ISSN: 2167-9851

RATS

RESEARCH AND TECHNICAL STUDIES

Research and Technical Studies
Specialty Group Postprints

From the 47th Annual Meeting
New England
May 13-18, 2019

Volume 7
2019

american
institute for
conservation
**Preserving Cultural
Heritage**

American Institute for Conservation

The Research and Technical Studies Specialty Group
of the
American Institute for Conservation

2018-2019 Officers
Chair
Corina Rogge
Program Chair
Matthew Clarke
Assistant Program Chair
Gregory Bailey
Secretary/Treasurer
Courtney VonStein Murray
Publications Chair
Amanda Norbutus
Chair Emeritus
Kristin deGhetaldi

2019-2020 Officers
Chair
Matthew Clarke
Program Chair
Gregory Bailey
Assistant Program Chair
Federica Pozzi
Secretary/Treasurer
Courtney VonStein Murray
Publications Chair
Molly McGath
Chair Emeritus
Corina Rogge

Research and Technical Studies Specialty Group Postprints

Abstracts, Extended Abstracts, and PowerPoint™ presentations from the 47th Annual Meeting of the American Institute for Conservation in New England, May 13 – 18, 2019

RATS 2019 Annual Meeting Program Committee
Matthew Clarke (Program Chair), Gregory Bailey and Corina Rogge

Compiler

Molly McGath

Volume 7

2019

American Institute for Conservation

Volume 7

ISSN: 2167-9851

The manuscripts and presentations in this publication have been edited for grammar yet have not undergone a formal process of peer review. The contents of this volume were originally given as oral presentations at the Annual Meeting of the American Institute for Conservations (AIC). The materials, methods, results, and conclusions described herein are the opinion of the contributors and do not reflect the policies or opinions of AIC or RATS. All rights reserved by individual authors.

This online publication is intended for all members of AIC. Copies of this publication are available only in electronic format and may be downloaded.

American Institute for Conservation
757 15th Street, NW, Suite 500, Washington, DC 20005-1714
www.culturalheritage.org

Table of Contents

Research and Technical Studies Specialty Group Presentations

Acoustic Emission of Humidity-Induced Damage to Model Wood Structures

Eric Hagan

Reducing the energy intensity of museums, galleries and other spaces with heritage collections is increasingly important due to the high cost of fuel, and the global need to lower greenhouse gas emissions. At the front line, institutions are seeking to lower energy consumption by addressing inefficiencies related to building design, HVAC and lighting equipment, and environmental control strategies. In a parallel effort, researchers are rethinking the necessity of precise museum environment tolerances, by investigating the risk of damage to specific materials exposed to fluctuating relative humidity (RH) and temperature. The goal of this latter body of work is to define the conditions that achieve an acceptable balance between facility energy consumption and the risk of collection damage. As a contribution to this effort, a research project is currently underway at the Canadian Conservation Institute that uses acoustic emission (AE) testing to monitor, or 'listen', to model wooden structures during exposure to humidity extremes. Under conditions causing physical damage, acoustic signals are emitted by the test materials, which are subsequently detected and analysed through the AE instrumentation. One of the many challenges with optimising the museum environment is the dependence of humidity sensitivity on exposure history. It is reasonable to assume that sensitive objects exposed to RH extremes have experienced past damage, and similar repeated fluctuations will have little or no harm. This is known as the Kaiser effect in AE terminology, or the concept of 'proofed fluctuations' in the field of heritage conservation. There are, however, foreseeable exposure histories where the Kaiser effect may fail or, at least, require further attention. For example, the resetting of hide glue in wooden assemblies at high RH may lead to further damage at a repeated low RH cycle. In order to study the effects of both humidity magnitude and history, a custom environmental chamber was constructed to generate fluctuations through various control modes: square wave, sinusoidal, custom array, and cloning of an external environment through cellular communication. Samples exposed to prescribed RH conditions in this low-noise test chamber were monitored with a multi-channel AE system to detect damage. This talk will provide an overview of research work to date, with a focus on the apparatus design and ongoing experiments. Preliminary test results highlight the response of simple wooden joints and veneered assemblies, which were bonded with animal glue and exposed to cycling humidity. The findings complement other research involving AE as an early warning monitoring tool for collection damage.

Biological Mortar Application for Micro-Crack Remediation in Travertines of Historic Monuments

Elif Sırt Çıplak, K. Goze Akoglu, Kivanc Bilecen, Neriman Sahin Guchan

Traditional conservation methods for the preservation of historical stones including applications with inorganic and organic polymers are often inadequate and results in introduction of new deterioration problems to historic structures. At this point, consolidating a stone by re-creating a structure similar to original microstructure of stone is a new approach developed to ensure the maximum compatibility by comparison to the traditional conservation techniques. In this study it was aimed to develop a sustainable and an eco-friendly repair material, biological mortar (BM)/infill, to be used in conservation interventions for healing micro-cracks (<1 mm) in travertines of historical monuments. This new repair material contains an environmental strain of a known bacteria species. In this context, bacterial isolation and identification were carried out from thermal spring water resources in Pamukkale Travertines (Denizli). Bacillus cereus, already known to have high calcite production capacity, was selected for BM development studies within isolated strains. Upon specifying all components of BM in details, mortar set up was performed in defined proportions and applied to micro-cracks of artificially aged test stones. Performance of this repair material was examined through physical, physico-mechanical, microstructural, and morphological analyses. Consequently, a strong bond between the grains and matrix of BM was determined in relation with the calcite production activities of B. cereus. Moreover, in all samples where BM applications were performed, interface of biological mortar and original material showed continuous and coherent structure. Hence, biological mortar and production substructure developed in this study, could be used for remediation of micro-cracks and micro-voids in historical travertine structures such as sculptures, ornaments, figures, capitals, and elements. In future studies, to increase the rate and concentration of bacterial calcite precipitation in mortar, some parameters in the experimental procedure could be improved by adding specific enzymes or macromolecules having potential to induce nitrogen cycle pathways to the nutritive medium, using large fermenters that could yield high quantities of bacteria, using multiple bacterial assembles that might also increase the amount of calcite production and identifying genes related with the mineral production process and with the adjustment of these genes to bring out large quantities of macromolecules that might induce calcite precipitation.

Challenges in the Detection and Identification of Proteins in Paintings and Works of Arts and Archaeological Objects

Ilaria Bonaduce, Anna Lluveras-Tenorio, Maria Perla Colombini, Sibilla Orsini

Staining, immunological, spectroscopic, chromatographic, and mass spectrometric based analytical methods have been shown to have the potential of being able to successfully detect, and in some cases, identify, proteins in selected samples from cultural heritage, such as paintings and works-of-arts, archaeological and paleontological findings1. Each of these approaches has its own strengths, but also its own drawbacks, most of which may be related to modifications undergone by proteins as an effect of human handling and ageing. Research in the recent years has demonstrated that several changes may take place in proteins as an effect of manufacturing processes (painting, cooking, etc.), interaction with the surrounding environment (pigments, paint support, vase, conservation treatment, etc.) and the external ageing conditions (temperature, light, RH% etc). Data indicate that amino acids modifications (such as deamidation, hydroxylation and several types of oxidations), hydrolysis and structural modifications are main pathways of degradation that may be encountered 2-6. In particular changes in the protein structure are very difficult to investigate at the molecular level, and are, as a consequence, not yet well understood. These include the formation of intermolecular and intramolecular aggregates stabilised by weak hydrophobic and hydrogen bonds, covalent cross-linking and formation of strong complexes with cations. Such modifications, though, may hamper the detection and identification of proteins in artistic and archaeological objects, as they may compromise the specificity of the protein pyrolytic pattern, may compromise the antigen/antibody interaction, may cause an irreversible loss of solubility, challenging the protein extraction necessary for chromatographic and proteomics techniques and may affect the degree of access of cleavage enzymes in proteomics experiments. As a consequence of all this, detection and identification of proteins in degraded samples from artistic, archaeological and paleontological objects still present several challenges, which are strongly interconnected. These include advancing scientific methods, dedicating more resources to better understand degradation phenomena, and developing reliable models for data interpretation. And when facing the analysis of a sample of unknown composition and of unknown conservation conditions, multi-analytical approaches and an open mind in the analysis of data are our most powerful tools. References (1) Dallongeville, S., Garnier, N., Rolando, C., Tokarski, C. Chemical Reviews 2016, 116, 2-79. (2) Orsini, S., Bramanti, E., Bonaduce, I. Journal of Analytical and Applied Pyrolysis 2018, 133, 59-67. (3) Orsini, S., Parlanti, F., Bonaduce, I. Journal of Analytical and Applied Pyrolysis 2017, 124, 643-657. (4) Orsini, S., Yadav, A., Dilillo, M., McDonnell, L. A., Bonaduce, I. Analytical Chemistry 2018, 90, 6403-6408. (5) Duce, C., Bramanti, E., Ghezzi, L., Bernazzani, L., Bonaduce, I., Colombini, M. P., Spepi, A., Biagi, S., Tine, M. R. Dalton Transactions 2013, 42, 5975-5984. (6) Mackie, M., Rüther, P., Samodova, D., Di Gianvincenzo, F., Granzotto, C., Lyon, D., Peggie, D. A., Howard, H., Harrison, L., Jensen, L. J. Angewandte Chemie International Edition 2018.

Effects of Binder Layer and Bath pH on Pt-Ag Replacement Reactions as Applied to Photographic Toning Practices

Dr. Joan M. Walker[1]*, Ronel Namde[2], Dr. Keana Scott[3], and Dr. Alline Myers[4]

Effects of Binder Layer and Bath pH on Pt-Ag Replacement Reactions as Applied to Photographic Toning Practices

Joan M. Walker and Ronel Namde
National Gallery of Art, Washington, DC
Keana Scott and Alline Myers
National Institute of Standards and Technology

American Institute for Conservation Annual Meeting | Research and Technical Studies Session | May 15, 2019

[1]Conservation Scientist, National Gallery of Art, Washington, DC

[2]Photograph Conservator, National Gallery of Art, Washington, DC

[3]Physical Scientist, Materials Measurement Science Division, National Institute of Standards and Technology

[4]Physical Scientist, Center for Nanoscale Science and Technology, National Institute of Standards and Technology

*jm-walker@nga.gov
Presented at the RATS session
47th Annual Meeting
American Institute for Conservation (AIC)
New England, May 13-17, 2019

Effects of Binder Layer and Bath pH on Pt-Ag Replacement Reactions as Applied to Photographic Toning Practices

Joan M. Walker and Ronel Namde
National Gallery of Art, Washington, DC
Keana Scott and Alline Myers
National Institute of Standards and Technology

American Institute for Conservation Annual Meeting | Research and Technical Studies Session | May 15, 2019

Nineteenth-century paper-based photographic images consist of metallic nanoparticles embedded in carbohydrate or protein matrices, where the properties and local environments of these particles determine the aesthetic tonality of the print. Salted paper prints and gelatin printed-out prints are both silver-based processes that naturally produce prints with a reddish-to-brown coloration. From an early date, photographers manipulated the tones of these photographs with the use of precious metal baths containing gold or platinum salts. As in modern nanomaterials chemistry, traditional chemical photographic printing methods require tightly controlled reaction conditions to influence product morphology and access specific optical properties.

In this study, a suite of silver prints toned with platinum was generated following historic recipes and analyzed by X-ray fluorescence spectroscopy, scanning electron microscopy, and colorimetry to investigate the interplay between metal content and perceived tone. Thin sections of the samples were also prepared by focused ion beam milling and imaged using scanning transmission electron microscopy to visualize the metal particles in situ. Prints toned in an acidic platinum bath undergo galvanic replacement of silver for platinum, converting nanoscale aggregates of silver to evenly distributed bimetallic particles that impart a neutral gray hue. Those toned in an alkaline platinum bath experience metal deposition, which increases the print's optical density. For gelatin prints, these reaction mechanisms are further influenced by the protonation state of the binder layer.

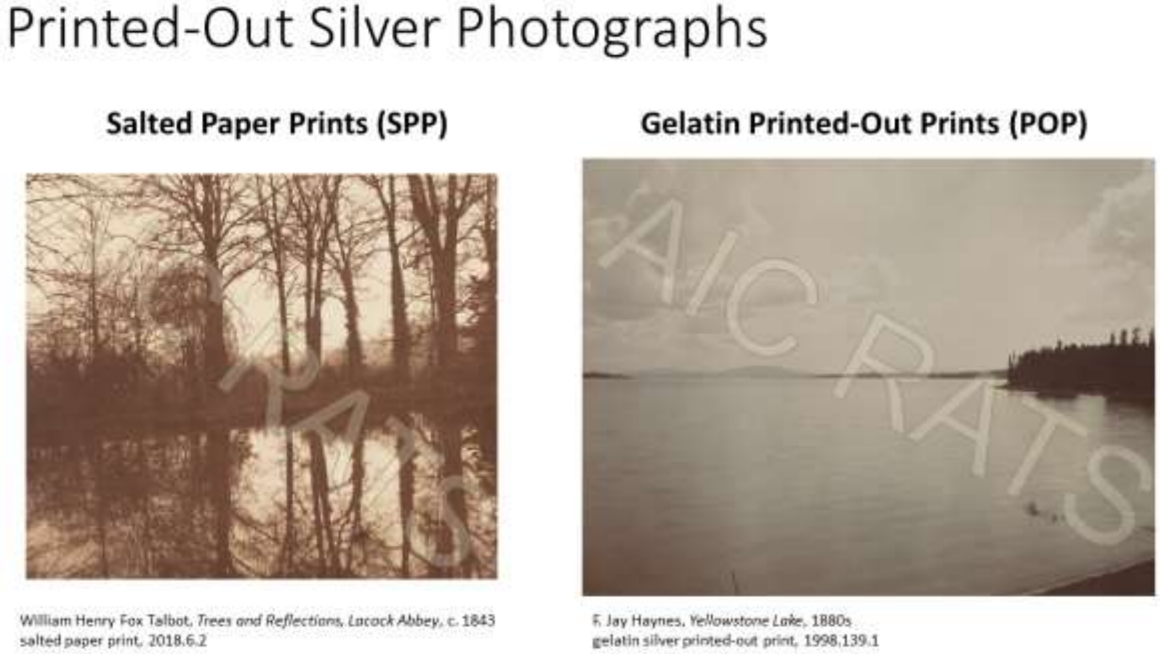

Printed-Out Silver Photographs

Salted Paper Prints (SPP)

Gelatin Printed-Out Prints (POP)

William Henry Fox Talbot, *Trees and Reflections, Lacock Abbey*, c. 1843
salted paper print, 2018.6.2

F. Jay Haynes, *Yellowstone Lake*, 1880s
gelatin silver printed-out print, 1998.139.1

This research focuses on two photographic processes that were popular in the 19th century: salted paper printing and gelatin print-out printing. Both of these processes are printed-out, that is, the image forms completely during exposure. Other types of photographs are developed-out, meaning that the image requires a chemical developer bath to complete image formation during processing.

Image credits (images.nga.gov):

William Henry Fox Talbot (British, 1800-1877) Trees and Reflections, Lacock Abbey, c. 1843, salted paper print, 16.4 x 19.2 cm (image), National Gallery of Art (2018.6.2), Purchased as a Gift of the Richard King Mellon Foundation.

F. Jay Haynes (American, 1853-1921) Yellowstone Lake, 1880s, gelatin silver printed-out print, 43.5 x 55.9 cm (sheet), National Gallery of Art (1998.139.1), Robert B. Menschel Fund.

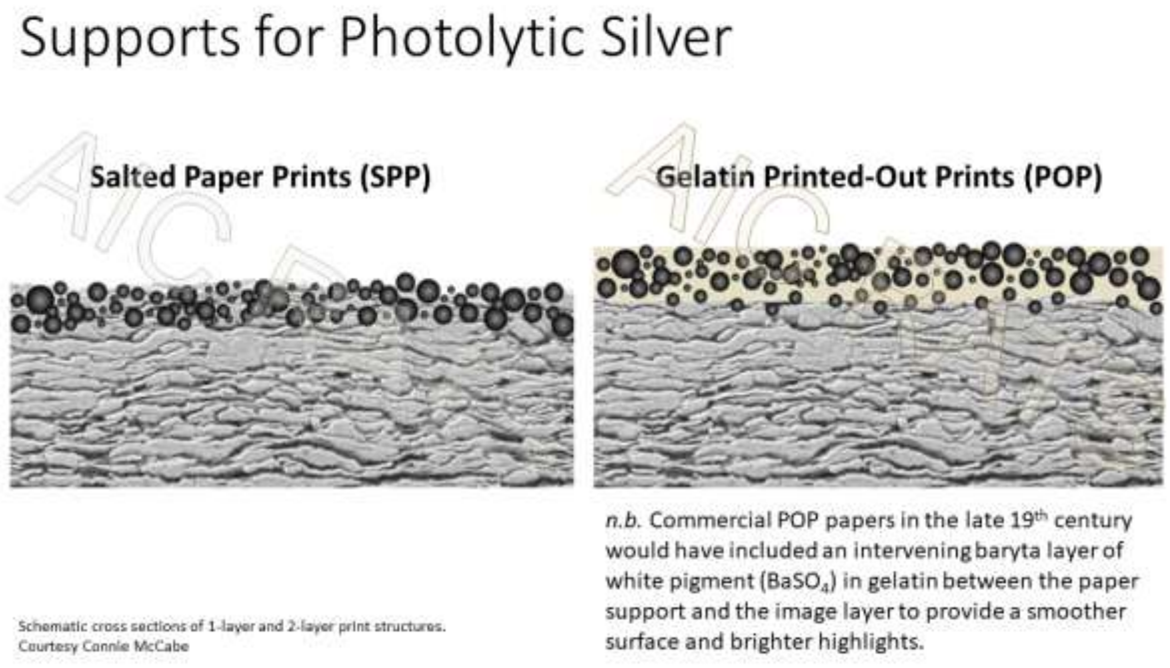

Supports for Photolytic Silver

Salted Paper Prints (SPP)

Gelatin Printed-Out Prints (POP)

n.b. Commercial POP papers in the late 19^{th} century would have included an intervening baryta layer of white pigment ($BaSO_4$) in gelatin between the paper support and the image layer to provide a smoother surface and brighter highlights.

Schematic cross sections of 1-layer and 2-layer print structures.
Courtesy Connie McCabe

Structurally, salted paper prints (SPP) are one of the simplest types of photographs, consisting of printed-out (i.e. photolytic) silver particles embedded in the surface of a paper support. In a gelatin printed-out print (POP), the silver image particles are located in the gelatin binder layer, which sits on top of the paper. Thus, the silver particles experience very different chemical environments between the two processes: carbohydrate (cellulose) or protein (gelatin).

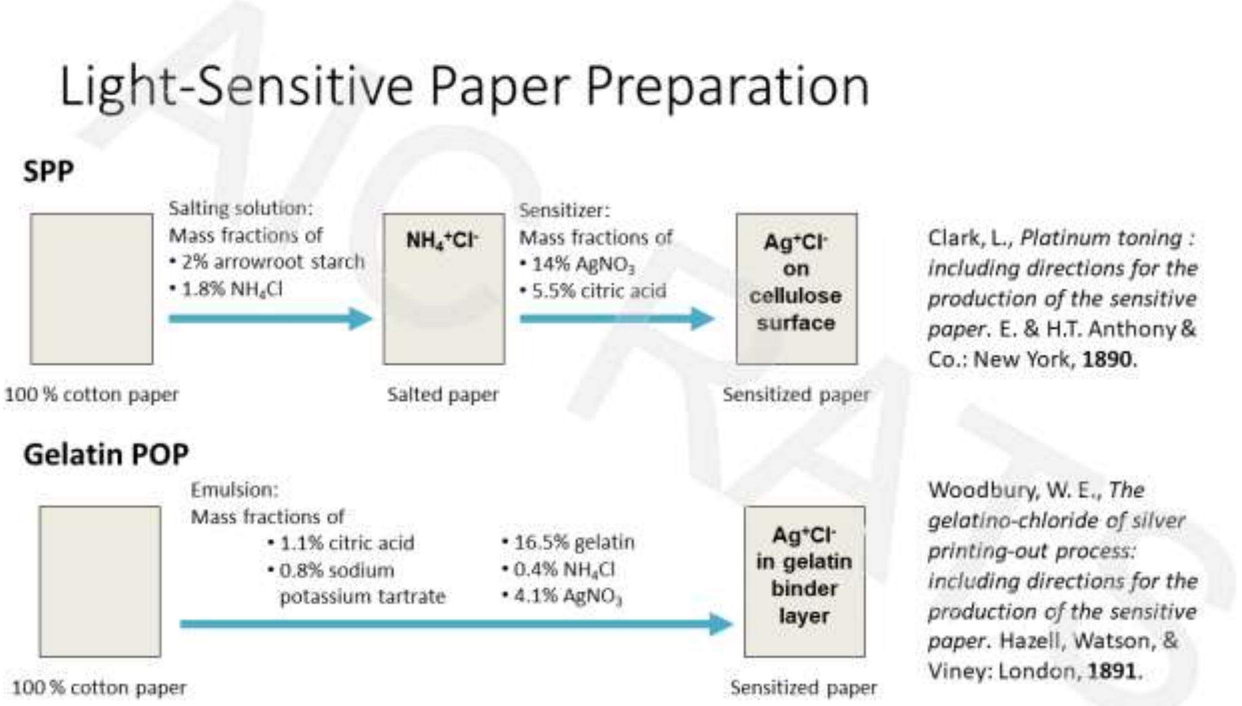

Light-Sensitive Paper Preparation

SPP

Salting solution:
Mass fractions of
- 2% arrowroot starch
- 1.8% NH_4Cl

Sensitizer:
Mass fractions of
- 14% $AgNO_3$
- 5.5% citric acid

100 % cotton paper → **$NH_4^+Cl^-$** Salted paper → **Ag^+Cl^- on cellulose surface** Sensitized paper

Clark, L., *Platinum toning : including directions for the production of the sensitive paper*. E. & H.T. Anthony & Co.: New York, **1890**.

Gelatin POP

Emulsion:
Mass fractions of
- 1.1% citric acid
- 0.8% sodium potassium tartrate
- 16.5% gelatin
- 0.4% NH_4Cl
- 4.1% $AgNO_3$

100 % cotton paper → **Ag^+Cl^- in gelatin binder layer** Sensitized paper

Woodbury, W. E., *The gelatino-chloride of silver printing-out process: including directions for the production of the sensitive paper*. Hazell, Watson, & Viney: London, **1891**.

The samples in this study were prepared following 19th century recipes published in manuals intended for use by both amateur and professional photographers wishing to make their own photographic papers.

The salted paper is made in two steps. First, a sheet of high quality 100% cotton paper (Arches Platine) is coated with a solution containing ammonium chloride and arrowroot starch. After drying, the sheets are sensitized with a solution of silver nitrate and citric acid to form silver chloride in situ.

For gelatin prints, photographic grade gelatin is dissolved in warm water, and various salts are added (ammonium chloride, citric acid, and sodium potassium tartrate). To this warm, stirring solution, silver nitrate is added dropwise to form a cloudy emulsion of silver chloride crystals. The sheets of paper are coated with the emulsion and hung to dry in the darkroom.

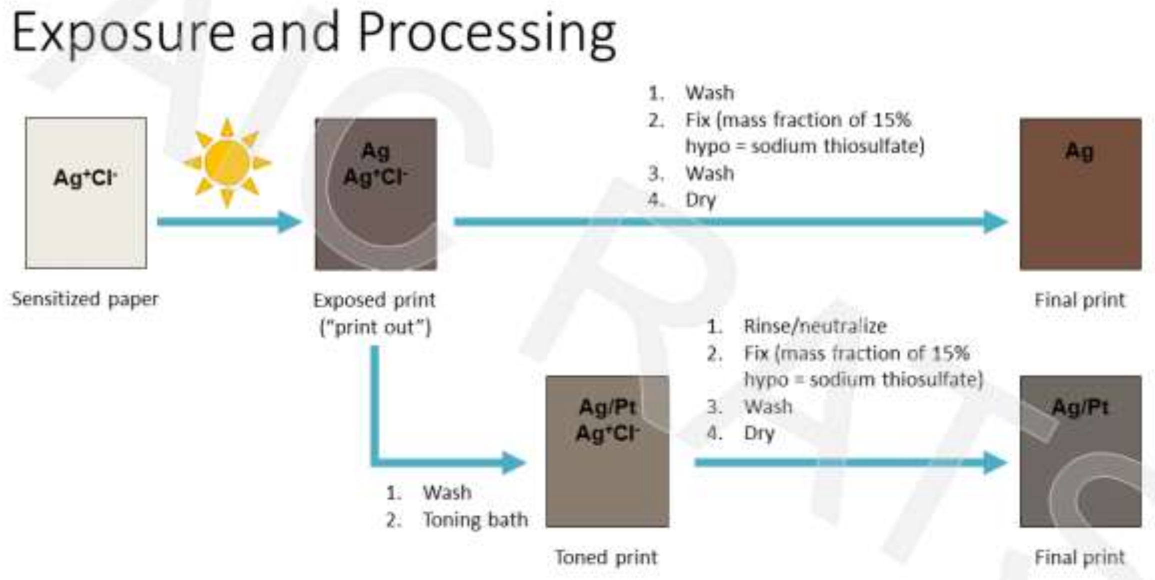

Exposure and Processing

1. Wash
2. Fix (mass fraction of 15% hypo = sodium thiosulfate)
3. Wash
4. Dry

1. Rinse/neutralize
2. Fix (mass fraction of 15% hypo = sodium thiosulfate)
3. Wash
4. Dry

1. Wash
2. Toning bath

For both salted paper and gelatin print-out printing, the procedures for exposure and processing are similar, and a simplified cartoon representation of these steps is shown. The dried sheets are contact printed under a 21-step gray scale negative in a UV exposure unit. For an untoned print (upper path), the processing steps include initial washing in water to remove soluble salts, followed by fixing in sodium thiosulfate (hypo) to remove any light-sensitive halides that remain in the photograph, and a final wash. To prepare a toned print (lower path), the sheet is introduced to a toning bath after its initial wash but before fixing. The toning baths tested contain platinum salts and additional chemicals intended to influence the toning action. After the toning bath, the print is rinsed, and the rest of the processing proceeds as for the untoned print.

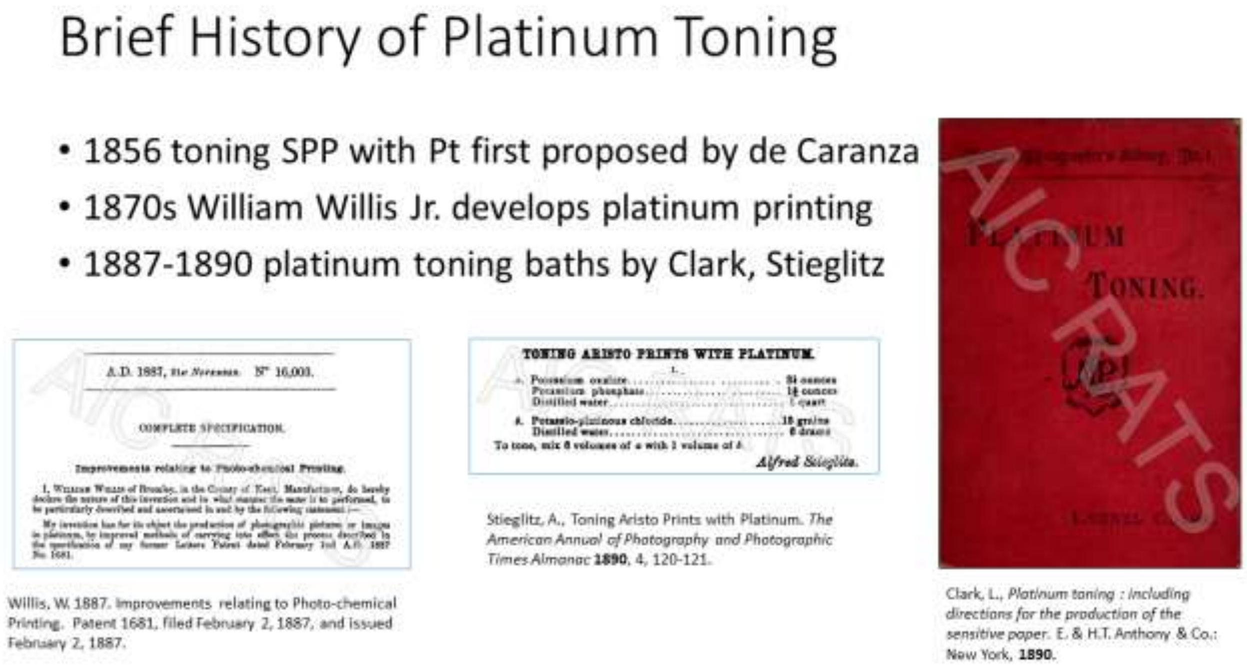

Brief History of Platinum Toning

- 1856 toning SPP with Pt first proposed by de Caranza
- 1870s William Willis Jr. develops platinum printing
- 1887-1890 platinum toning baths by Clark, Stieglitz

A.D. 1887, 21st November. Nº 16,003.

COMPLETE SPECIFICATION.

Improvements relating to Photo-chemical Printing.

I, William Willis of Bromley, in the County of Kent, Manufacturer, do hereby declare the nature of this invention and in what manner the same is to be performed, to be particularly described and ascertained in and by the following statement:—

My invention has for its object the production of photographic pictures or images in platinum, by improved methods of carrying into effect the process described in the specification of my former Letters Patent dated February 2nd A.D. 1887 No. 1681.

Willis, W. 1887. Improvements relating to Photo-chemical Printing. Patent 1681, filed February 2, 1887, and issued February 2, 1887.

TONING ARISTO PRINTS WITH PLATINUM.

1.

a. Potassium oxalate .... 3½ ounces
Potassium phosphate .... 1½ ounces
Distilled water .... 1 quart

b. Potassio-platinous chloride .... 15 grains
Distilled water .... 6 drams

To tone, mix 6 volumes of a with 1 volume of b.

Alfred Stieglitz.

Stieglitz, A., Toning Aristo Prints with Platinum. *The American Annual of Photography and Photographic Times Almanac* **1890**, 4, 120-121.

Clark, L., *Platinum toning : including directions for the production of the sensitive paper*. E. & H.T. Anthony & Co.: New York, **1890**.

Platinum toning dates to at least 1856, when Ernest de Caranza published a recipe for toning salted paper prints with platinum salts in France. The procedures investigated in this study were developed later in the century, when platinum printing was popular. William Willis Jr. invented platinum printing, a developed-out process, in the 1870s. In 1887 Willis patented a platinum-containing developer bath, which other photographers, including Lyonel Clark and Alfred Stieglitz, quickly adapted as a toner for silver prints.

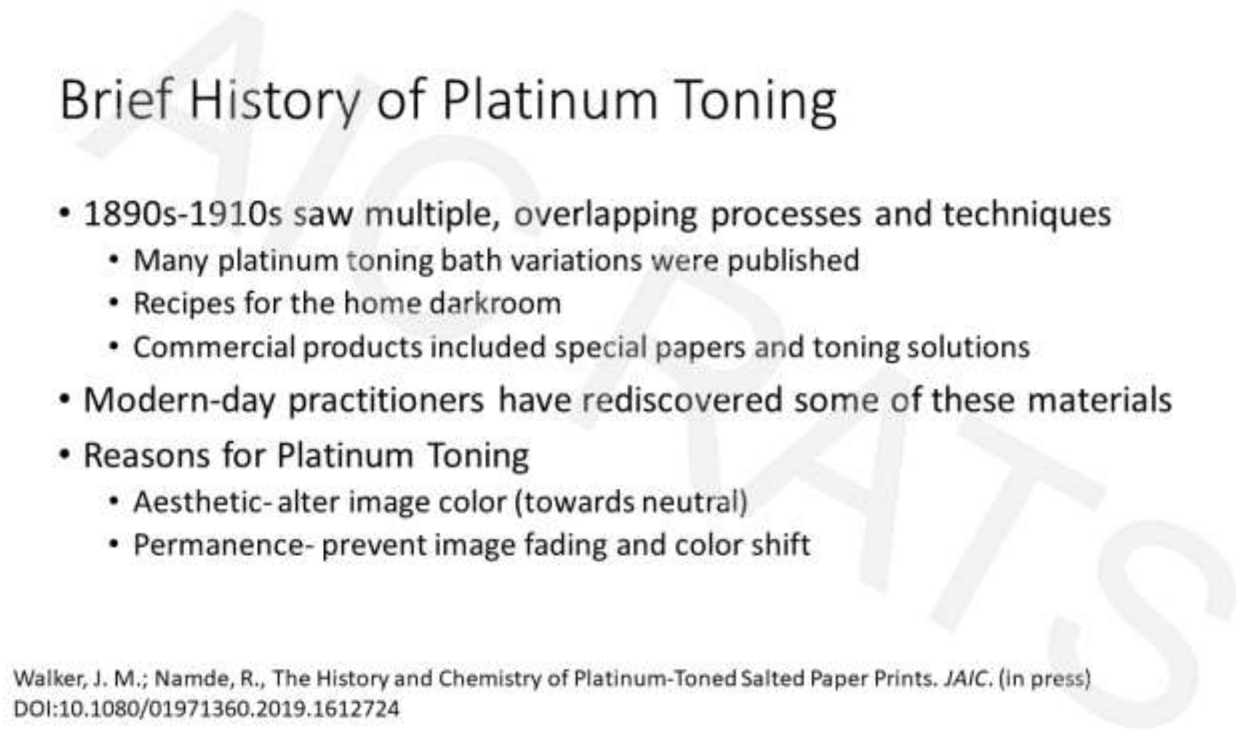

Brief History of Platinum Toning

- 1890s-1910s saw multiple, overlapping processes and techniques
  - Many platinum toning bath variations were published
  - Recipes for the home darkroom
  - Commercial products included special papers and toning solutions
- Modern-day practitioners have rediscovered some of these materials
- Reasons for Platinum Toning
  - Aesthetic- alter image color (towards neutral)
  - Permanence- prevent image fading and color shift

Walker, J. M.; Namde, R., The History and Chemistry of Platinum-Toned Salted Paper Prints. *JAIC*. (in press)
DOI:10.1080/01971360.2019.1612724

The decades surrounding the turn of the 20th century were very rich in photographic technology and innovation. A diverse array of materials and techniques were available to photographers. Some of this larger context for platinum toning is the subject of a forthcoming publication in JAIC (https://dx.doi.org/10.1080/01971360.2019.1612724). It is also important to note that the modern-day alternative process community is actively engaged in rediscovering and experimenting with platinum toning and other historic processes. The reasons for toning with platinum (and other precious metals) remain the same: to alter the appearance of a print and to improve its longevity.

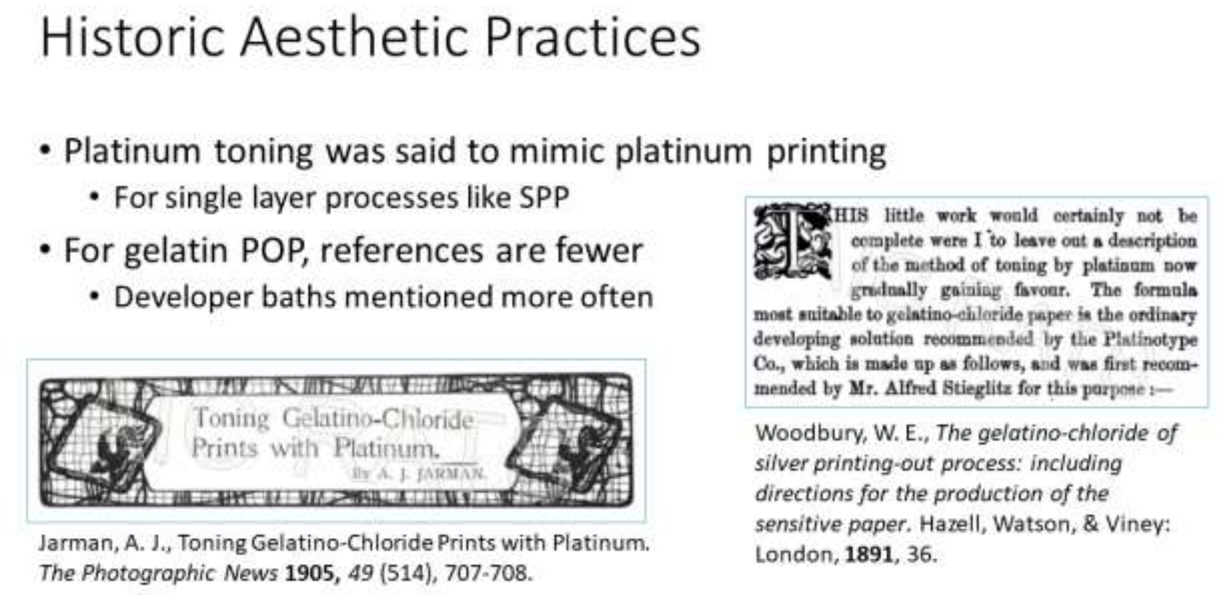

Historic Aesthetic Practices

- Platinum toning was said to mimic platinum printing
  - For single layer processes like SPP
- For gelatin POP, references are fewer
  - Developer baths mentioned more often

Toning Gelatino-Chloride Prints with Platinum.
By A. J. JARMAN.

Jarman, A. J., Toning Gelatino-Chloride Prints with Platinum. *The Photographic News* **1905,** *49* (514), 707-708.

THIS little work would certainly not be complete were I to leave out a description of the method of toning by platinum now gradually gaining favour. The formula most suitable to gelatino-chloride paper is the ordinary developing solution recommended by the Platinotype Co., which is made up as follows, and was first recommended by Mr. Alfred Stieglitz for this purpose :—

Woodbury, W. E., *The gelatino-chloride of silver printing-out process: including directions for the production of the sensitive paper.* Hazell, Watson, & Viney: London, **1891**, 36.

From an aesthetic perspective, toning silver photographs with platinum was purported to mimic the appearance of a platinum print. In fact, some authors included directions for toning salted paper prints in manuals for platinum printing. Platinum toning specifically for gelatin printed-out prints was written about less often than for salted paper. While most toning bath recipes for SPP were acidic, those recommended for POP were more often alkaline, like the Willis developer bath. This study applies baths of various compositions, acidic to alkaline, to both types of prints in order to understand the mechanism of toning action for these processes.

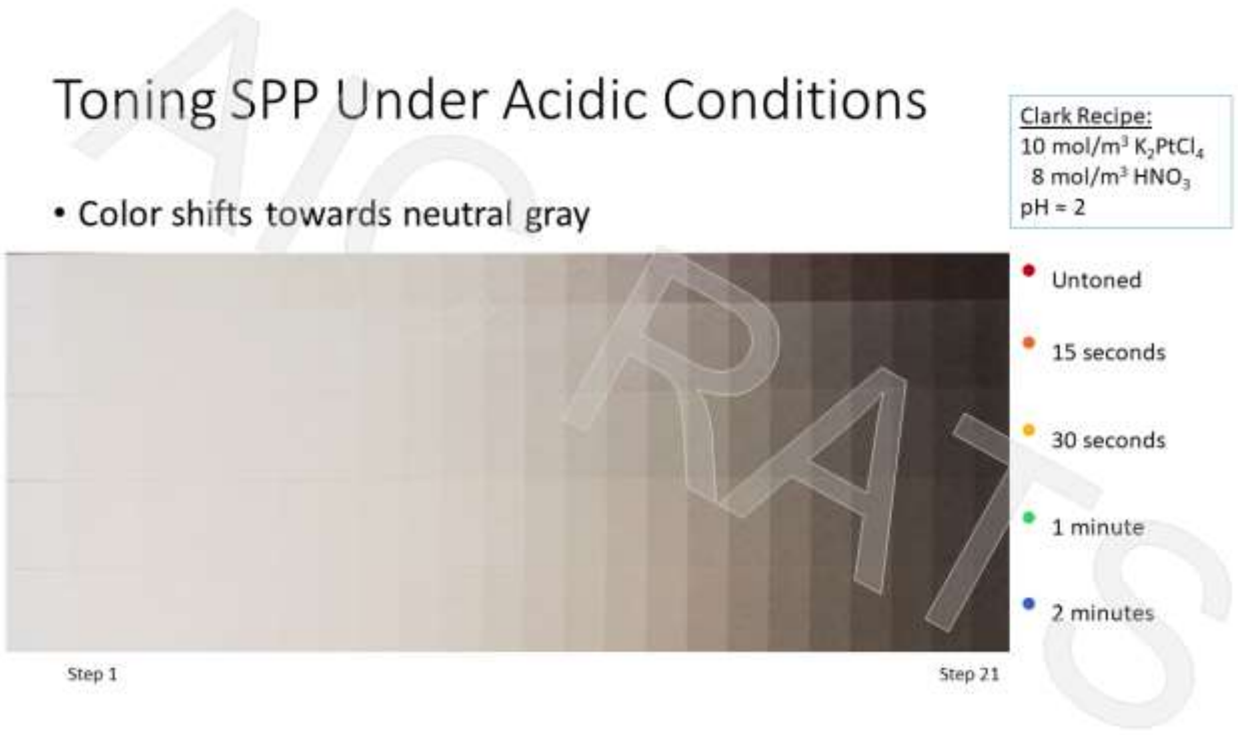

Toning SPP Under Acidic Conditions

- Color shifts towards neutral gray

Clark Recipe:
10 mol/m³ K_2PtCl_4
8 mol/m³ HNO_3
pH = 2

● Untoned
● 15 seconds
● 30 seconds
● 1 minute
● 2 minutes

When the salted paper print is introduced into an acidic toning bath, it undergoes a dramatic color shift from brick red to neutral-to-warm gray. Subtle variations in color and the speed of reaction are apparent with different bath formulations. However, the results for samples toned with a bath prepared according to Lyonel Clark's recipe containing potassium tetrachloroplatinate and nitric acid are representative of the acidic baths tested.

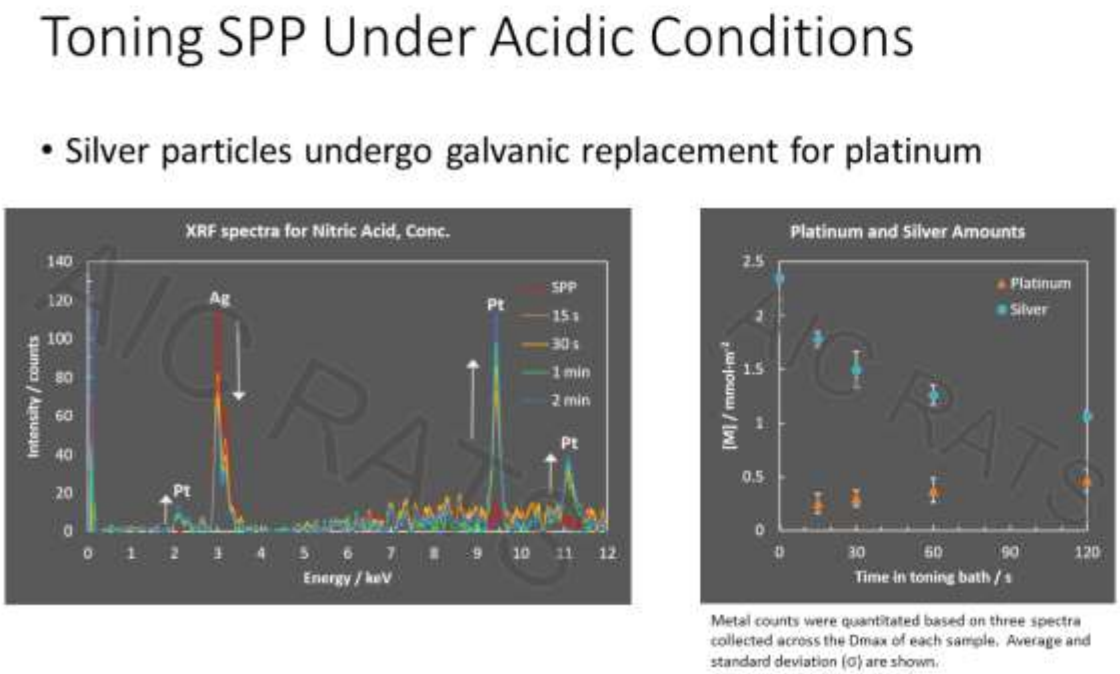

Toning SPP Under Acidic Conditions

- Silver particles undergo galvanic replacement for platinum

Metal counts were quantitated based on three spectra collected across the Dmax of each sample. Average and standard deviation (σ) are shown.

The metallic content of the prints is analyzed with X-ray fluorescence spectroscopy (XRF). The platinum content increases and the silver counts decrease with longer times in the toning bath. This trend indicates that the platinum is replacing silver in the print.

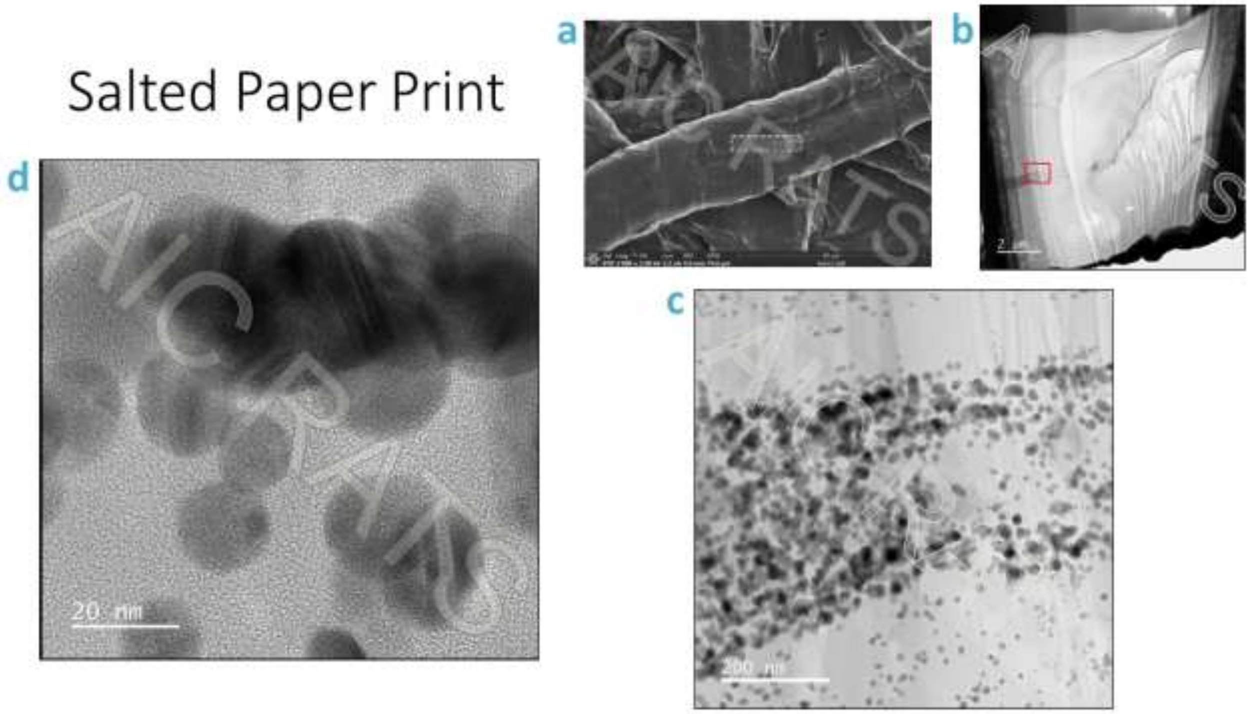

A cross section of a surface paper fiber (a) is prepared using focused ion beam milling in a scanning electron microscope (FIB-SEM). The structures of the image particles in the thinned section (b) are observed with high resolution transmission electron microscopy (HRTEM). For the untoned SPP, the silver particles are roughly spherical in shape and range to a few tens of nanometers in diameter (c, d).

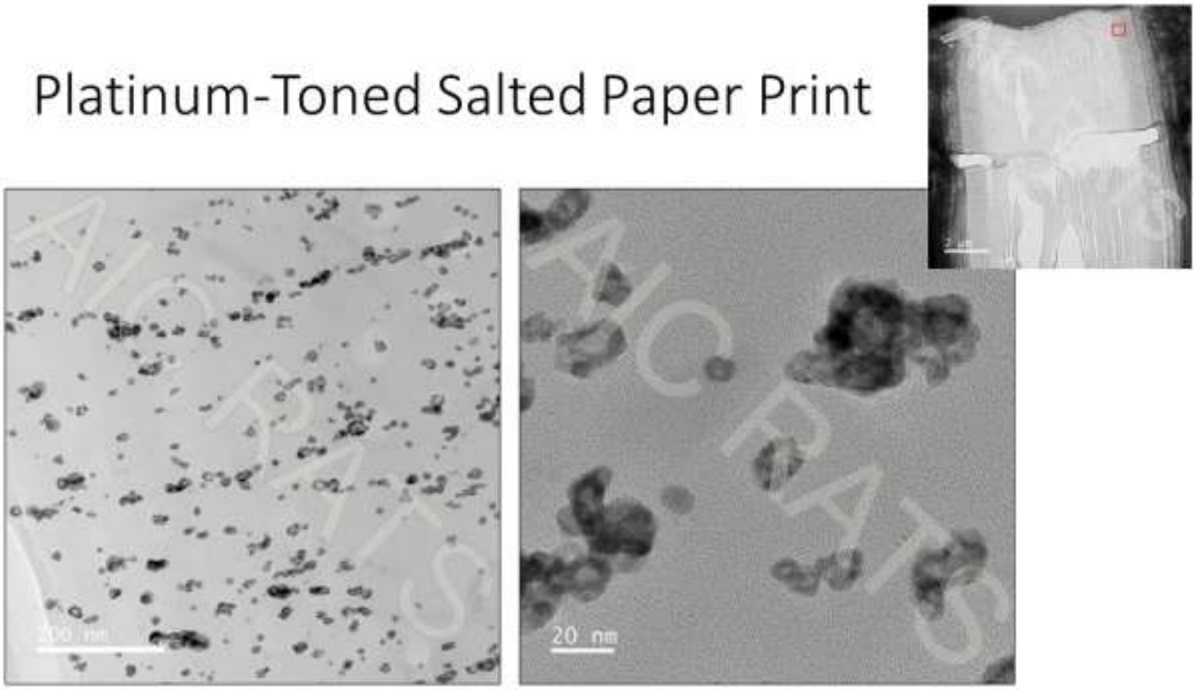

Platinum-Toned Salted Paper Print

For the platinum-toned sample, a different particle morphology is observed, and the metallic particles appear hollow.

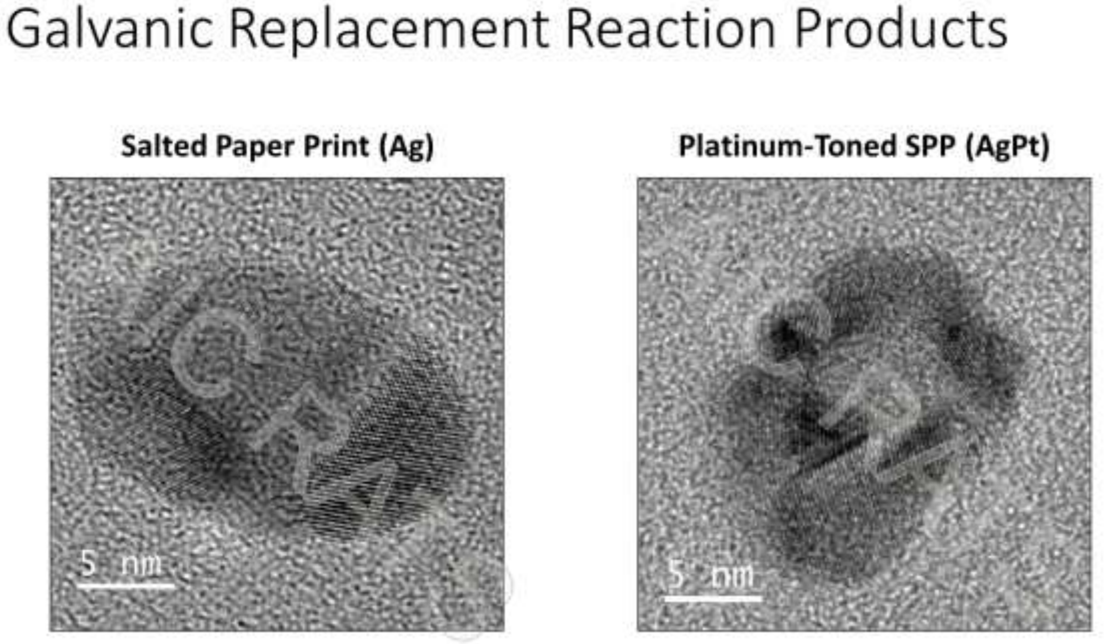

Galvanic Replacement Reaction Products

Salted Paper Print (Ag)

Platinum-Toned SPP (AgPt)

These particle morphologies are characteristic of a galvanic replacement reaction, in which a solid silver starting material is used as a sacrificial template for the overgrowth of a more noble metal. Here, the final products are bumpy, hollow structures containing both silver and platinum domains.

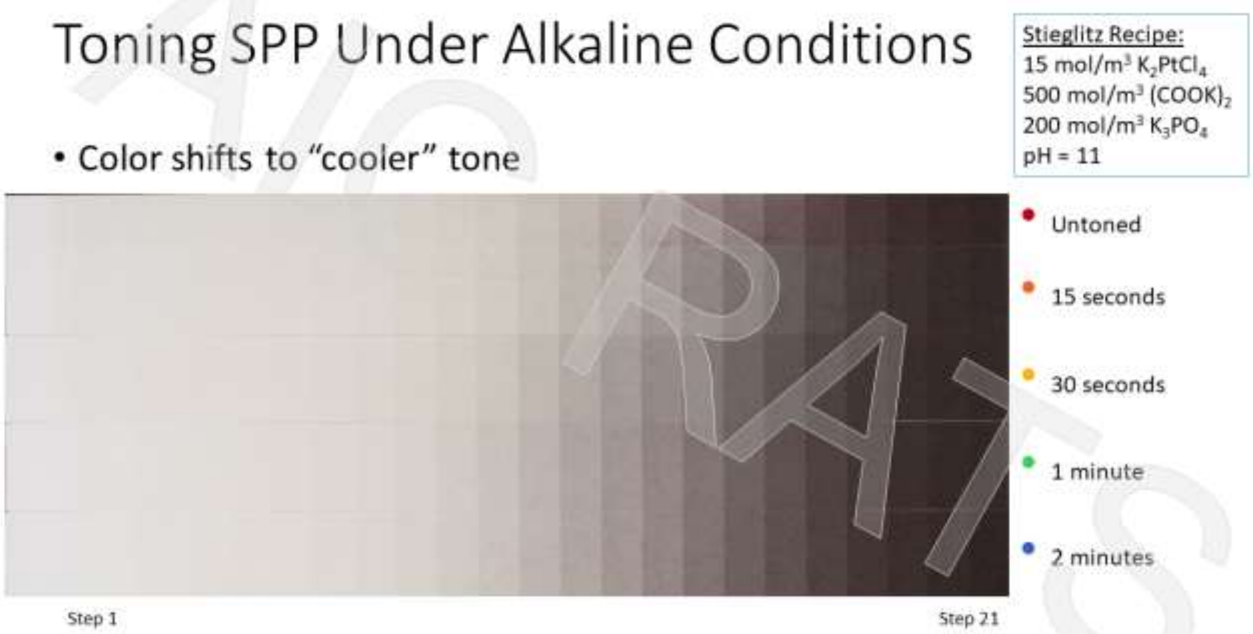

Toning SPP Under Alkaline Conditions

- Color shifts to “cooler” tone

Stieglitz Recipe:
15 mol/m^3 K_2PtCl_4
500 mol/m^3 $(COOK)_2$
200 mol/m^3 K_3PO_4
pH = 11

● Untoned
● 15 seconds
● 30 seconds
● 1 minute
● 2 minutes

Platinum toning salted paper prints proceeds differently under alkaline conditions. The most alkaline bath tested, based on a recipe published by Alfred Stieglitz, contains potassium tetrachloroplatinate, potassium oxalate, and potassium phosphate. The color of the print shifts, but the direction of change is toward a cooler tone than that observed with the acidic baths.

Toning SPP Under Alkaline Conditions

- Less platinum is deposited than in the acidic samples

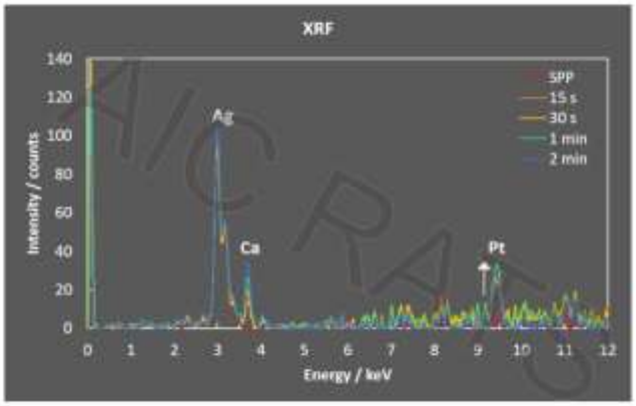

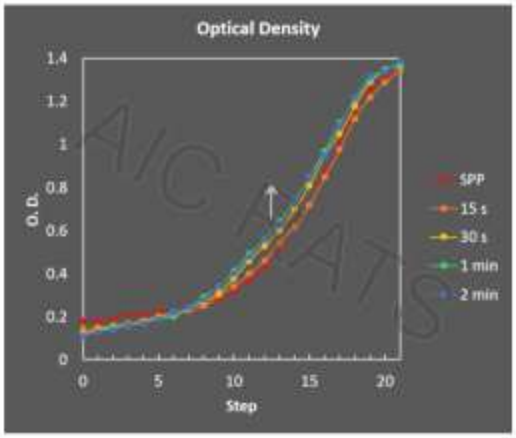

The alkaline-toned samples also show an increase in optical density, as measured with a reflectance spectrophotometer, but only minor gains in platinum counts in the XRF spectra.

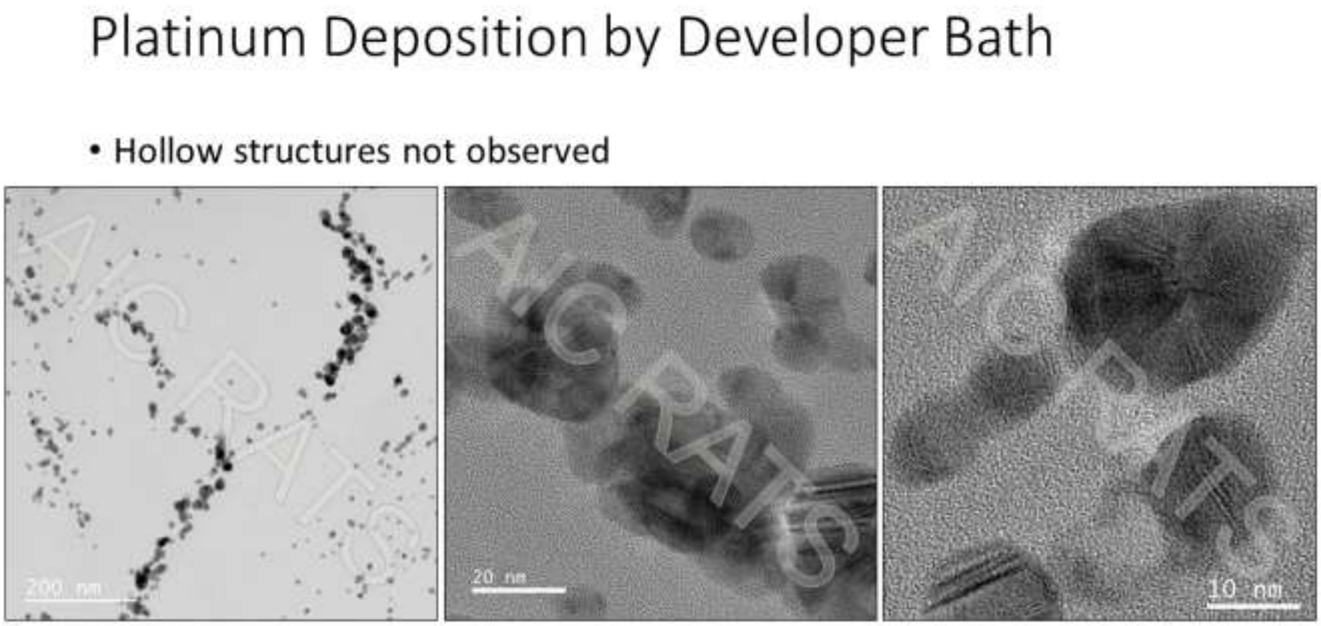

Platinum Deposition by Developer Bath

- Hollow structures not observed

Under the alkaline conditions, galvanic replacement is not operative, and no hollow AgPt structures are observed. Instead, small amounts of platinum are deposited on the silver image by the bath, which is similar in composition to the platinum-containing developers from the late 1880s.

Photolytic Silver in Two Processes

The optical properties of silver nanostructures are determined by size and shape, degree of aggregation, and local dielectric near their surfaces. Comparing the silver image particles in SPP and gelatin POP shows that they are similar in size and shape in both samples. However, in the POP sample, the silver particles are clustered into small groupings suspended in the protein matrix. These differences in nano-environment partly explain the visual characteristics that distinguish the two processes.

Gelatin POP : Dark Field STEM

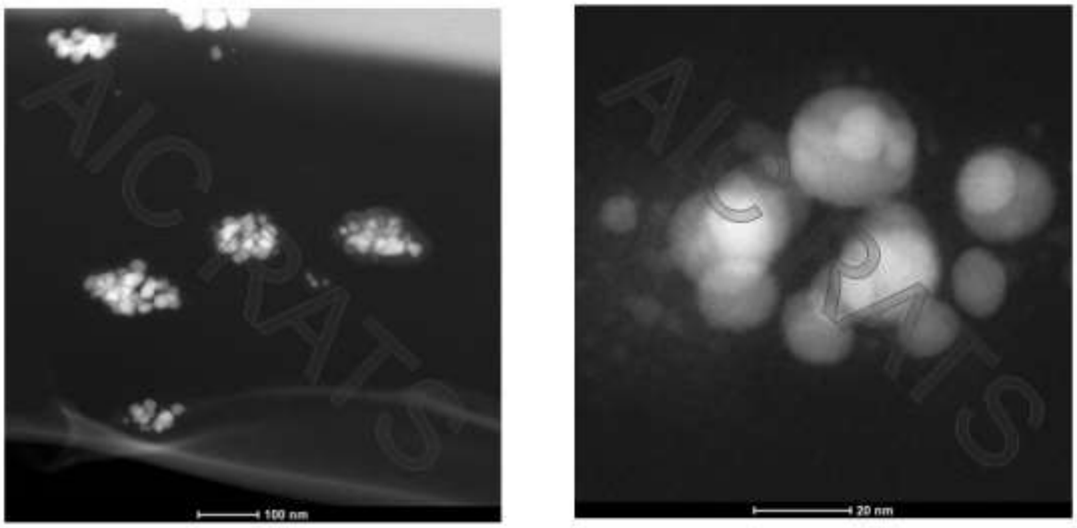

Because of the clustering of the silver particles in the gelatin sample, it is easier to view them in dark field scanning TEM. In these Z-contrast images, the metal appears as bright spots, and the individual spheres in each cluster can be distinguished.

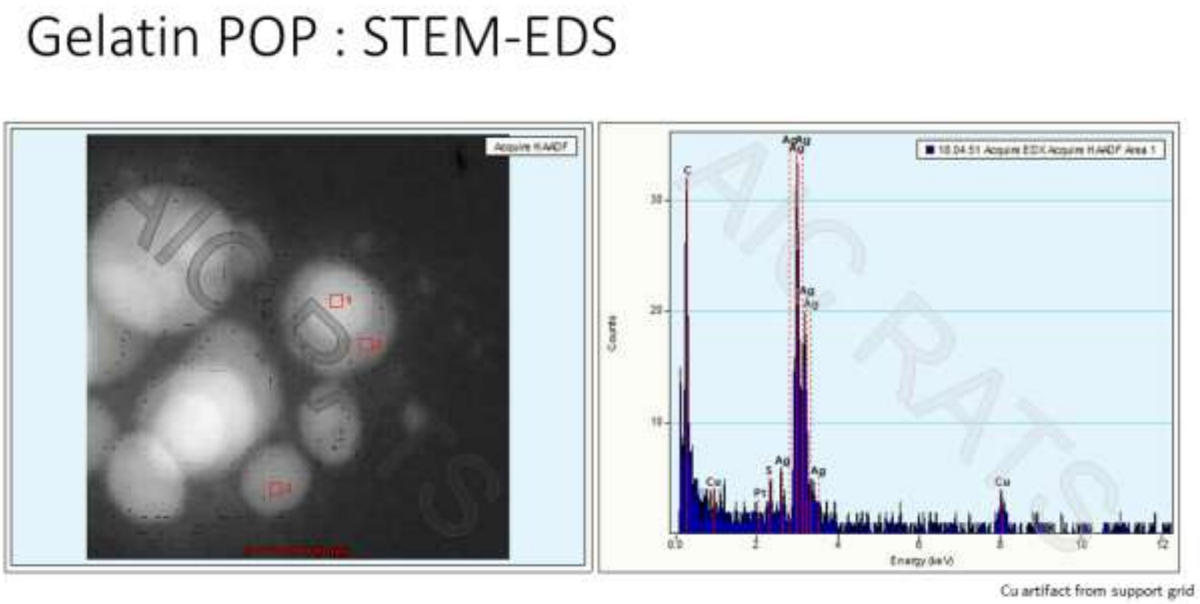

Gelatin POP : STEM-EDS

Cu artifact from support grid

Elemental data are acquired on selected areas of the samples using energy dispersive spectroscopy (EDS), which confirms that the particles contain silver.

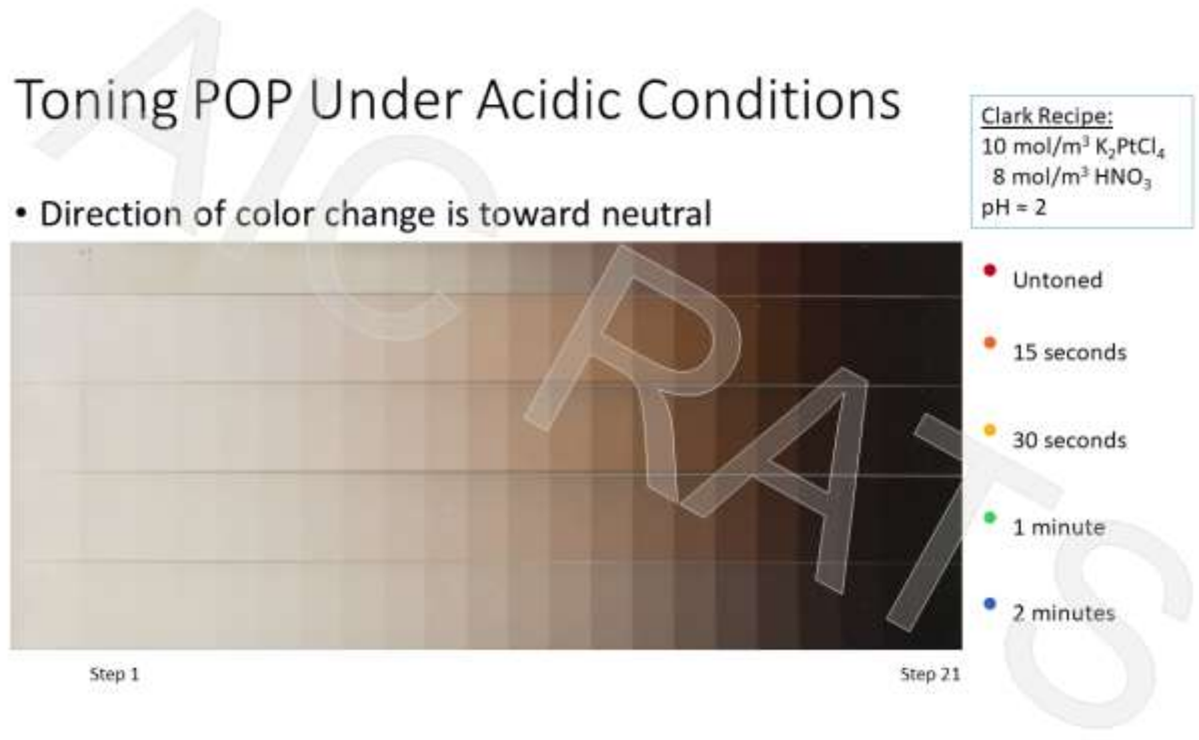

Toning POP Under Acidic Conditions

- Direction of color change is toward neutral

Clark Recipe:
10 mol/m^3 K_2PtCl_4
8 mol/m^3 HNO_3
pH = 2

● Untoned
● 15 seconds
● 30 seconds
● 1 minute
● 2 minutes

When the gelatin POP is introduced into the acidic platinum toning bath, the color begins to lose some of its reddishness and shift towards neutral.

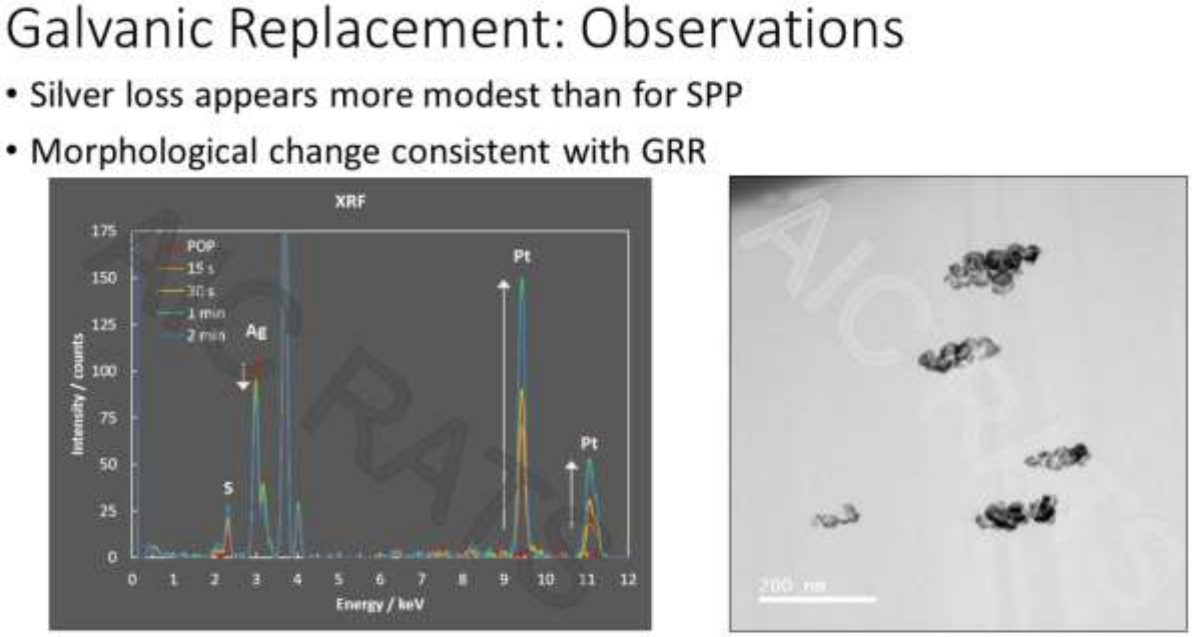

Galvanic Replacement: Observations

- Silver loss appears more modest than for SPP
- Morphological change consistent with GRR

Similar to the SPP samples, the XRF spectra and TEM images indicate a galvanic replacement reaction.

Product from Acidic Toning Bath

The morphology of the particles is more clearly seen in the STEM dark field images. The clusters of solid silver nanoparticles have been transformed into hollow shells.

Bumpy Ag-Pt Particles

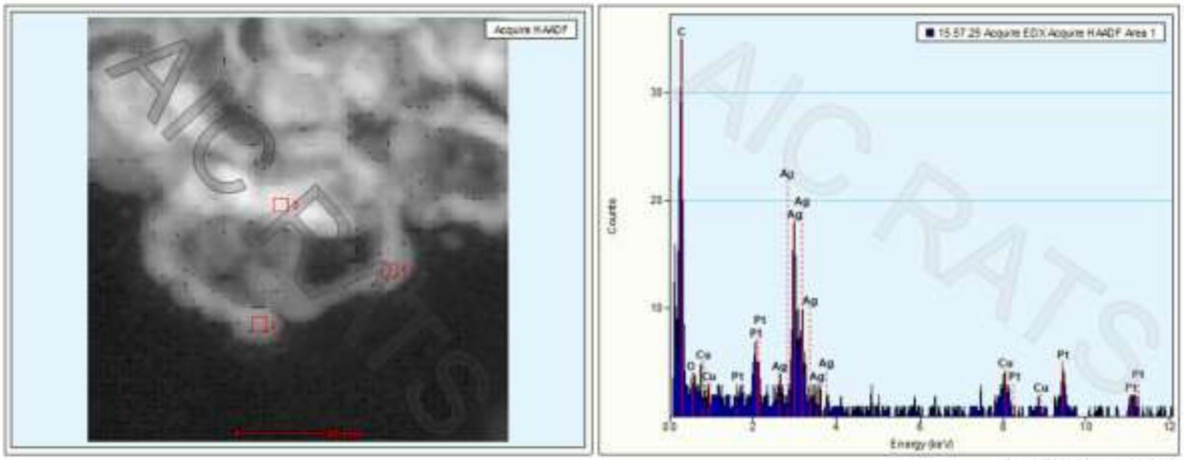

Cu artifact from support grid

The bumpy shells contain both silver and platinum.

Toning POP Under Alkaline Conditions

- Color change is different

Stieglitz Recipe:
15 mol/m^3 K_2PtCl_4
500 mol/m^3 $(COOK)_2$
200 mol/m^3 K_3PO_4
pH = 11

● Untoned
● 15 seconds
● 30 seconds
● 1 minute
● 2 minutes

When the alkaline bath is used for toning the gelatin POP, a less dramatic visual impact is observed than for the acidic bath or for the salted paper prints. The color shifts to a warm brown that does not appear to progress over the 2-minute toning period.

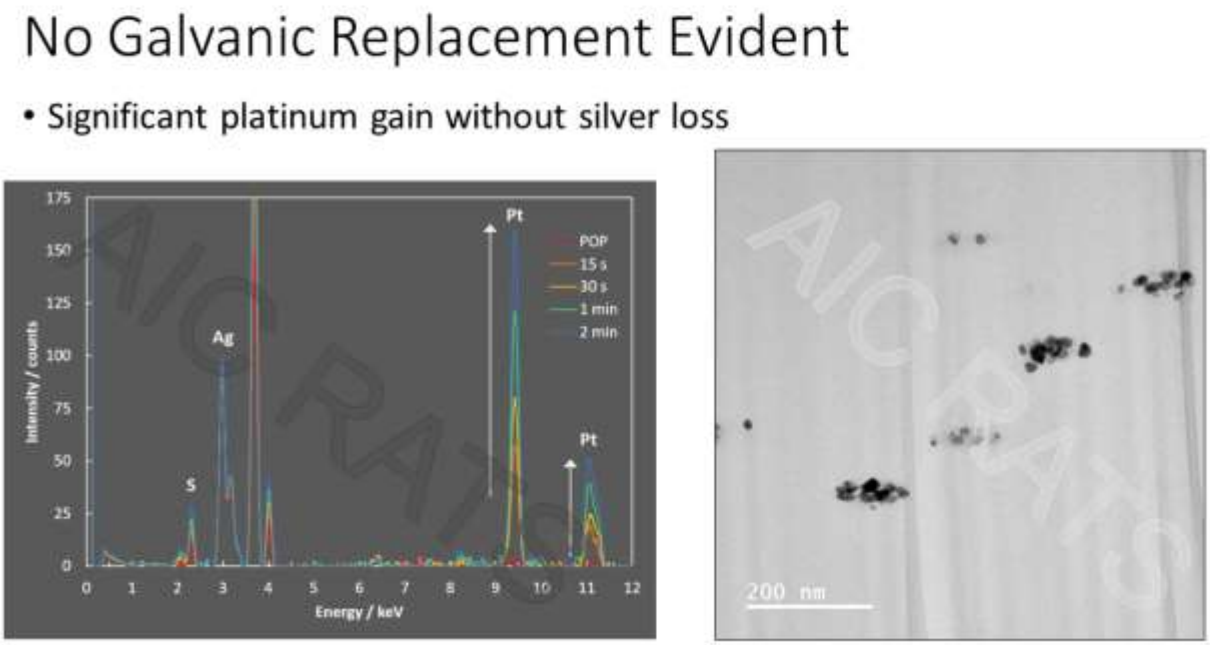

No Galvanic Replacement Evident

- Significant platinum gain without silver loss

In contrast to the alkaline-toned SPP, a significant increase in platinum counts in the XRF spectra is observed for the POP. However, the silver counts remain unchanged, indicating that no galvanic replacement is occurring.

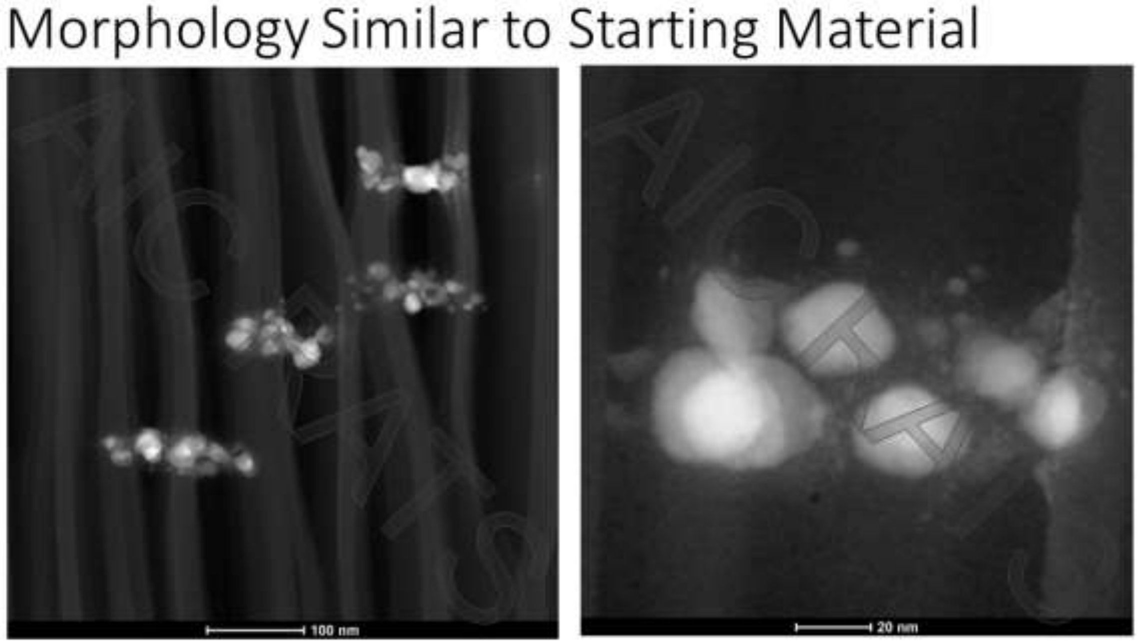

Morphology Similar to Starting Material

The morphology of the image particles confirms that they are not being reshaped by galvanic replacement.

Small Amount of Pt Associated with Ag

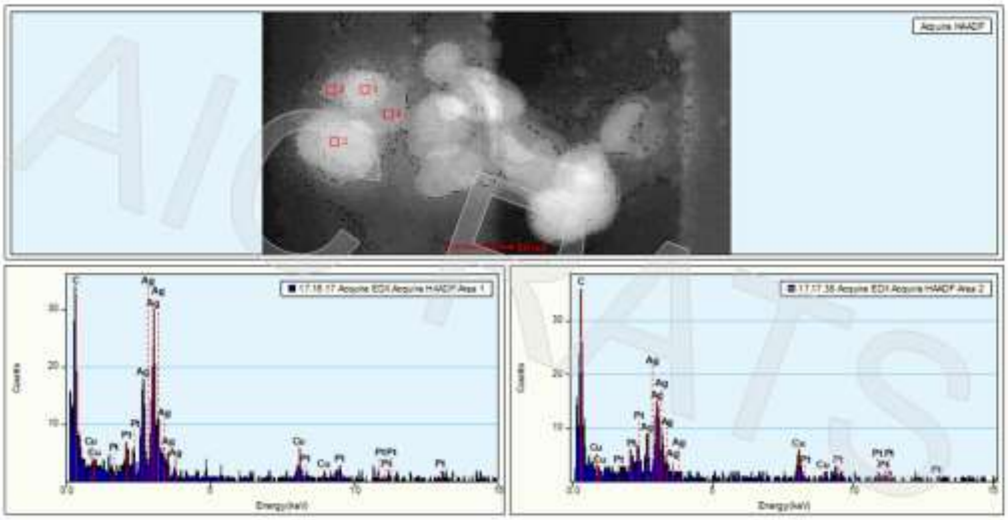

Cu artifact from support grid

In fact, very little platinum is detected in the clusters of image particles. This is in apparent contradiction to the XRF results showing high levels of platinum in these samples.

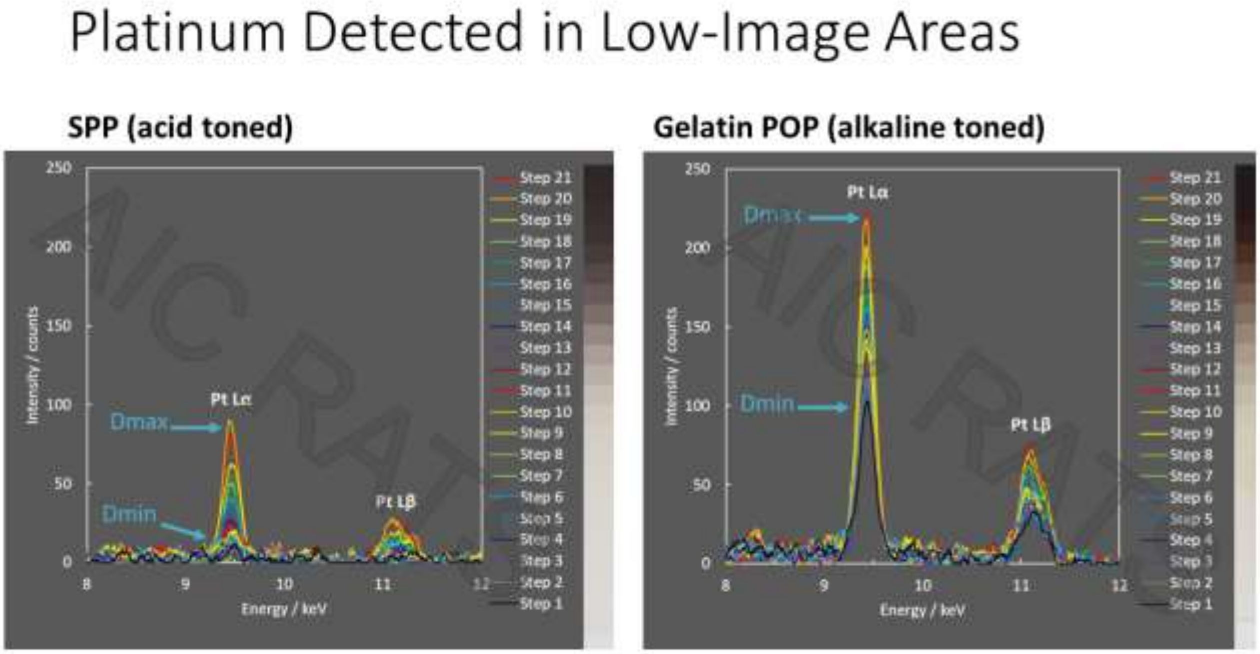

Platinum Detected in Low-Image Areas

SPP (acid toned)

Gelatin POP (alkaline toned)

The XRF data shown previously were acquired at the maximum image density (Dmax, Step 21) end of the step tablet because it is the most metal-rich area of the samples. The intensities of the peaks for platinum (and also for silver, not shown) decrease with decreasing image density; the limit of detection for platinum is reached by step 10 and below in the toned salted paper print. However, the toned gelatin printed-out print samples all show significant amounts of platinum in non-image areas.

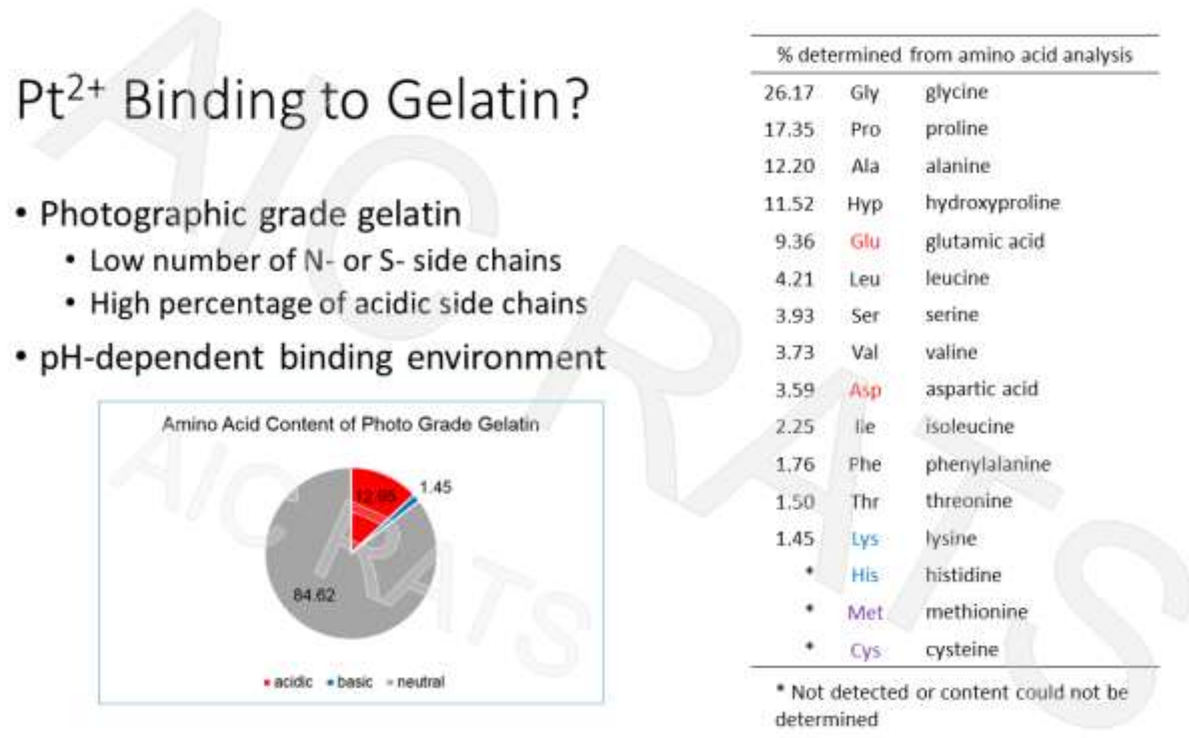

Pt^{2+} Binding to Gelatin?

- Photographic grade gelatin
  - Low number of N- or S- side chains
  - High percentage of acidic side chains
- pH-dependent binding environment

% determined from amino acid analysis		
26.17	Gly	glycine
17.35	Pro	proline
12.20	Ala	alanine
11.52	Hyp	hydroxyproline
9.36	Glu	glutamic acid
4.21	Leu	leucine
3.93	Ser	serine
3.73	Val	valine
3.59	Asp	aspartic acid
2.25	Ile	isoleucine
1.76	Phe	phenylalanine
1.50	Thr	threonine
1.45	Lys	lysine
*	His	histidine
*	Met	methionine
*	Cys	cysteine

* Not detected or content could not be determined

One potential explanation for the high platinum content in the toned samples is non-specific binding or absorption of Pt2+ ions from the toning bath by the gelatin protein. Photographic grade gelatin has very low levels of typical soft-metal binding side chains containing nitrogen or sulfur residues but a relatively high percentage of carboxylic acid groups. If the glutamic or aspartic acid residues are involved in Pt2+ uptake, this would argue for a pH-dependent binding environment.

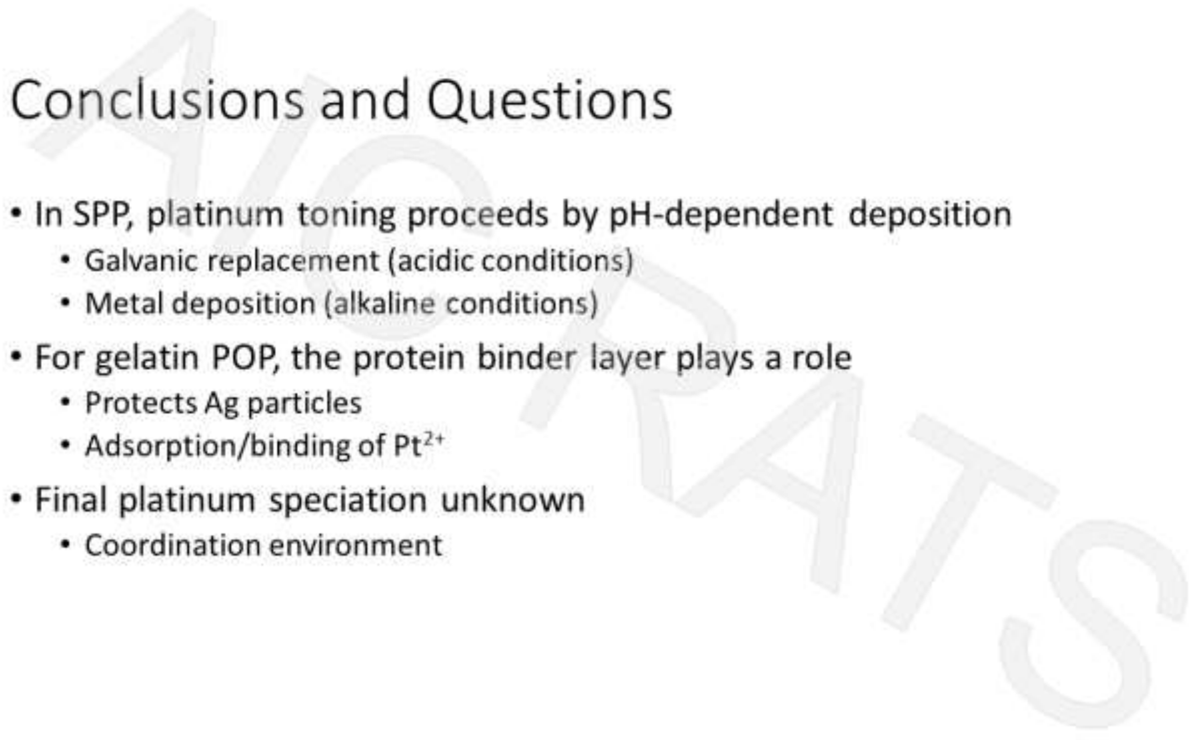

Conclusions and Questions

- In SPP, platinum toning proceeds by pH-dependent deposition
  - Galvanic replacement (acidic conditions)
  - Metal deposition (alkaline conditions)
- For gelatin POP, the protein binder layer plays a role
  - Protects Ag particles
  - Adsorption/binding of Pt^{2+}
- Final platinum speciation unknown
  - Coordination environment

The preliminary results of this study indicate that the toning of silver prints with platinum proceeds by a pH-dependent reaction mechanism. In acidic conditions, silver image particles are sacrificed for platinum reduction by galvanic replacement. For the alkaline case, small amounts of platinum deposit on the image. The presence of a gelatin binder layer further affects the action of the toning bath. Additional research continues to further elucidate the nature of the platinum-protein interaction.

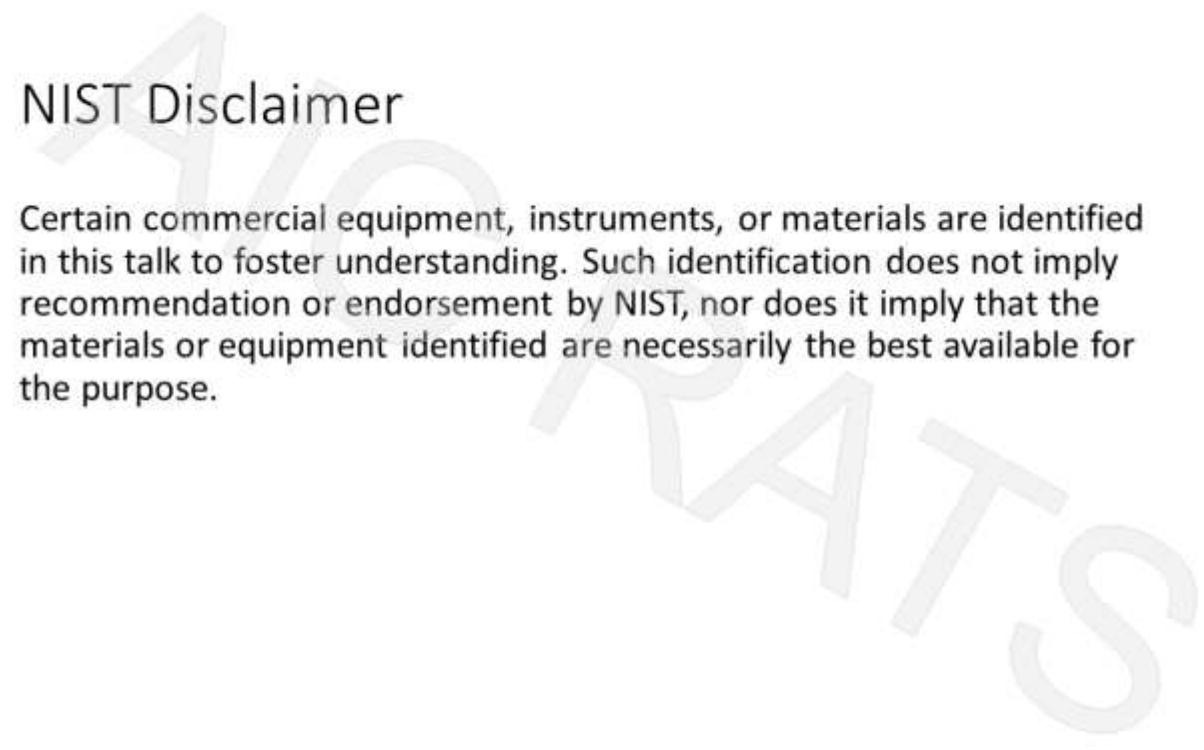

NIST Disclaimer

Certain commercial equipment, instruments, or materials are identified in this talk to foster understanding. Such identification does not imply recommendation or endorsement by NIST, nor does it imply that the materials or equipment identified are necessarily the best available for the purpose.

Effects of Relative Humidity and Temperature on Morphology and Chemical Composition of Debarked Maize Stems

Alfredo Adolfo Ortega-Ordaz, Carlos Cruz-Cárdenas, Emanuel Bojóquez-Quintal, Esteban Sánchez-Rodríguez, Luis Rojas-Abarca, Ángela Ku-González

In New Spain – Mexico today –, maize stem was used in a lightweight sculpting technique that was a synthesis of the Prehispanic and European traditions. These sculptures are mostly made from the stem of the maize plant, with or without bark. The use of stems may have two functions: structural, when the stem is used as the structural core, and volumetric, when it is used as a modeling paste (milled maize stem agglutinated with animal glue). Despite the importance of maize stem sculptures in Latin America and Spain, little is known about its degradation mechanisms and appropriate methods for their conservation. Therefore, this research determines the effects of different relative humidity and temperature treatments on morphology and chemical composition of the debarked maize stems. Also, dissociated and naturally aged samples from a New Spain sculpture were analyzed and compared with the treatments results. The maize stems treated samples were classified into lower and upper sections according to the distance from the root plant, while the New Spain samples were obtained from a New Spain temple in Michoacán, México. The samples underwent nine treatments: T1 (25%RH/25°C), T2 (25%RH/50°C), T3 (25%RH/75°C), T4 [control] (50%RH/25°C), T5 (50%RH/50°C), T6 (50 %RH/75°C), T7 (75%RH/25°C), T8 (75%RH/50°C) and T9 (75%RH/75°C). Morphology was determined using SEM and histochemical staining methods applying toluidine, safranine and phloroglucinol-HCl. For chemical characterization, cellulose and hemicellulose content was determined by sodium chlorite method, while lignin was quantified according to the Klason method. In addition, FTIR-ATR spectroscopy was used for identification of chemical groups. The chemical characterization shows that the upper section stems have a higher hemicellulose content than the lower section and that the higher temperatures decrease the percent of this component, such effect is aggravated by increasing the relative humidity, even beginning to affect cellulose. By morphological characterization, it was observed that the lower section stems tissues are weaker and as the hemicellulose decreases, the non-lignified cell walls become more susceptible to deformations and ruptures, mainly in parenchyma and phloem. For FTIR-ATR spectroscopy, it was identified that the higher parameters of relative humidity and temperature decrease the transmittance of the signal 1736 cm-1 that is related with stretching vibrations in the C=O alkyl-ester bonds that form the hemicellulose and pectin of the cell walls. In addition, the New Spain samples characterization determined a drastic low hemicellulose and cellulose percentage supporting the treatments results. The principal contributions of this study are the identification of the more vulnerable structural components in the maize stems, provide different methods to diagnose their degradation degree, and recognize the riskier relative humidity and temperature treatments, these allows to improve and develop accurate preventive and conservation methods. In further studies, mechanical resistance of the treated samples will be tested and compared with thus far obtained results.

Examination of Metal Soap Efflorescence on Selected Oil-On-Canvas Studies by Edwin Austin Abbey

Richard R. Hark, Aniko Bezur, Cynthia Schwarz, Katherine Schilling, Kelsey Wingel, Pablo Londero

Edwin Austin Abbey (1852-1911) was an American painter and a prominent illustrator who was born in Philadelphia, Pennsylvania but moved to England in his early thirties. His works include murals for the Boston Public Library and the Pennsylvania State Capitol Building in Harrisburg. He also received the royal commission to paint the coronation of King Edward VII of England. The Yale University Art Gallery (YUAG) collection holds over 600 oil paintings by Abbey. Many are unvarnished or selectively varnished preparatory studies for larger compositions and over half exhibit surface efflorescence. The presence and formation of efflorescence vary within the collection: on some paintings, efflorescence appears in amorphous, apparently random patches while, on other works, it correlates to form, color, or varnishes selectively applied by the artist. This research, initiated to inform conservation treatments in preparation for an upcoming exhibition, aims to identify the morphology and composition of the efflorescence while examining its relationship to both the locally applied varnishes and the materials within the stratigraphy of several paintings executed as part of Abbey's preparation for his Harrisburg commission. Efflorescence, ground layer, and paint samples from several of Abbey's oil-on-canvas studies were analyzed with visible and ultraviolet light microscopy, Fourier transform infrared spectroscopy (FTIR), field emission scanning electron microscopy/energy dispersive spectroscopy (FE-SEM/EDS), gas chromatography-mass spectrometry (GC/MS), portable x-ray fluorescence spectroscopy (pXRF), and macro x-ray fluorescence spectroscopy (MA-XRF). For example, FE-SEM analysis of surface samples removed from Abbey's The Spirit of Light (226.7 x 64.5 cm) revealed that the efflorescence appears as plate-like structures (1-2 microns wide and less than 1 micron thick) on the surface of the painting, and EDS showed that the efflorescence is composed primarily of carbon and zinc. FTIR analysis of these samples suggested that the efflorescence was composed of zinc soaps while GC/MS confirmed that the efflorescence contains metal carboxylates and free fatty acids (azelate, palmitate, and stearate). EDS analysis of a cross-section indicated the presence of a double ground containing layers of calcium carbonate and zinc sulfide/barium sulfate. MA-XRF element maps of the entire work were also obtained to see if the location of the efflorescence correlates with particular pigments. Our results for this painting and three studies for the large mural The Passage of the Hours will be presented along with possible explanations for the formation of efflorescence.

Glass Analysis Combining Elemental Imaging from Nanometer to Centimeter Scale with Quantitative Bulk Analysis: Characterizing a Carchesium with Silver Stain Enamel

Pablo Londero, Aniko Bezur, Brian McIntyre, Elena Torok, Nicholas Bigelow, Patrick Degryse, Ralph Wiegandt

Silver stain luster and enameling of glass from the Syro-Palestine area is known to be critical for understanding the development of silver staining techniques. However, given the material complexity of objects possessing these features, they can be challenging to characterize. Key features must be understood at the nanometer (silver nanoparticles), micrometer (nanoparticle distribution and luster/enamel thickness), and bulk (base glass composition) scales. Consequently, there are relatively few studies of such breadth. This paper details a technical study that combines nano, micro, and macro material imaging techniques, as well as bulk quantitative analysis to elucidate the nature of a glass carchesium with hand-painted enamel decoration that was suspected to be a 1st c. Roman vessel at the time of acquisition. A variety of imaging techniques were combined with bulk analysis to characterize the object, including transmission electron microscopy (TEM), scanning electron microscopy with energy dispersive spectroscopy (SEM-EDS), imaging and bulk XRF measurements, strontium isotope analysis by multi-collector inductively coupled plasma mass spectrometry (MC-ICP-MS), and inductively coupled plasma optical emission spectroscopy (ICP-OES). The carchesium was purchased in 1922 from New York dealer Fahim Kouchakji by Mrs. William H. Moore, who donated it to the Yale University Art Gallery in 1955. At the time of purchase the object was suspected to be 1st century Roman based on form, blue glass body, olive branch decorative elements, and splash glass decorative elements. The object, which recently underwent conservation treatment and was studied during that time, is significantly corroded in a manner consistent with a burial environment. Microscopic examination revealed that the decorative material was inset in the glass, with a layered structure consisting of alternating orange-brown and blue-green bands. Initial XRF point- and imaging-based measurements showed that the decorative enameling contained silver, and no other element that could easily explain the coloring. SEM/EDS and TEM measurements revealed the presence of silver nanoparticles and characterized their depth-dependent size and shape. Strontium isotope analysis suggested the lime was derived from a calcareous sand deposit rather than limestone. Quantitative XRF and ICP-OES measurements reveal a soda-lime base glass and an overall composition more consistent with Roman glass made in the Syro-Palestine area during the fourth to eight centuries. Work is ongoing to characterize the glass in the enamel layers quantitatively and model light-matter interactions with the nanoparticles to confirm they are responsible for the observed coloring. Additional future efforts will focus on the location of potentially similar objects in other collections.

Hyperspectral Imaging on the Microscopic Scale: Challenges and Successes of Instrument Design for Materials Characterization

Lindsay Oakley, Marc Sebastian Walton, Victoria Cooley

Hyperspectral imaging has become an increasingly ubiquitous tool for the technical study of cultural heritage objects. It has been used to non-invasively characterize pigments and binding media on painted surfaces, as well as a variety of other object types from manuscripts to wood, over a wide field of view. However, the interpretation of hyperspectral data cubes can be complicated by the nonlinear mixing response of two or more colorants present below the resolution limits of the camera. Consequently, complimentary point analysis techniques, such as Raman or FTIR spectroscopy, are usually employed to obtain ground truth detailed material information. When possible, samples are removed and mounted in resin for further elemental and molecular characterization. However, some challenges are encountered with traditional analytical techniques when used to map molecular phases in these samples, notably the contaminating fluorescence background which can swamp the signal in Raman microspectrometry or the low signal-to-noise ratio in FTIR which can necessitate long integration times prohibitive for imaging. Avoiding these obstacles, a hyperspectral imaging technique with high spatial resolution would offer advantages for characterizing at the sub-micron range, with little additional sample prep or need to access more expensive equipment such as electron microscopy. As of yet, hyperspectral microscope configurations are rarely applied outside of the biological sciences. However, a recent hyperspectral optical microscopy experiment demonstrated excellent spatial resolution for the detection of single silver nanoparticles down to 100 nm diameters using a high numerical aperture objective, indicating the technique's potential for material studies across many disciplines. This work presents the design and development of a simple dark field, reflectance hyperspectral microscope system for the purpose of extracting high spatially- and spectrally-resolved information, particularly for pigmented samples. Using a tunable light source to illuminate monochromatically over a range of visible to Near Infrared wavelengths, diffusely reflected light was collected with a long working distance, 20x objective. The challenges of fully automating and mechanizing the experimental construction of the hyperspectral data cube will be discussed as well as best practices determined for normalizing the acquired reflectance spectra as the surface texture of reflectance standards can become problematic under magnification. The developed microscope was used to characterize the pigment distribution in the stratigraphy of painting cross sections as well as other materials systems such as red opaque glass.

Normalized Peak Area Distributions with HPLC-DAD-MS as a Tool for Differentiating Madder and Cochineal Lakes in Easel Paintings

Jing Han*[1], Beatriz Fonseca[2], Monica Ganio[3], Douglas MacLennan[4], Michael R. Schilling[5]

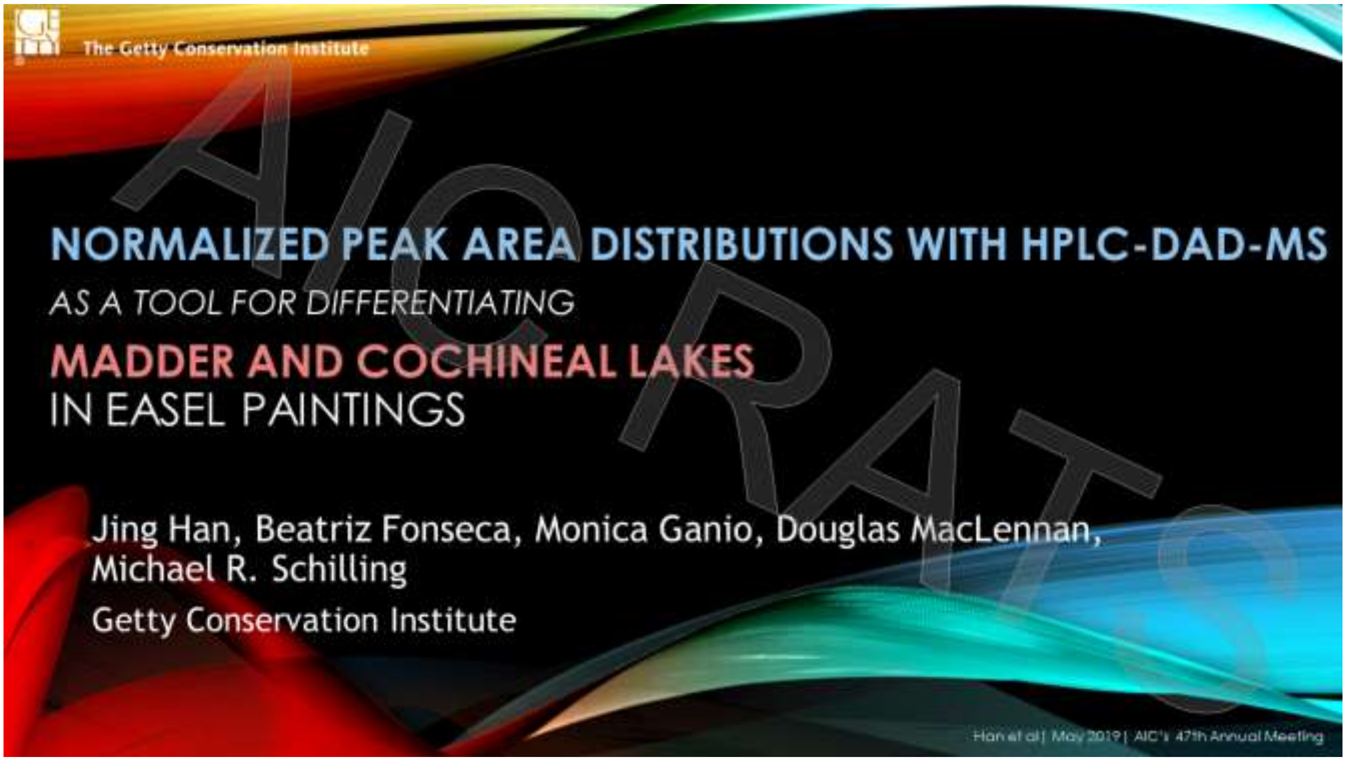

The Getty Conservation Institute

NORMALIZED PEAK AREA DISTRIBUTIONS WITH HPLC-DAD-MS

AS A TOOL FOR DIFFERENTIATING

MADDER AND COCHINEAL LAKES

IN EASEL PAINTINGS

Jing Han, Beatriz Fonseca, Monica Ganio, Douglas MacLennan,
Michael R. Schilling

Getty Conservation Institute

Han et al | May 2019 | AIC's 47th Annual Meeting

1 Professional Fellow, Getty Conservation Institute
2 Graduate Intern, Getty Conservation Institute
3 Assistant Scientist, Getty Conservation Institute
4 Research Lab Associate, Getty Conservation Institute
5 Senior Scientist, Getty Conservation Institute

Presented at the RATS session
47th Annual Meeting of
The American Institute for Conservation of Historic and Artistic Works (AIC)
Mohegan Sun , Uncasville, Connecticut, May13-17, 2019

Contact information

*jihan@getty.edu, jinghan8706@hotmail.com

1200 Getty Center Drive, Los Angeles 90049, CA

Abstract

Historically, organic dyestuffs played an important role not only in coloring textiles but also in producing lake pigments for paintings. The dye sources and recipes of organic lake pigments varied based on the geographical regions and time periods of production. The ability to identify the dye composition in lake pigments provides important information about their source and even the manufacturing techniques used to prepare the pigment. This paper presents the results of novel research on the dye composition of madder and cochineal pigments prepared in different binding media following historical recipes as well as from unknown samples removed from paintings using high performance liquid chromatography coupled with diode array detection and mass spectrometry.

Results show that extraction using a solution of 4% boron trifluoride in methanol is more suitable than extraction with oxalic acid and hydrochloric acid solutions. By this method, the bonds between dye molecules and the surrounding organic binding media are broken up effectively, while glycosidic bonds are preserved. Mass spectrometer detector provides a much clearer separation of co-eluting components than detection by diode array detector, which facilitates study of the individual dyestuffs. Results of normalized peak area distributions are reproducible and the amount of sample analyzed or the presence of binding media has limited influence on the results, except for oil, but a smaller amount of sample of pigments painted with oil helps. Different pigment recipes and dye sources result in variability in normalized peak area distributions. Results of historical samples show characteristics in normalized peak area distributions, but the small sample amount makes it difficult to draw conclusions on dye sources and recipes.

To the best of our knowledge the first comprehensive protocol for the composition of organic dyes in paintings is established. This protocol constitutes a solid foundation for further study on the diverse sources, methods of lake production, and preservation of organic dyes in easel paintings.

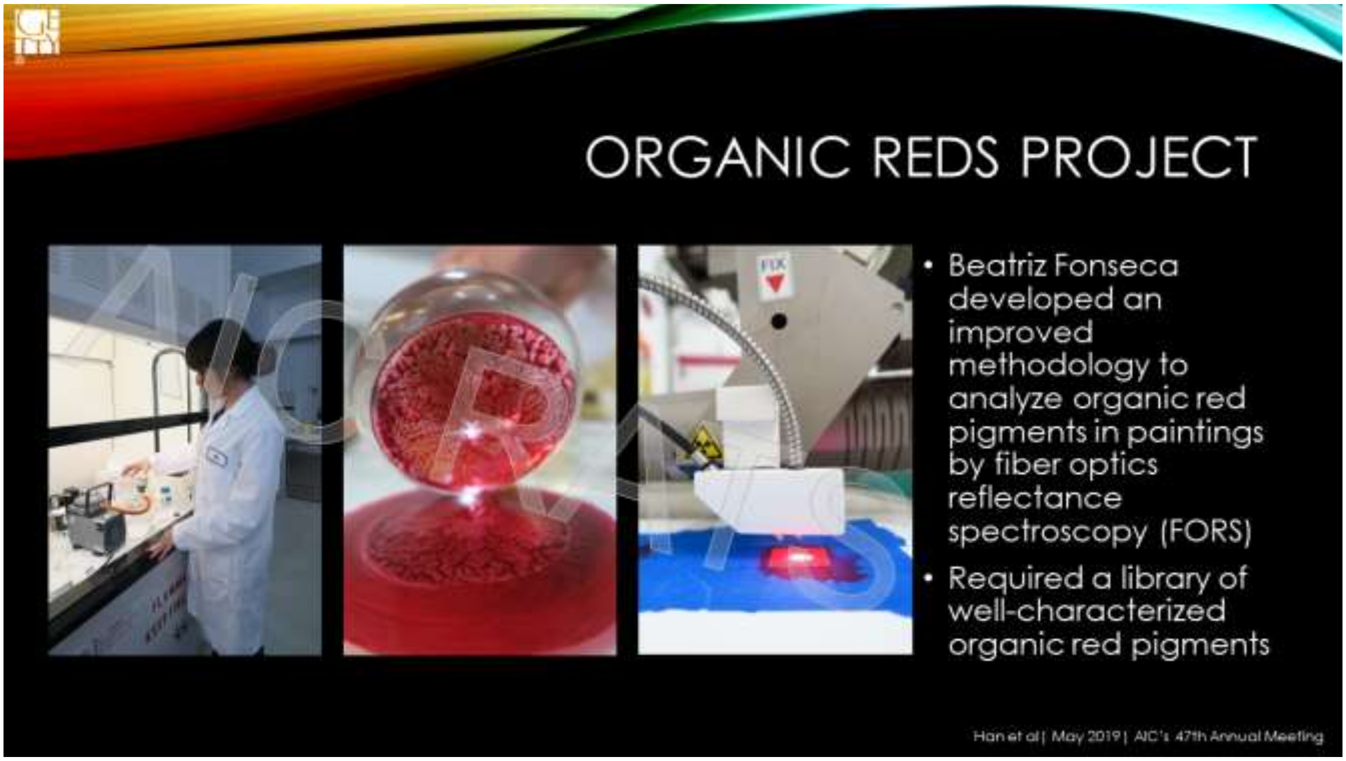

ORGANIC REDS PROJECT

- Beatriz Fonseca developed an improved methodology to analyze organic red pigments in paintings by fiber optics reflectance spectroscopy (FORS)
- Required a library of well-characterized organic red pigments

Han et al | May 2019 | AIC's 47th Annual Meeting

The research presented in this talk is part of Organic Reds project which aims to analyze organic red pigments in paintings by Fiber Optic Reflectance Spectroscopy (FORS). The analytical protocol presented in this talk is used for the characterization of dye components in the pigments and painting samples in order to provide support to the FORS analyses.

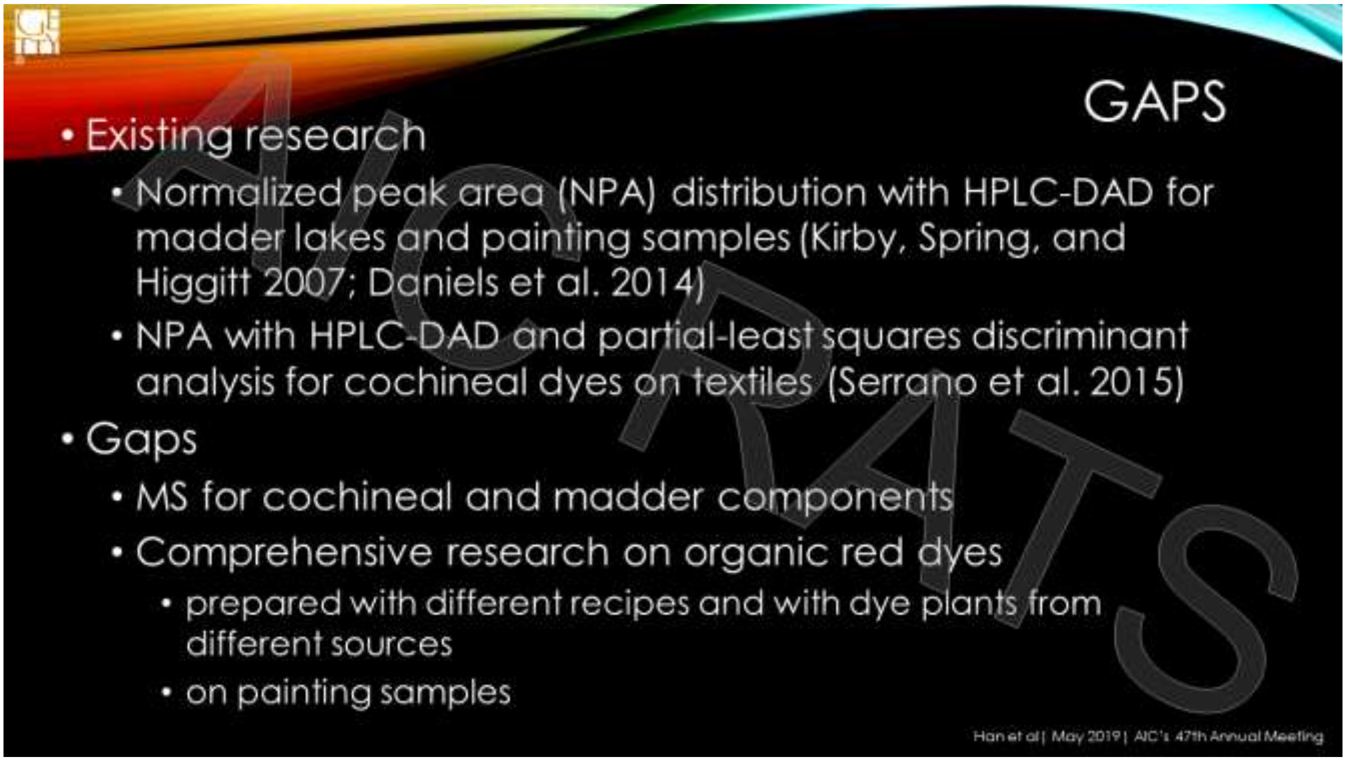

GAPS

- Existing research
  - Normalized peak area (NPA) distribution with HPLC-DAD for madder lakes and painting samples (Kirby, Spring, and Higgitt 2007; Daniels et al. 2014)
  - NPA with HPLC-DAD and partial-least squares discriminant analysis for cochineal dyes on textiles (Serrano et al. 2015)
- Gaps
  - MS for cochineal and madder components
  - Comprehensive research on organic red dyes
    - prepared with different recipes and with dye plants from different sources
    - on painting samples

Han et al| May 2019| AIC's 47th Annual Meeting

This research involves novel application of a MS detector coupled with LC-DAD for normalized peak area (NPA) studies. A wide range of pigments and painting samples made from madder and cochineal are studied.

MATERIALS

- 8 cochineal recipes
- 9 madder recipes for madder
  - Kremer Pigmente
  - Locally grown madder
- Different substrates: alumina, Ca containing alumina, metal complexes of Sn and Al.
- Reuse of dyed fleece (wool) and silk

(Kirby, van Bommel, and Verhecken 2014)

Han et al | May 2019 | AIC's 47th Annual Meeting


The Getty Conservation Institute

1. METHOD DEVELOPMENT

Han et al | May 2019 | AIC's 47th Annual Meeting

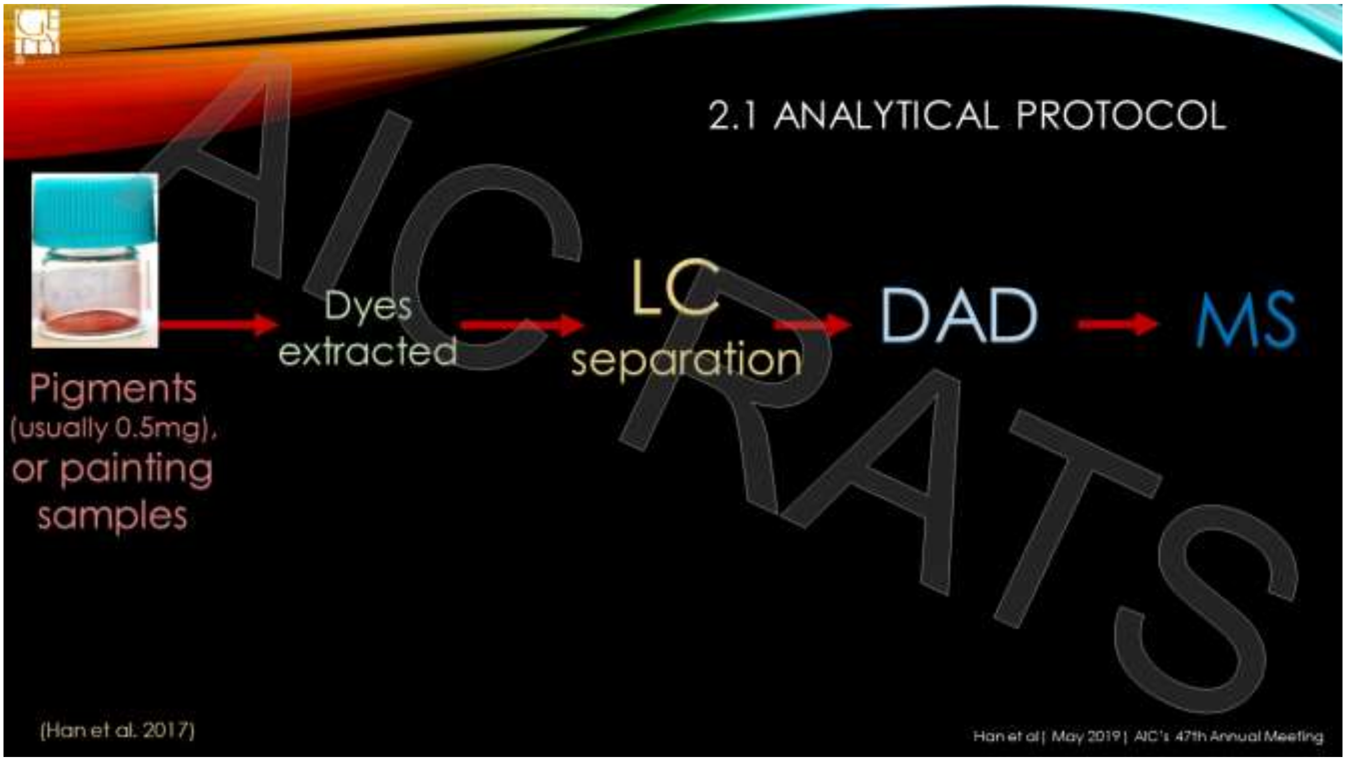

2.1 ANALYTICAL PROTOCOL

Pigments (usually 0.5mg), or painting samples → Dyes extracted → LC separation → DAD → MS

(Han et al. 2017)

Han et al | May 2019 | AIC's 47th Annual Meeting

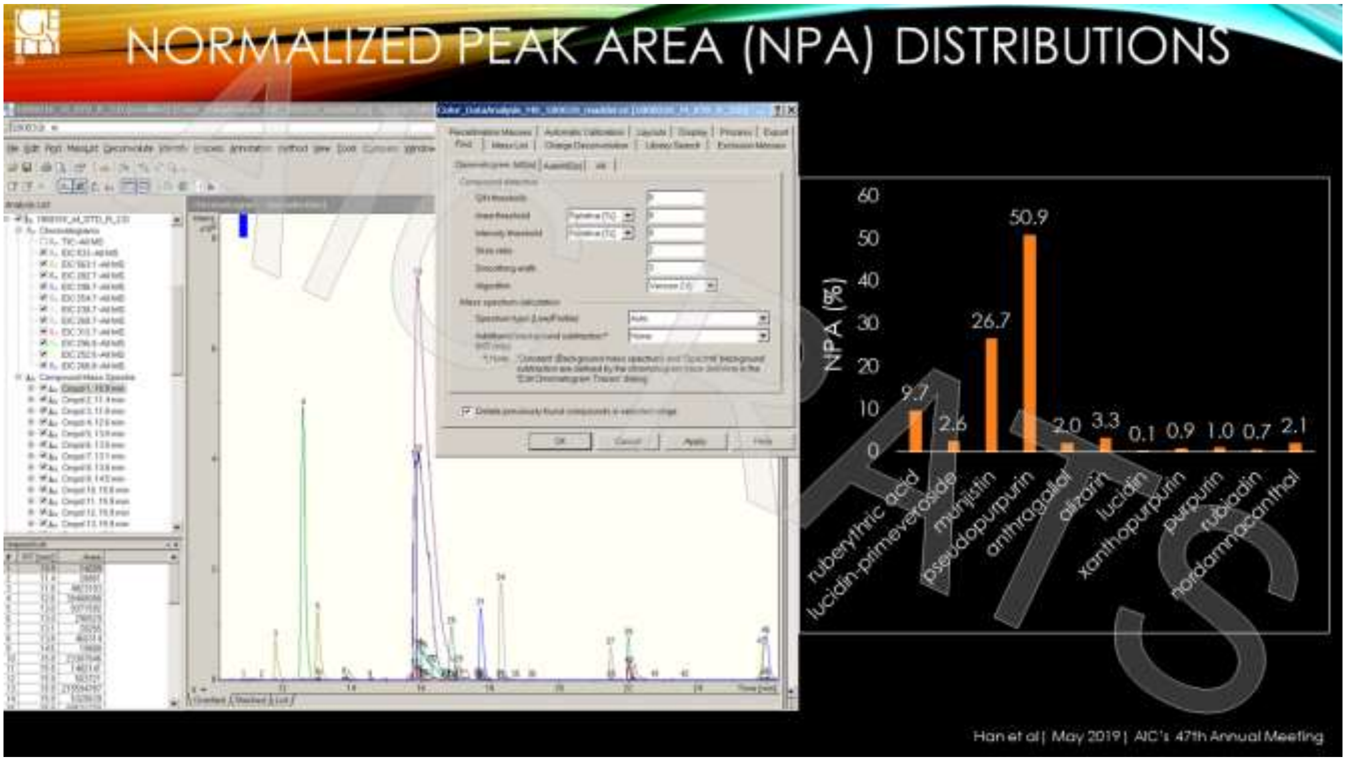
NORMALIZED PEAK AREA (NPA) DISTRIBUTIONS

Han et al| May 2019| AIC's 47th Annual Meeting

Each peak in the chromatogram stands for a component. Peak areas of the dye components are calculated by the instrument software, then normalized and presented in a bar graph. Each bar shows the normalized peak area (also known as relative peak area) of a dye component.

The NPA distributions obtained mainly indicate differences in the relative amount of the same dye between samples, rather than the relative amount of different dyes in individual samples or their absolute amounts. The latter two depends on other factors including the extraction efficiency and instrument response factor of individual dyes. For example, the bar graph does NOT indicate there is a higher amount of pseudopurpurin than munjistin in this sample.

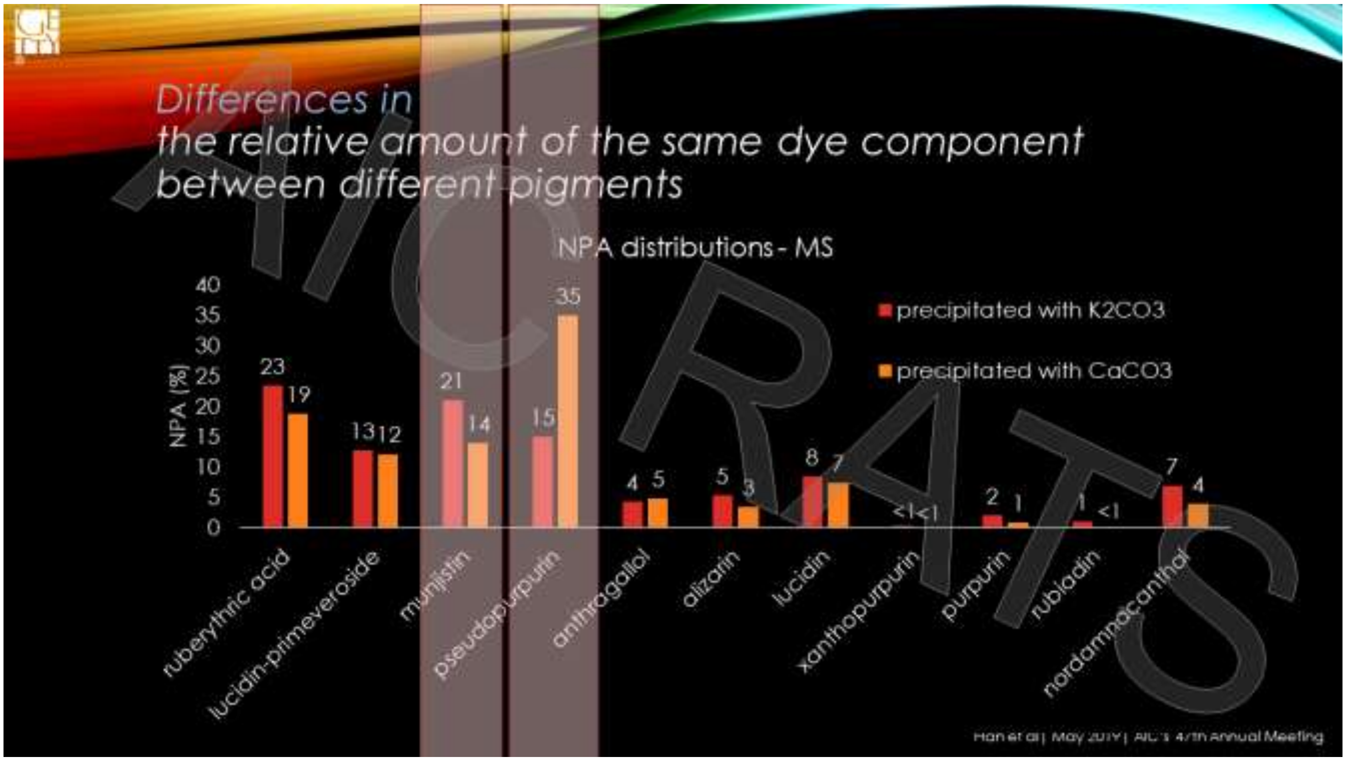

Differences in
the relative amount of the same dye component
between different pigments

Han et al | May 2019 | AIC's 47th Annual Meeting

NPA distribution graphs make more sense when two or more samples are compared with each other. Comparing these 2 samples, we can say in the first sample there is higher relative amount of munjistin and lower relative amount of pseudopurpurin. In the first sample there are also higher amounts of ruberythric acid and several other dye components.

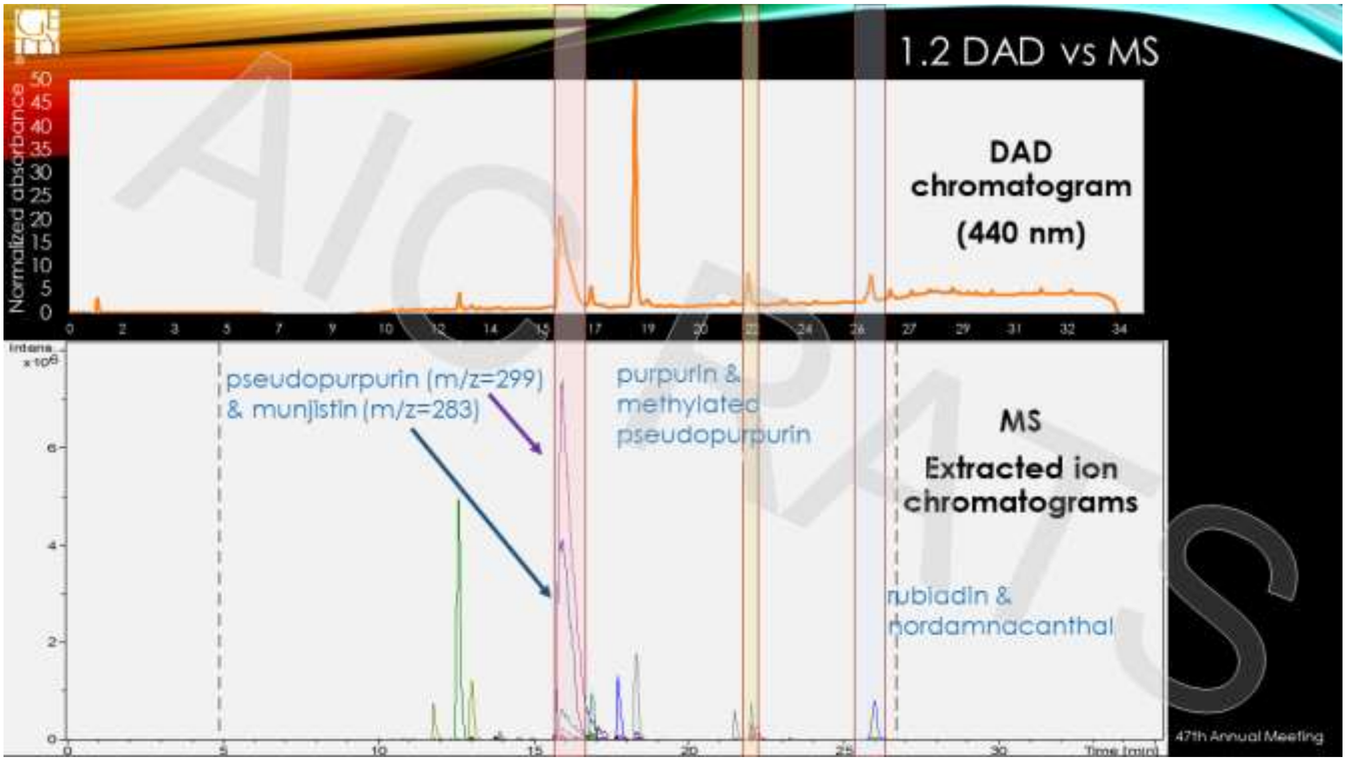

1.2 DAD vs MS

DAD chromatogram (440 nm)

MS Extracted ion chromatograms

MS has a main advantage over DAD in that MS facilitates the study of individual dye components in the case of co-elution by calculating the area of individual mass-to-charge ratio peaks. Co-eluting dye component pairs include munjistin and pseudopurpurin, purpurin and methylated pseudopurpurin, rubiadin and nordamnacanthal (the above are madder dyes), and flavokermesic acid and kermesic acid (these are cochineal dyes). It is difficult to separate some of the co-eluting pairs with usual LC conditions. As the co-eluting dye component pairs are often also of similar spectral characteristics and can not be separated in DAD chromatograms, the peak areas of the two components have to be calculated together as a whole, inevitably resulting in the loss of important information.

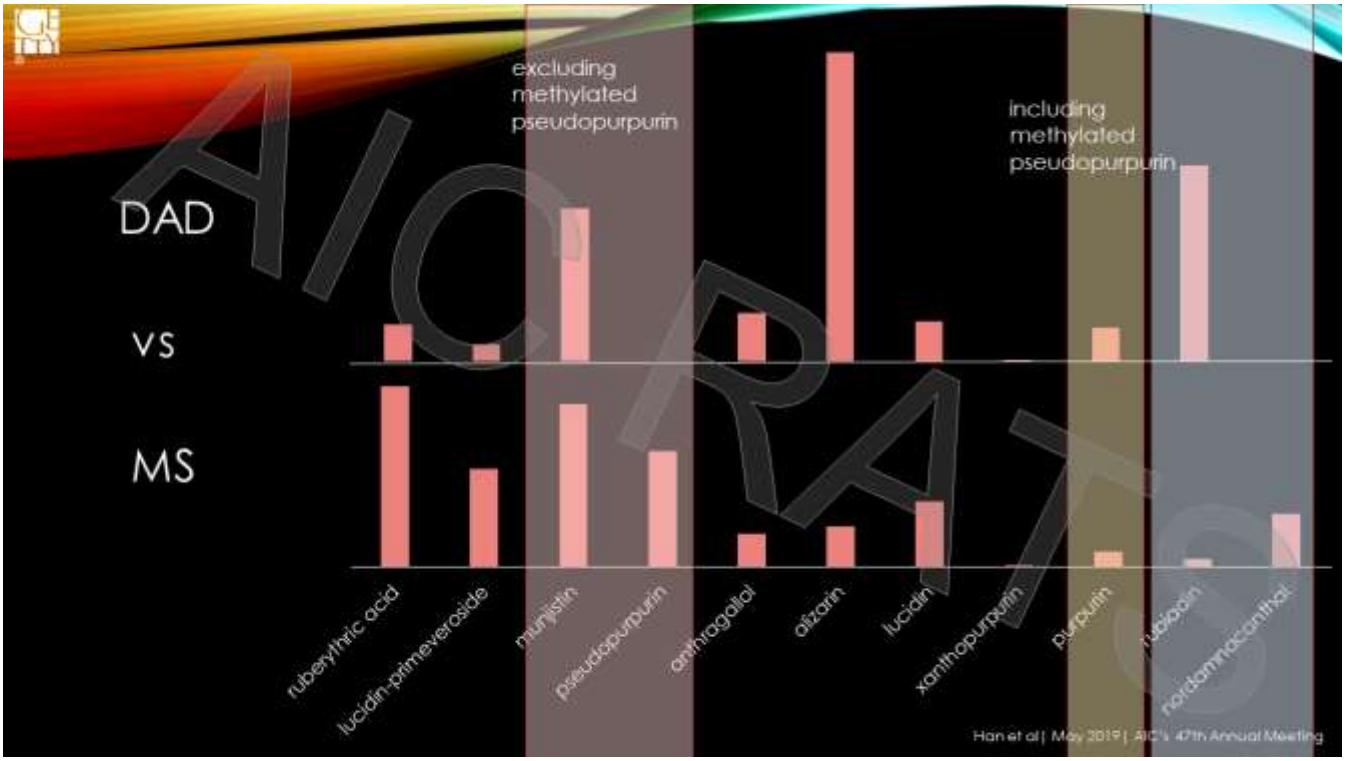

Han et al | May 2019 | AIC's 47th Annual Meeting

The DAD peak areas of the co-eluting components have to be calculated together as a whole.

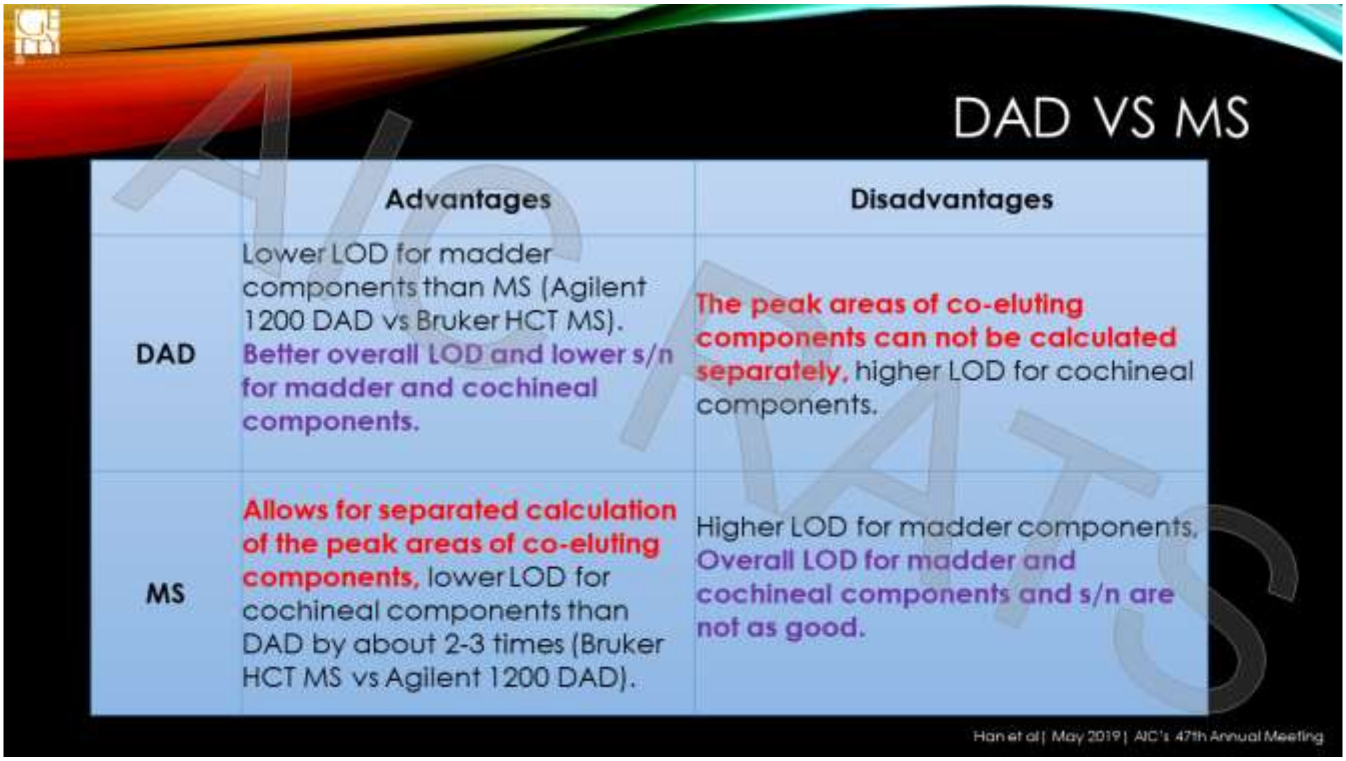

DAD VS MS

	Advantages	Disadvantages
DAD	Lower LOD for madder components than MS (Agilent 1200 DAD vs Bruker HCT MS). **Better overall LOD and lower s/n for madder and cochineal components.**	**The peak areas of co-eluting components can not be calculated separately,** higher LOD for cochineal components.
MS	**Allows for separated calculation of the peak areas of co-eluting components,** lower LOD for cochineal components than DAD by about 2-3 times (Bruker HCT MS vs Agilent 1200 DAD).	Higher LOD for madder components. **Overall LOD for madder and cochineal components and s/n are not as good.**

Han et al| May 2019| AIC's 47th Annual Meeting

Therefore, NPA distributions with MS were chosen to analyze the reference samples. It is to be noted that DAD has overall lower detection limit and signal-to-noise ratio for madder and cochineal components, therefore more suitable for the identification of dye components of small amounts.

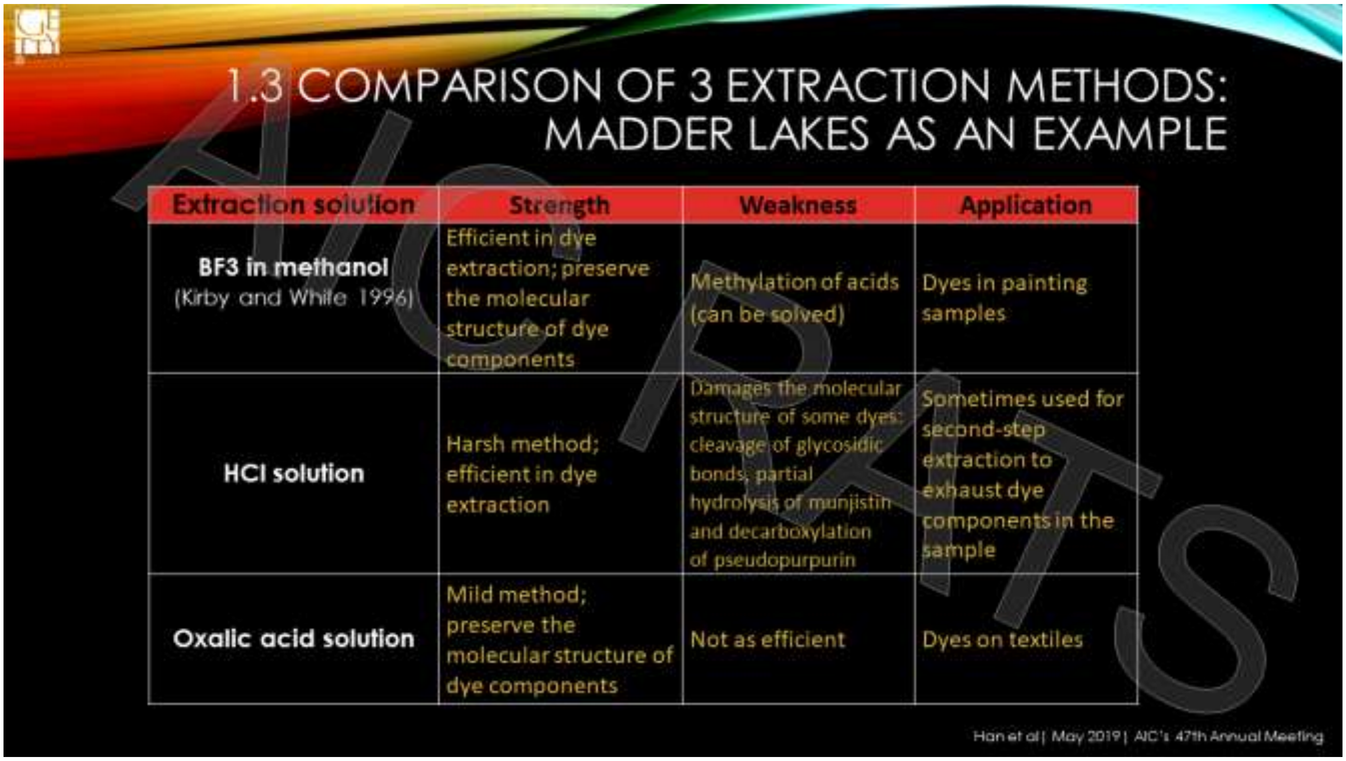

1.3 COMPARISON OF 3 EXTRACTION METHODS: MADDER LAKES AS AN EXAMPLE

Extraction solution	Strength	Weakness	Application
BF3 in methanol (Kirby and White 1996)	Efficient in dye extraction; preserve the molecular structure of dye components	Methylation of acids (can be solved)	Dyes in painting samples
HCl solution	Harsh method; efficient in dye extraction	Damages the molecular structure of some dyes: cleavage of glycosidic bonds, partial hydrolysis of munjistin and decarboxylation of pseudopurpurin	Sometimes used for second-step extraction to exhaust dye components in the sample
Oxalic acid solution	Mild method; preserve the molecular structure of dye components	Not as efficient	Dyes on textiles

Han et al | May 2019 | AIC's 47th Annual Meeting

BF3 solution was chosen to extract dyes from the pigment and painting samples in this study. Details are shown in the table. For historical samples of very small amounts, a second-step extraction with HCl solution was sometimes applied to the sample residue after extraction with BF3 solution.

Details of extraction with BF3 solution:

A sample was placed in an Agilent vial with a 300 µL fixed insert (5188-6591). 6 µl 4% boron trifluoride / methanol was added into the vial. The vial was agitated for 10 mins in a Branson 1510 ultrasonic bath and left overnight at room temperature. An additional of 10 µl reagent was added the following morning to dilute the concentrated dye solution to avoid overloading the LC column. The vial was shaken gently and agitated for 5 mins in the ultrasonic bath to disperse the dye components evenly in the solution, and then centrifuged with an IEC Clinical centrifuge (International Equipment Co.) at speed 7 for 20 mins to precipitate the particulates. The supernatant (about 6-8 µl) was carefully drawn up by a micropipette with observation through a magnifier to avoid drawing up fine particulates, and then transferred into another Agilent vial of the same kind for HPLC-DAD-MS analyses.

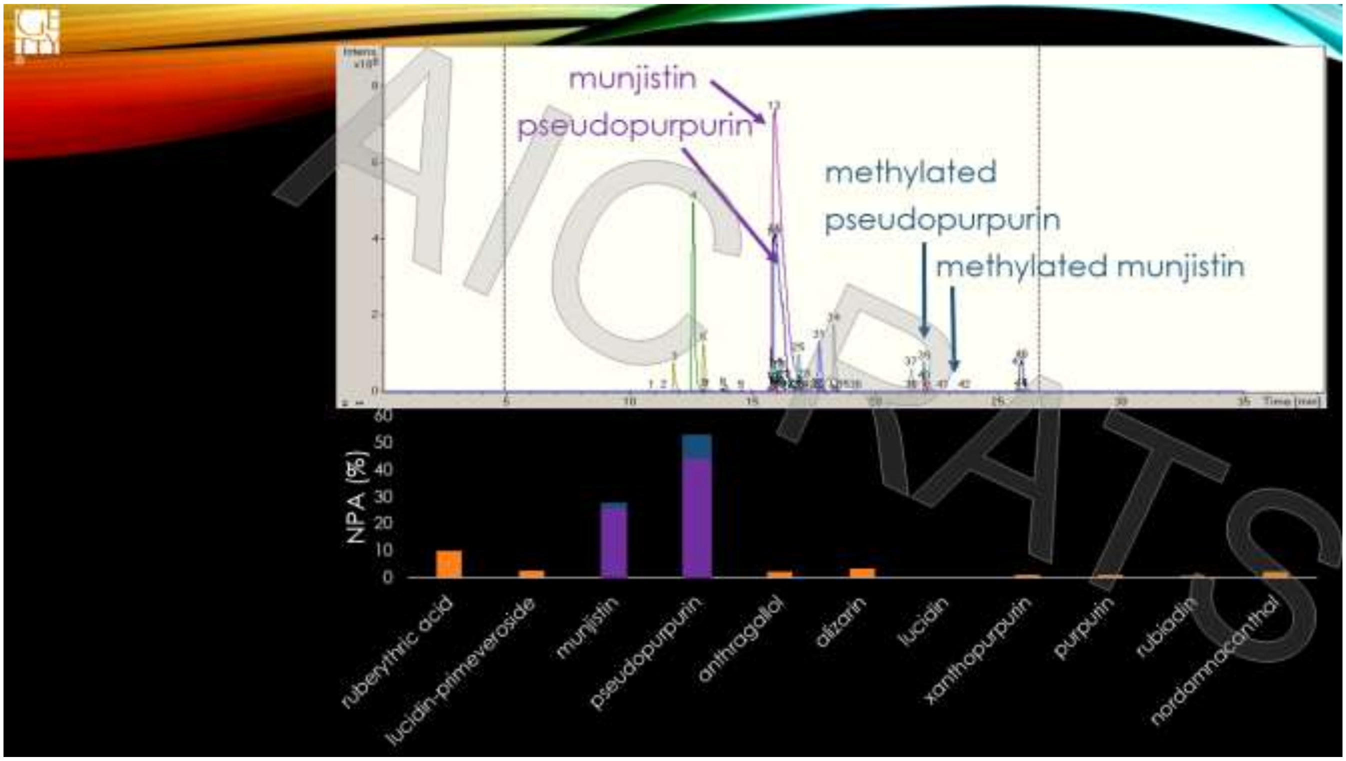

Acid components are partially methylated during BF3 extraction, shown in the chromatogram as two peaks – respectively the original acid component and its methylated component. The peak areas were added together.

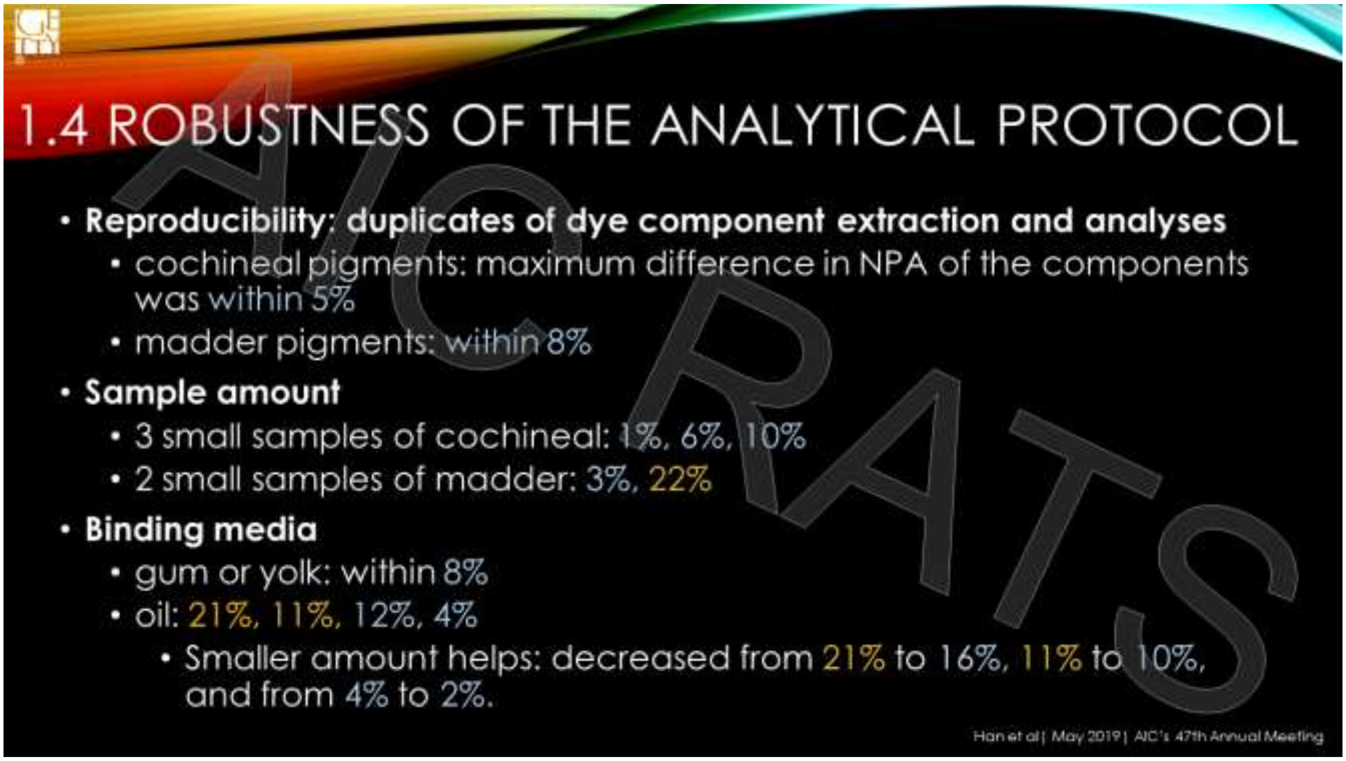

1.4 ROBUSTNESS OF THE ANALYTICAL PROTOCOL

- **Reproducibility: duplicates of dye component extraction and analyses**
  - cochineal pigments: maximum difference in NPA of the components was within 5%
  - madder pigments: within 8%
- **Sample amount**
  - 3 small samples of cochineal: 1%, 6%, 10%
  - 2 small samples of madder: 3%, 22%
- **Binding media**
  - gum or yolk: within 8%
  - oil: 21%, 11%, 12%, 4%
    - Smaller amount helps: decreased from 21% to 16%, 11% to 10%, and from 4% to 2%.

Han et al | May 2019 | AIC's 47th Annual Meeting

The variabilities of results in terms of reproducibility and different samples amounts mainly come from variations in samples, sampling, pretreatment process, instrumentation, lab conditions, computational analyzes, etc. Oil as binding media has a larger impact on NPA distributions, probably due to disturbance of dye extraction by reaction between oil components and the BF3/methanol solution during extraction, as well as ion suppression during ionization, but a smaller sample helps. Overall, in most cases the variability of results is within 10%

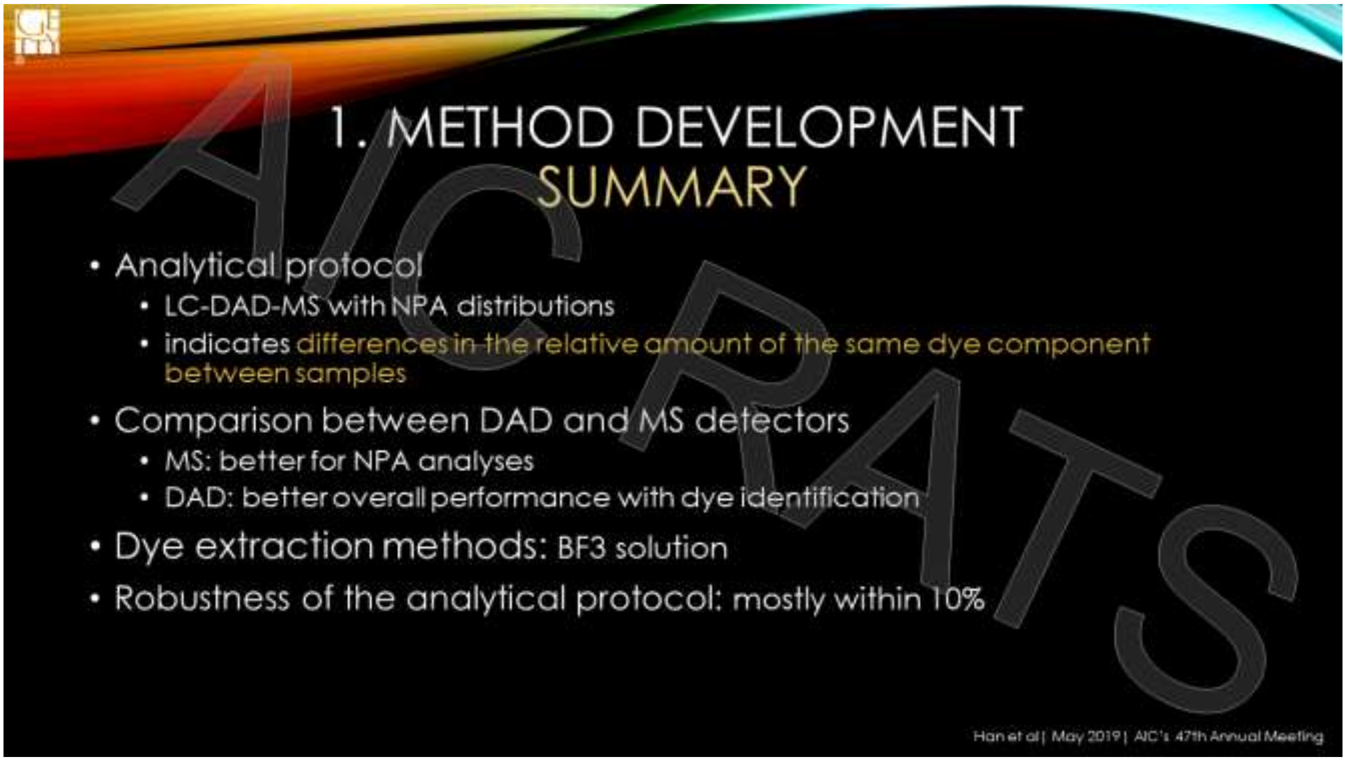

1. METHOD DEVELOPMENT
SUMMARY

- Analytical protocol
  - LC-DAD-MS with NPA distributions
  - indicates differences in the relative amount of the same dye component between samples
- Comparison between DAD and MS detectors
  - MS: better for NPA analyses
  - DAD: better overall performance with dye identification
- Dye extraction methods: BF3 solution
- Robustness of the analytical protocol: mostly within 10%

Han et al | May 2019 | AIC's 47th Annual Meeting

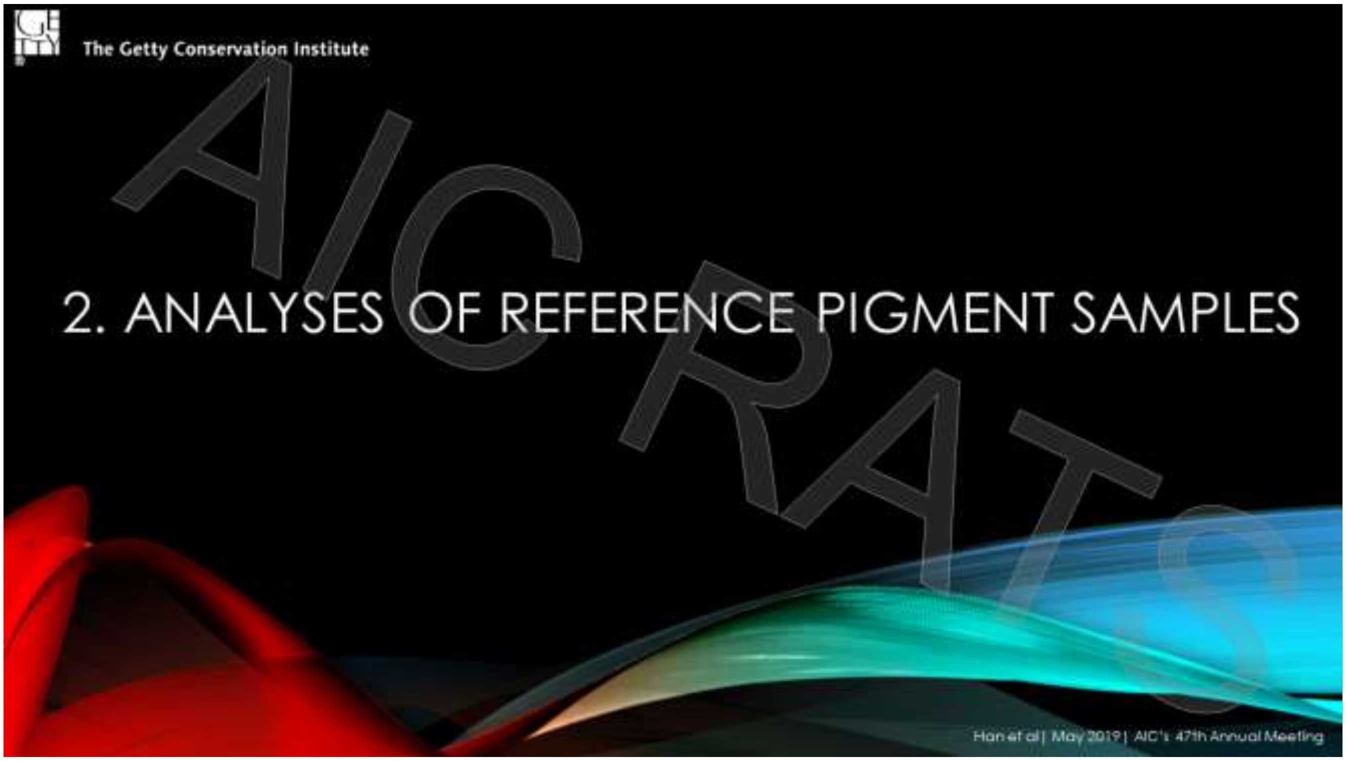

The Getty Conservation Institute

2. ANALYSES OF REFERENCE PIGMENT SAMPLES

Han et al | May 2019 | AIC's 47th Annual Meeting

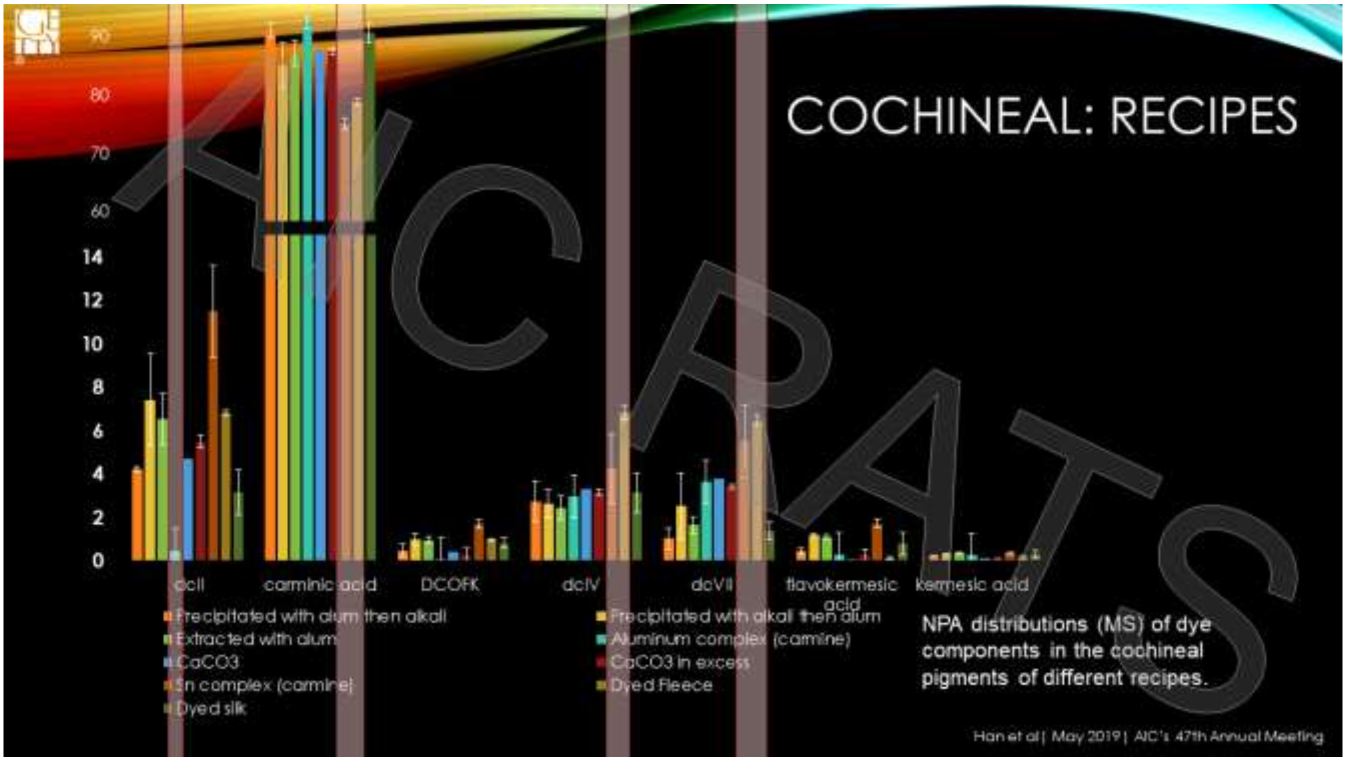

COCHINEAL: RECIPES

NPA distributions (MS) of dye components in the cochineal pigments of different recipes.

Han et al | May 2019 | AIC's 47th Annual Meeting

Here are the NPA distributions of cochineal pigments of the nine different recipes. Carminic acid has the highest NPA in all the cochineal pigments, ranging from 75% to 92%. This graph shows clear characteristics of pigments prepared with the different recipes. For example, the NPA of carminic acid of pigments with Sn (dark orange bars) and from dyed fleece (earth yellow bars) are about 10% lower than in the other pigments; and the NPA of dc II of alum carmine (light blue bars) is significantly lower than in the other pigments.

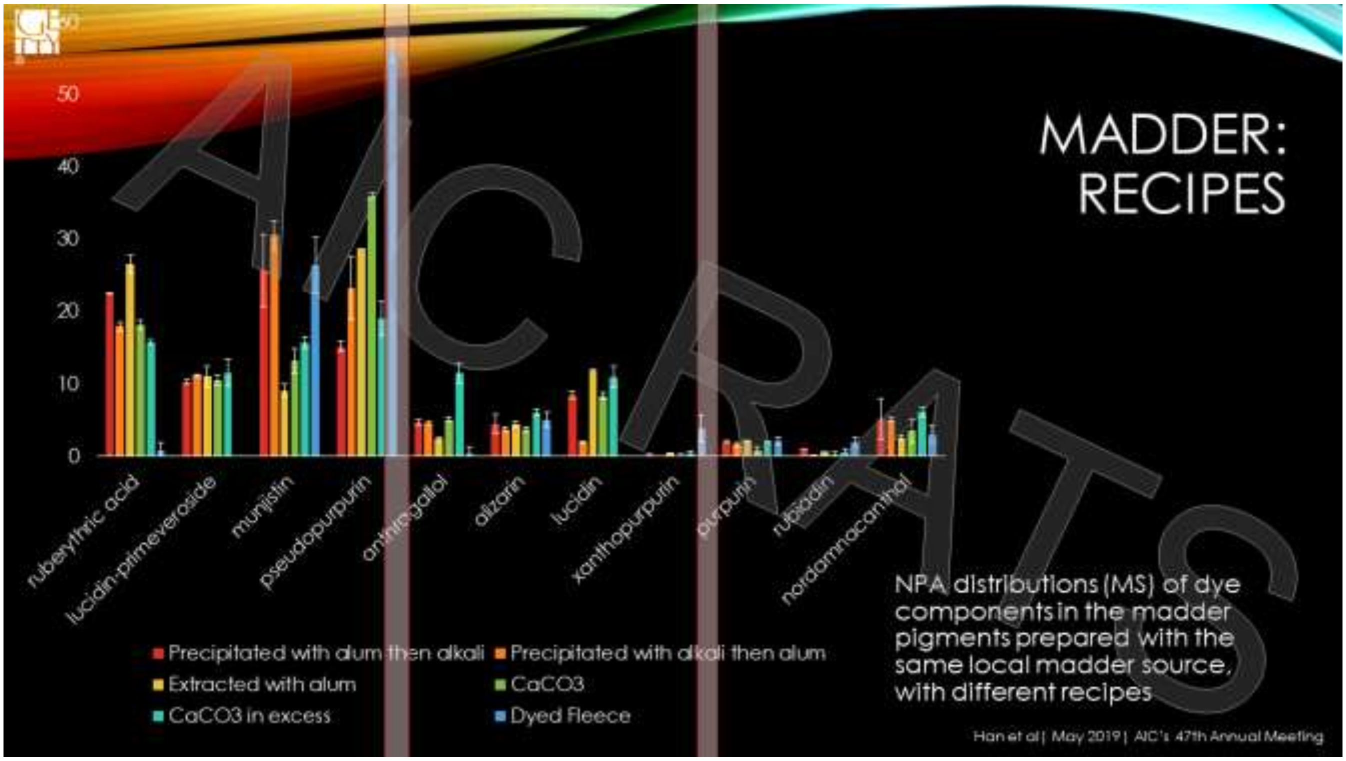

MADDER:
RECIPES

NPA distributions (MS) of dye components in the madder pigments prepared with the same local madder source, with different recipes

Han et al| May 2019| AIC's 47th Annual Meeting

The NPA distributions of madder pigments show a larger variability, due to both different sources of madder and pigment preparation recipes. First, pigments prepared with madder from the same source but with difference recipes show obvious characteristics in NPA distribution of dye components. For example, in pigments made from dyed fleece (blue bars), the contents of pseudopurpurin, xanthopurpurin, rubiadin and munjistin are high, while the contents of ruberythric acid, lucidin-primeveroside and lucidin are very low. Another example: pigments with alum extraction (yellow bars) contain higher content of ruberythric acid and lucidin. The NPA distributions of other recipes are also more or less characteristic. The differences in relative amount mainly come from different capability of precipitating dye components of different recipes. For pigments made from dyed fleece and dyed silk the differences also come from different behaviors of dye components in dyeing and the process of dye extraction from dyed fabrics. Further research is needed to explain the different dye composition due to various recipes.

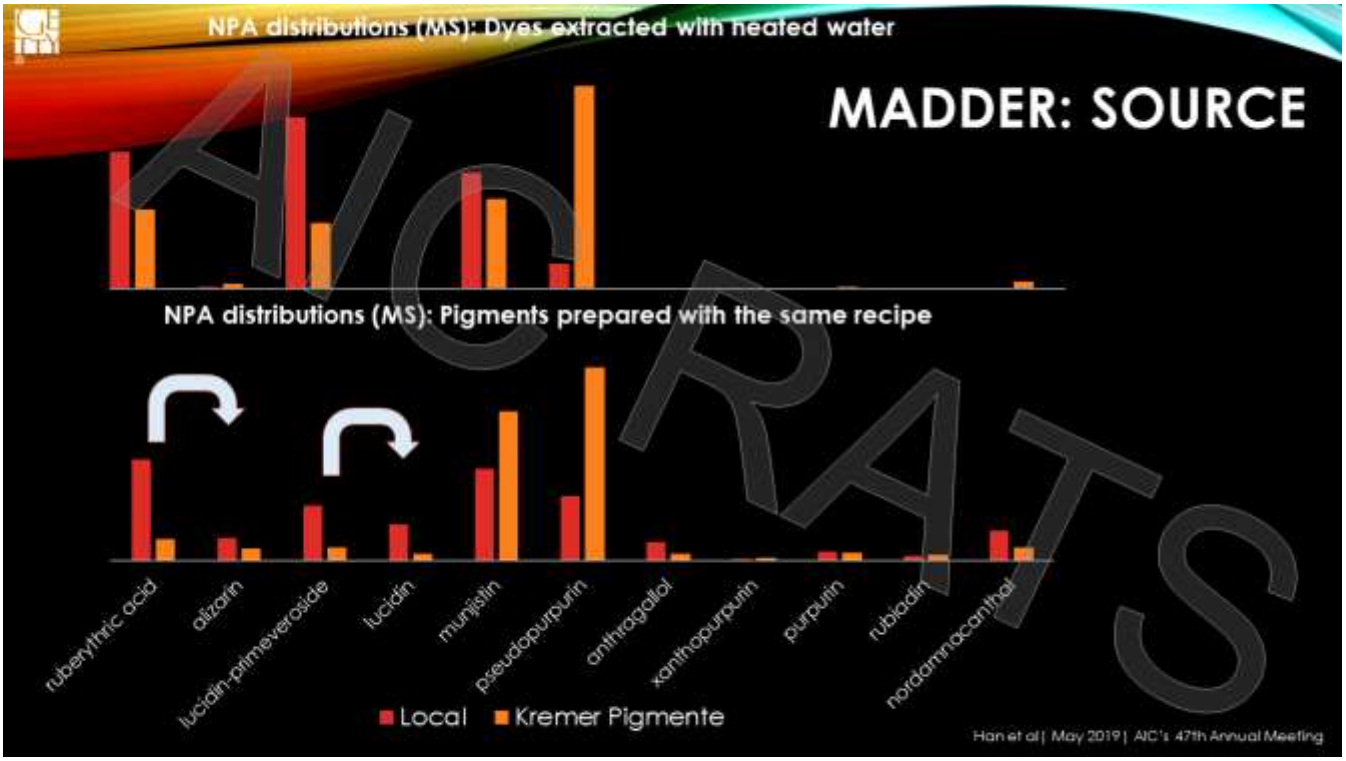

NPA distributions (MS): Dyes extracted with heated water

MADDER: SOURCE

NPA distributions (MS): Pigments prepared with the same recipe

Han et al| May 2019| AIC's 47th Annual Meeting

Second, dye source makes a great difference. The relative amount of dye components contained in madder from local madder and from Kremer Pigmente are different: the main differences include higher content of ruberythric acid, lucidin-primeveroside and munjistin, and lower content of pseudopurpurin in local madder than in madder from Kremer Pigmente. The differences in dye composition may result from different species, different production places, etc. A side note is that part of ruberythric acid and lucidin-primeveroside lose sugar groups and become respectively alizarin and lucidin. These difference in dye composition are more or less reflected in the madder pigments prepared with madder from the two sources with the same recipes. In the bar graph, for all the three pair of pigments, there is higher relative contents of ruberythric acid and lucidin-primeveroside in the pigment made from local madder. The relative contents of munjistin and pseudopurpurin in the pigments are also consistent with the relative contents in the dye sources in most cases.

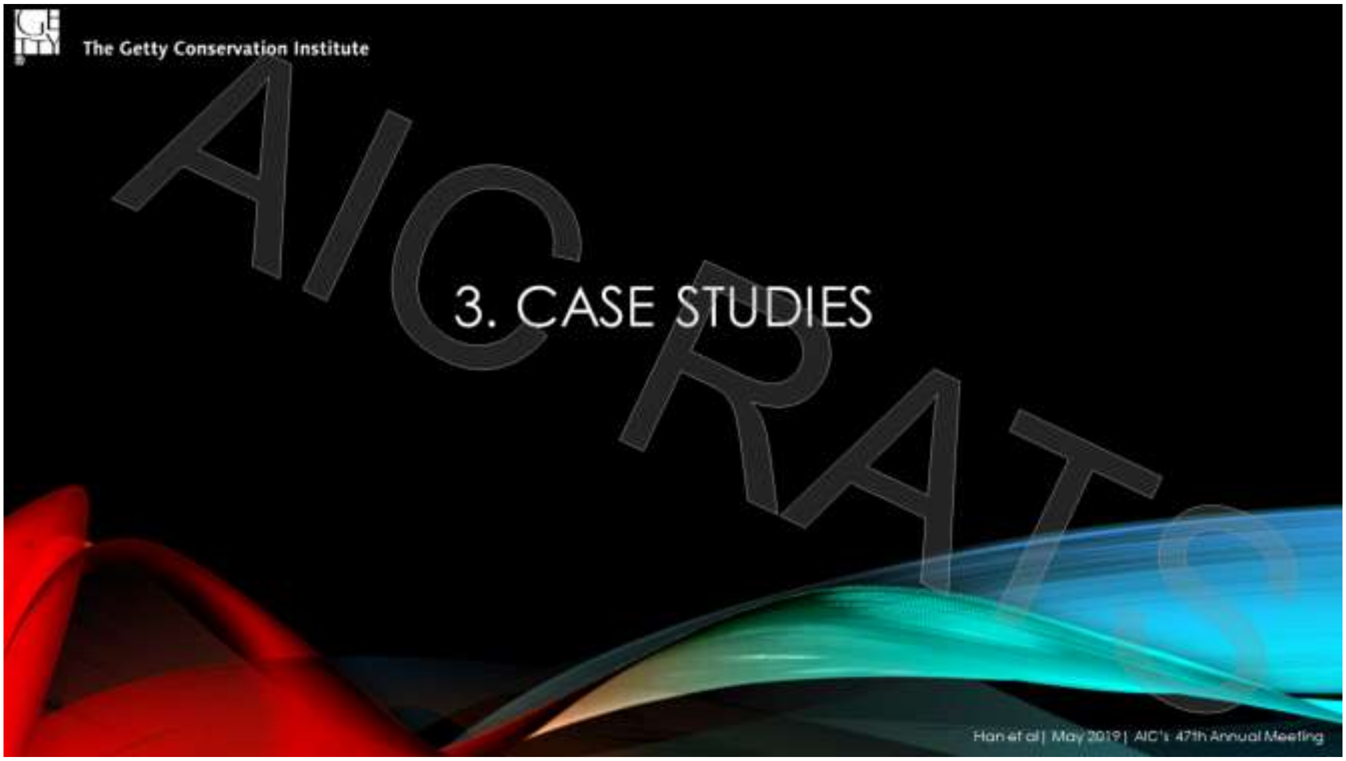

The Getty Conservation Institute

3. CASE STUDIES

Han et al | May 2019 | AIC's 47th Annual Meeting

Based on the above research, four samples from three easel paintings were studied.

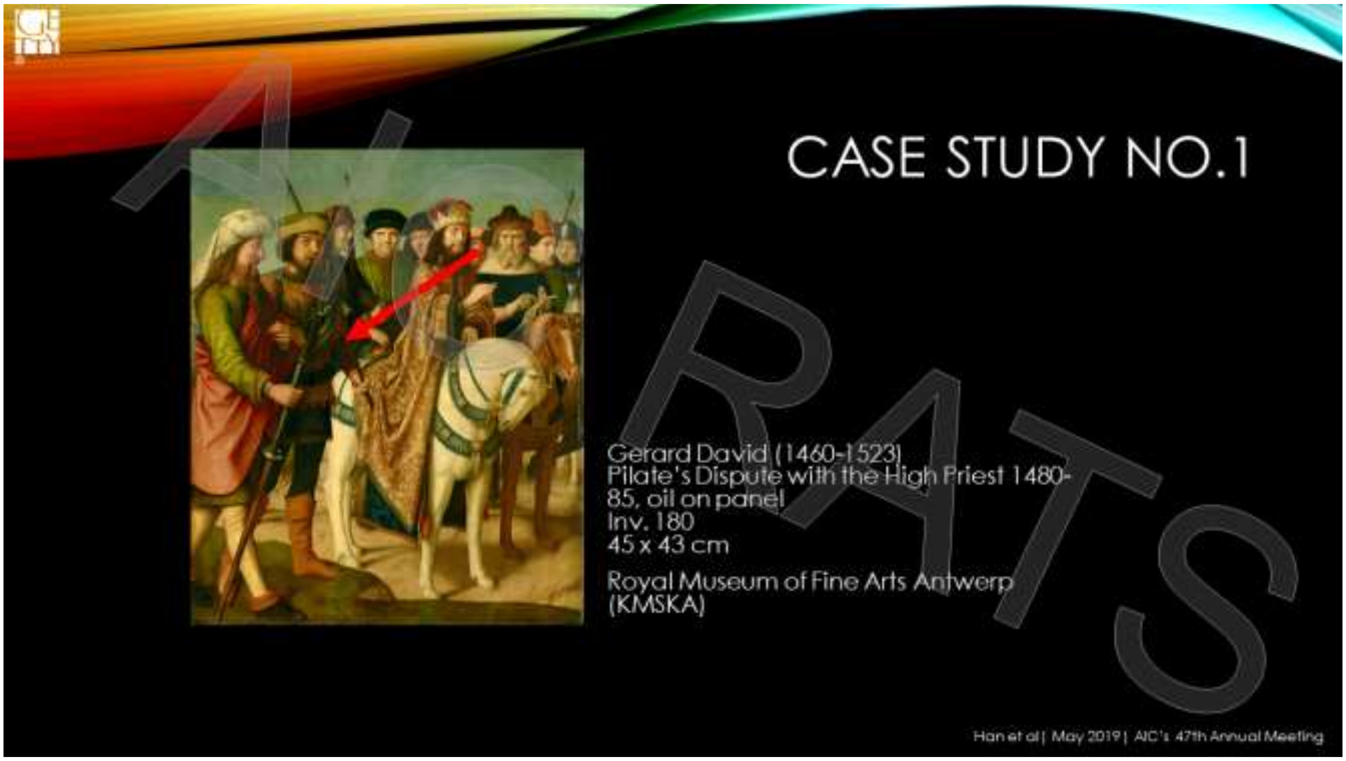

CASE STUDY NO.1

Gerard David (1460-1523)
Pilate's Dispute with the High Priest 1480-85, oil on panel
Inv. 180
45 x 43 cm

Royal Museum of Fine Arts Antwerp
(KMSKA)

Han et al| May 2019| AIC's 47th Annual Meeting

The first sample came from Gerard David's painting. BF3 solution was used for extraction.

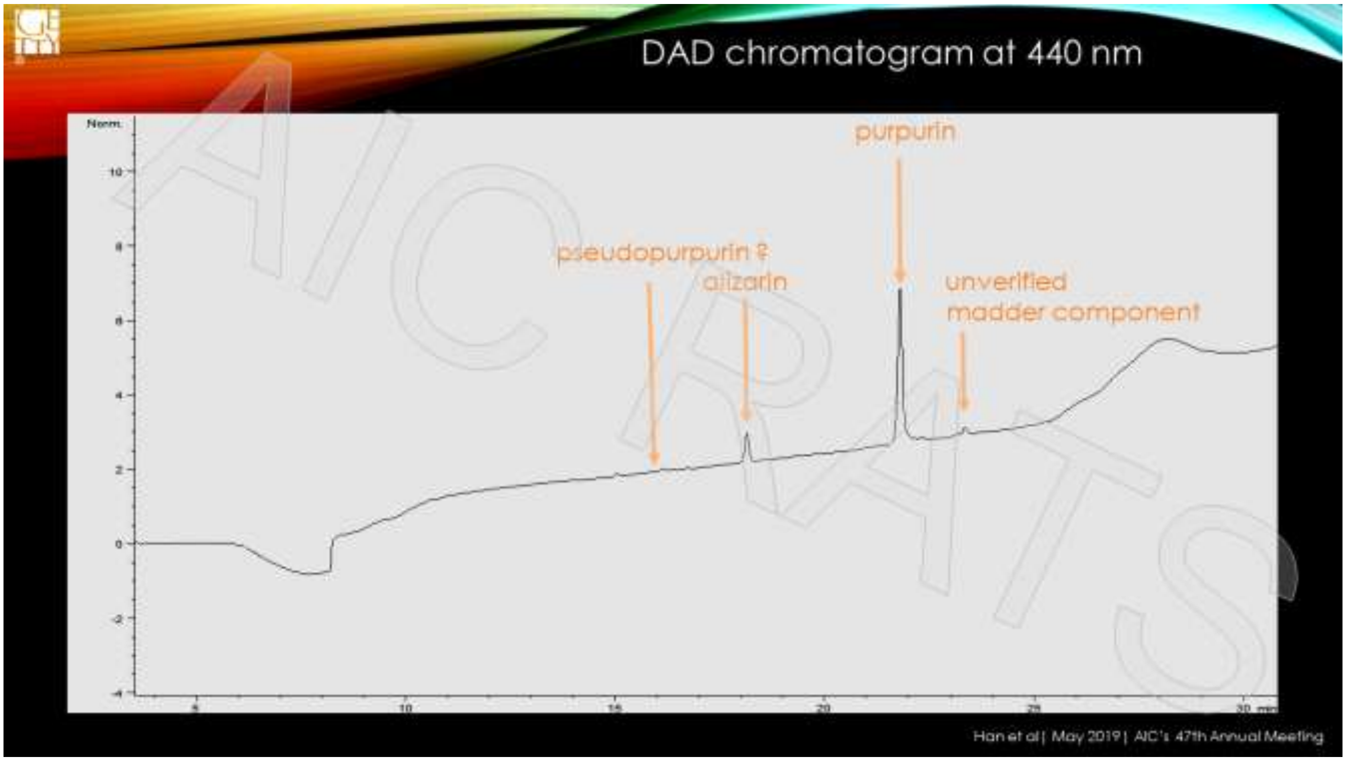

DAD chromatogram at 440 nm

Han et al | May 2019 | AIC's 47th Annual Meeting

Dye components identified included alizarin, purpurin and pseudopurpurin (maybe), and an unverified madder component was detected, all by the DAD. As the dye components were of very low amounts, none of them were detected by the MS detector.

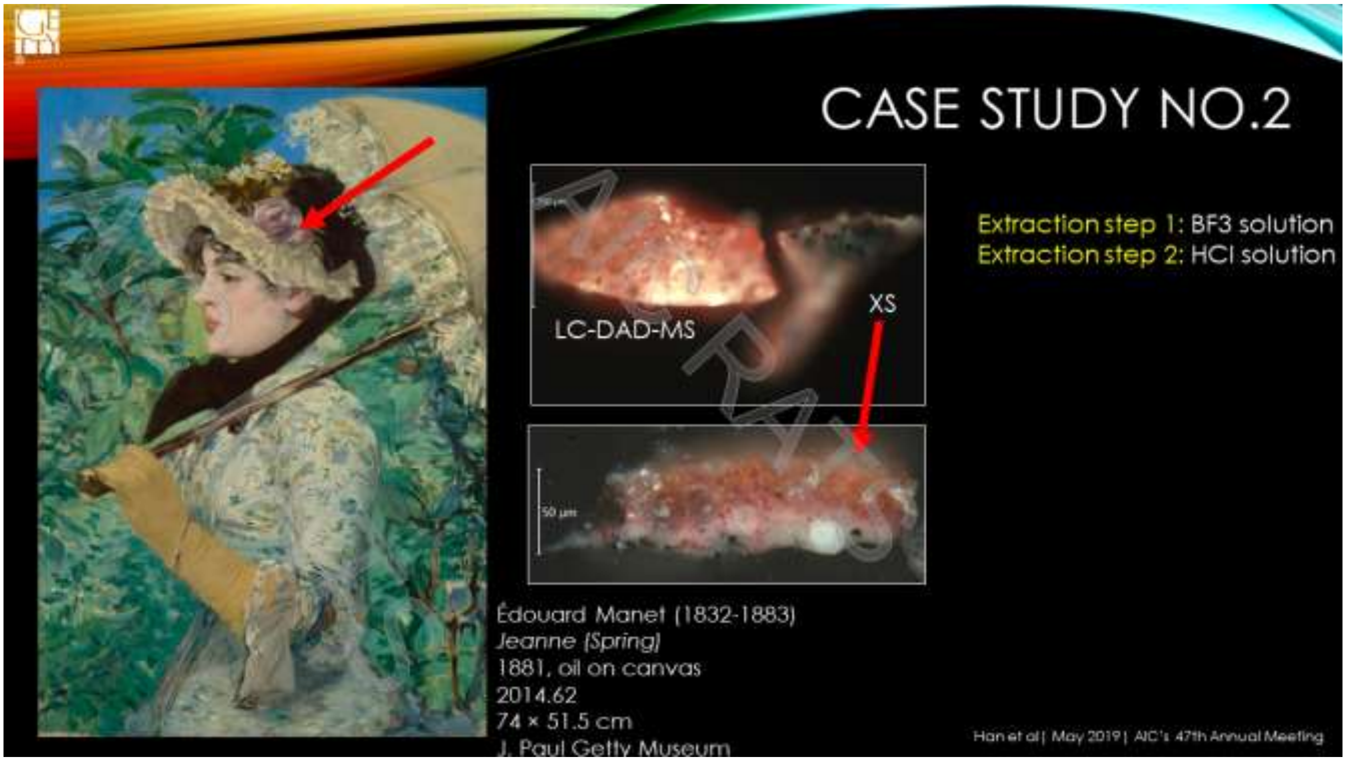

CASE STUDY NO.2

Extraction step 1: BF3 solution
Extraction step 2: HCl solution

Édouard Manet (1832-1883)
Jeanne (Spring)
1881, oil on canvas
2014.62
74 × 51.5 cm
J. Paul Getty Museum

Han et al| May 2019| AIC's 47th Annual Meeting

The second sample was from Manet's Spring. The red layer in the middle is abundant with organic dyes. By FORS, microscope and SEM, the scientist thought the dye is pure cochineal. LC-DAD-MS analysis was undertaken with a two-step extraction method as the sample was too tiny and there were only a few dye components present.

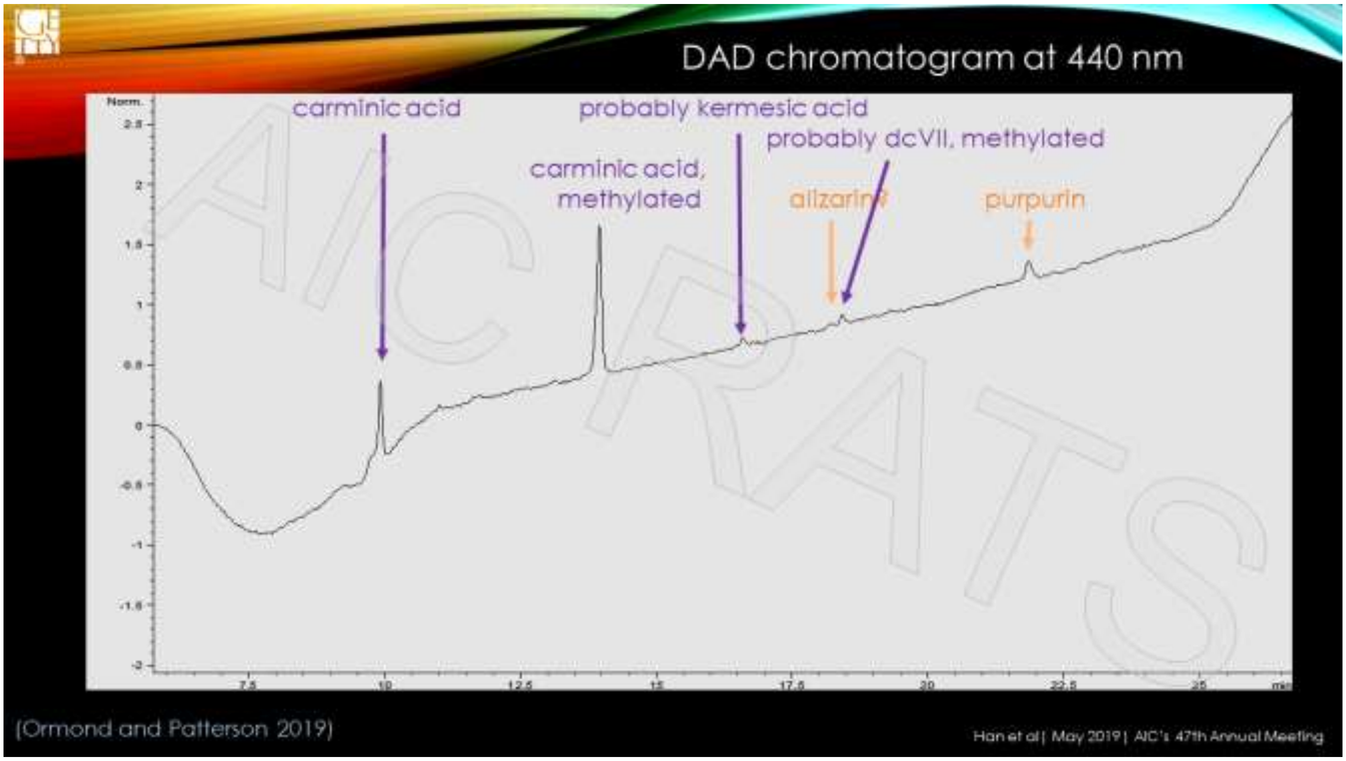

DAD chromatogram at 440 nm

(Ormond and Patterson 2019)

Han et al | May 2019 | AIC's 47th Annual Meeting

Results showed that actually apart from cochineal dyes, dye components of madder were also present, indicating the use of both. All dye components were detected with the DAD but only cochineal dyes were detected with the MS detector.

CASE STUDY NO. 3

Henri de Toulouse-Lautrec (1864-1901)
The Model Resting
1889, oil on cardboard
84.PC.39
65.4 × 49.2 cm
J. Paul Getty Museum

Han et al | May 2019 | AIC's 47th Annual Meeting

The next two samples were from Henri de Toulouse-Lautrec's The Model Resting. Similar analytical results were obtained. Both the two samples contained both madder and cochineal dyes.

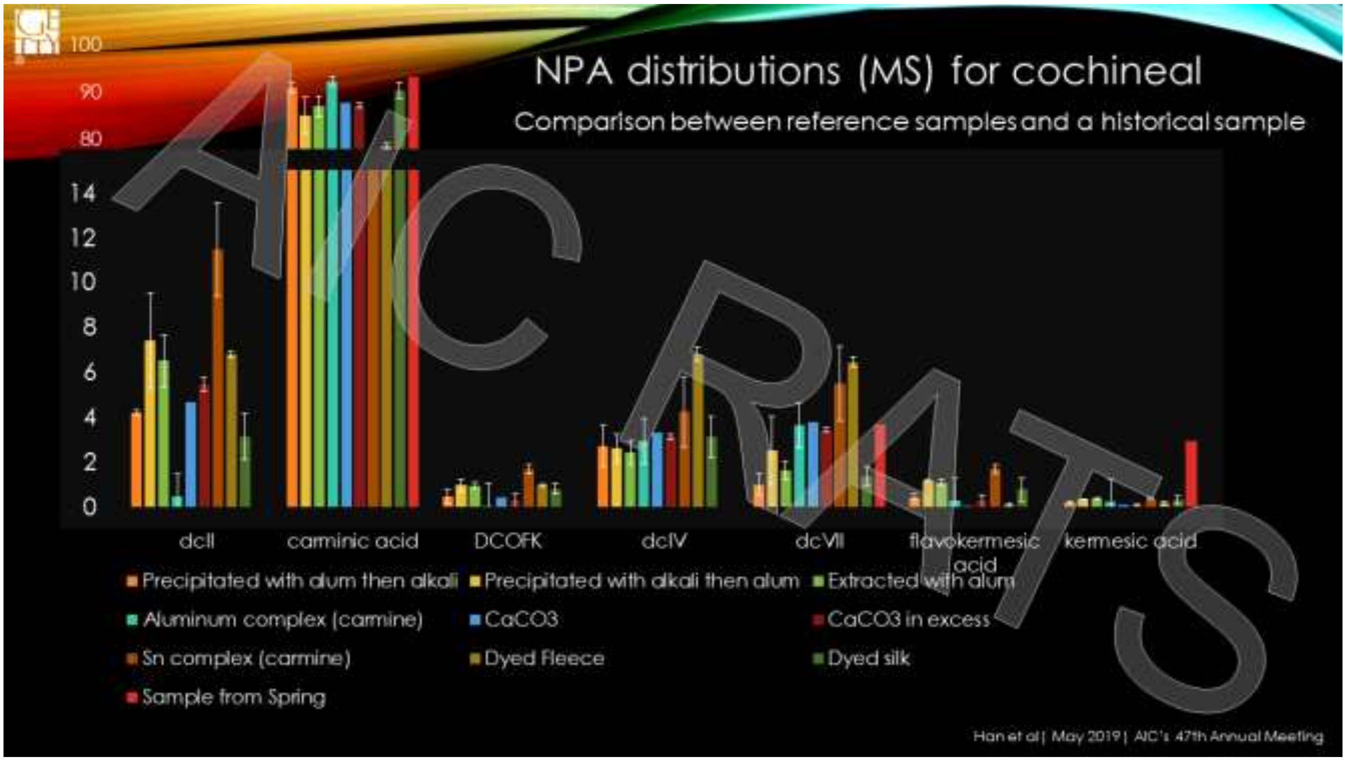

NPA distributions (MS) for cochineal

Comparison between reference samples and a historical sample

🟧 Precipitated with alum then alkali
🟨 Precipitated with alkali then alum
🟩 Extracted with alum
🟩 Aluminum complex (carmine)
🟦 CaCO3
🟥 CaCO3 in excess
🟫 Sn complex (carmine)
🟫 Dyed Fleece
🟩 Dyed silk
🟥 Sample from Spring

Han et al | May 2019 | AIC's 47th Annual Meeting

NPA distribution (MS) of the cochineal dye in the sample from Spring (red bars at the end of each group) shows comparative NPA of carminic acid and dc VII, and higher NPA of kermesic acid. As other components were not detected, and complementary extraction with hydrochloric acid solution was involved, it is difficult to determine which recipe is more likely to have been used for the pigment.

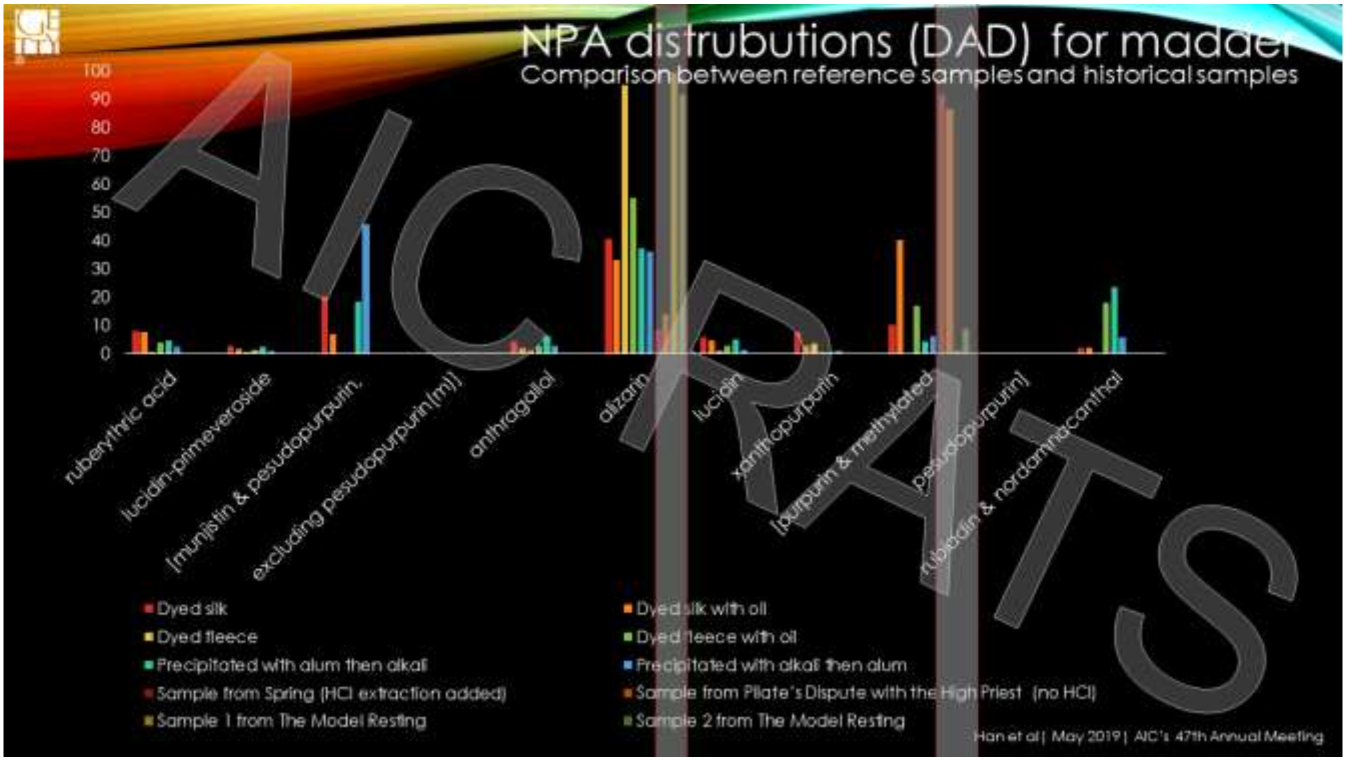
NPA distrubutions (DAD) for madder
Comparison between reference samples and historical samples

Han et al | May 2019 | AIC's 47th Annual Meeting

The NPA distributions (DAD) for madder of the four historical samples show the two samples from The Model Resting (the last two bars in each group) has higher NPA of alizarin, similar to the recipe dyed fleece. The other two samples (the last third and fourth bars in each group) has higher NPA of purpurin and methylated pseudopurpurin (calculated together). The madder pigments may result from a procedure similar to Kopp's purpurin extraction, whereby purpurin and pseudopurpurin are extracted from madder root by a particular process involving sulphurous acid (Kirby, Higgitt, and Spring 2017). NPA distributions of the madder samples provides important information on pigment recipes though it is difficult to draw solid conclusions.

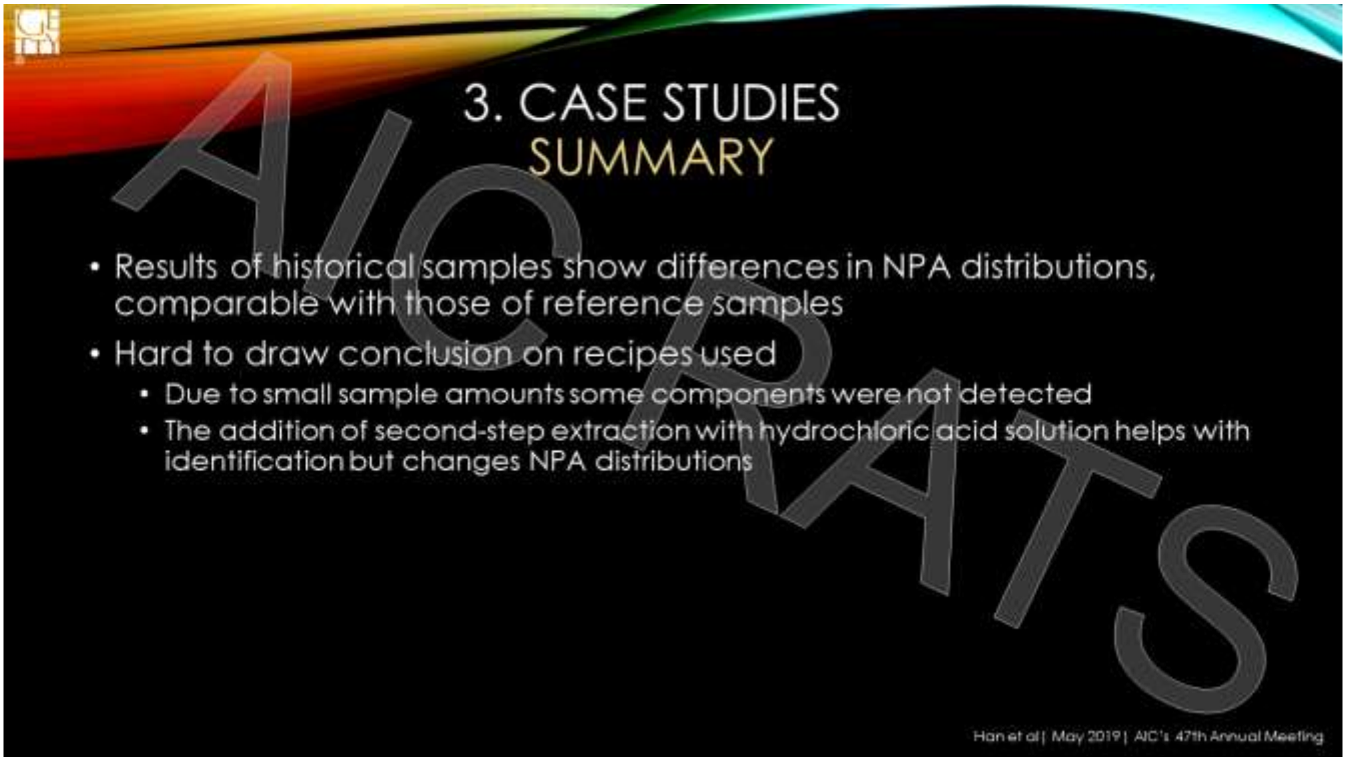

3. CASE STUDIES

SUMMARY

- Results of historical samples show differences in NPA distributions, comparable with those of reference samples
- Hard to draw conclusion on recipes used
  - Due to small sample amounts some components were not detected
  - The addition of second-step extraction with hydrochloric acid solution helps with identification but changes NPA distributions

Han et al | May 2019 | AIC's 47th Annual Meeting

Overall, results of historical samples show characteristics in NPA distributions, comparable with those of reference samples, but it is hard to draw a conclusion on recipes and dye sources, as some components were not detected and the addition of second-step extraction with hydrochloric acid solution helped with identification but changed NPA distributions. Further research to optimize the application of this protocol for samples from historical easel paintings is needed, e.g. by taking bigger samples.

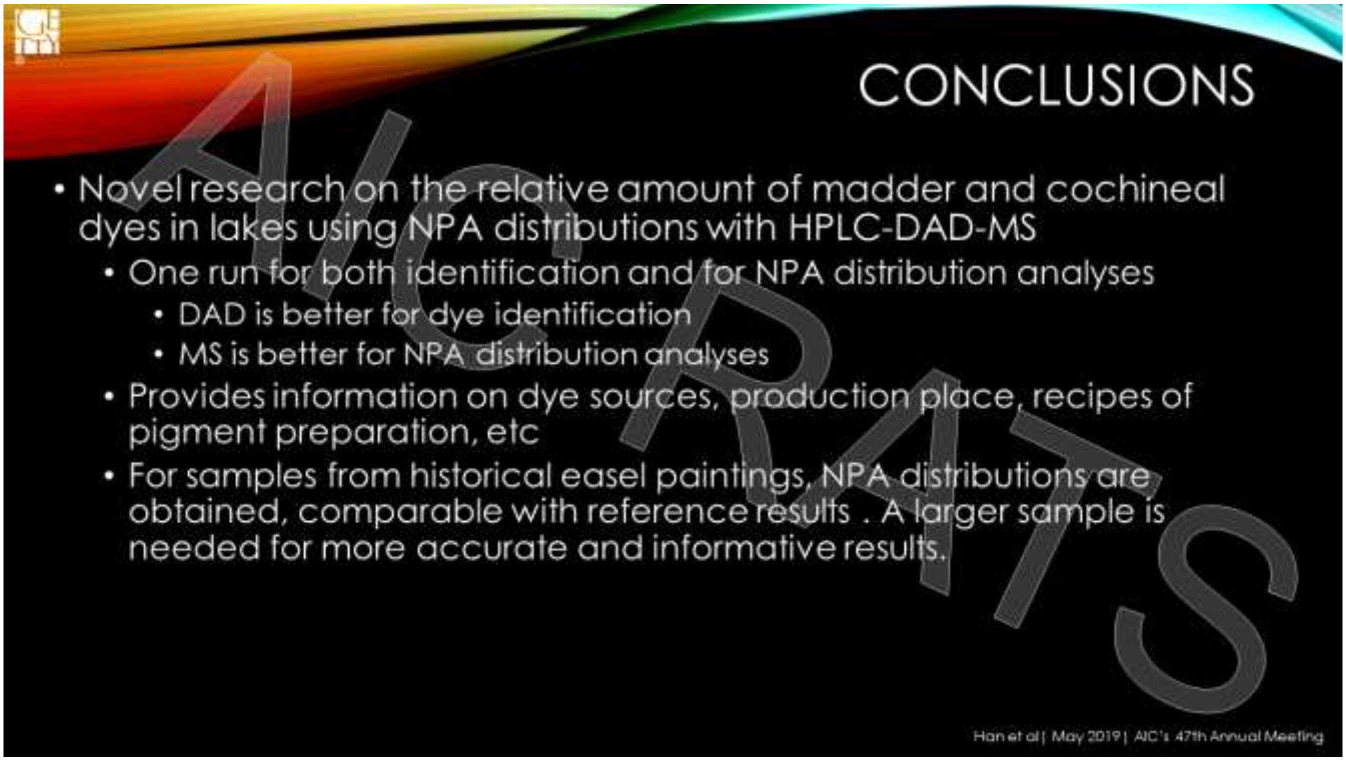

CONCLUSIONS

- Novel research on the relative amount of madder and cochineal dyes in lakes using NPA distributions with HPLC-DAD-MS
  - One run for both identification and for NPA distribution analyses
    - DAD is better for dye identification
    - MS is better for NPA distribution analyses
  - Provides information on dye sources, production place, recipes of pigment preparation, etc
  - For samples from historical easel paintings, NPA distributions are obtained, comparable with reference results . A larger sample is needed for more accurate and informative results.

Han et al| May 2019| AIC's 47th Annual Meeting

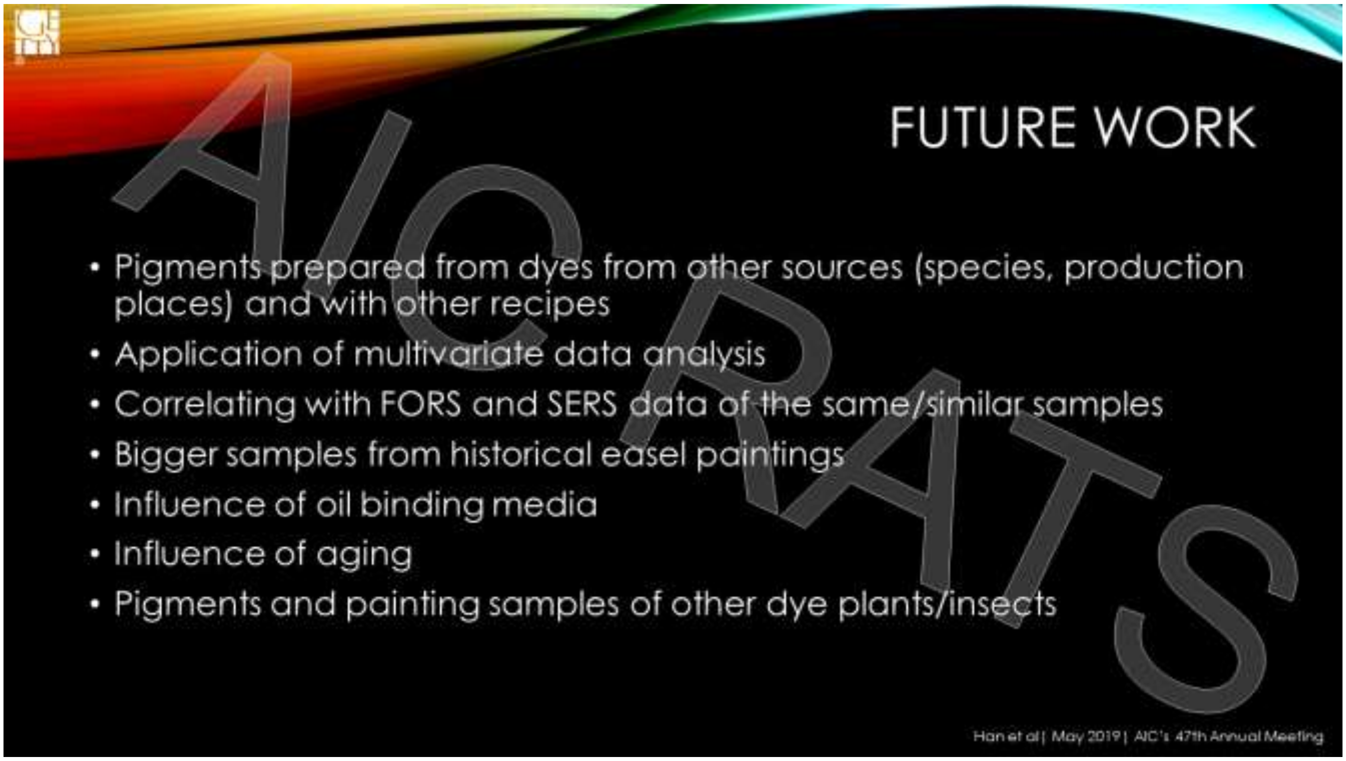

FUTURE WORK

- Pigments prepared from dyes from other sources (species, production places) and with other recipes
- Application of multivariate data analysis
- Correlating with FORS and SERS data of the same/similar samples
- Bigger samples from historical easel paintings
- Influence of oil binding media
- Influence of aging
- Pigments and painting samples of other dye plants/insects

Han et al| May 2019| AIC's 47th Annual Meeting

ACKNOWLEDGMENTS

- Jo Kirby and David Peggie at the National Gallery, London
- Joy Mazurek, Catherine Patterson and Karen Trentelman at The Getty Conservation Institute
- Jonathan Ashley-Smith (Independent teacher, researcher and consultant) for inspirations on 'Uncertainty in Cultural Heritage Conservation'
- Devi Ormond and Kat Harada at The J. Paul Getty Museum and Gwen Borms at Royal Museum of Fine Arts Antwerp (KMSKA) for providing easel painting samples
- Marie Svoboda at The J. Paul Getty Museum for providing madder roots

Thank you!

Jing Han et al
Getty Conservation Institute
jihan@getty.edu

Han et al | May 2019 | AIC's 47th Annual Meeting

REFERENCES

- Daniels, Vincent, Thibaut Deviese, Marei Hacke, and Catherine Higgitt. 2014. "Technological insights into madder pigment production in antiquity." *British Museum Technical Bulletin* 8:13-28.
- Han, Jing, Jantien Wanrooij, Maarten van Bommel, and Anita Quye. "Characterisation of Chemical Components for Identifying Historical Chinese Textile Dyes by Ultra Performance Liquid Chromatography-Photodiode Array-Electrospray Ionisation Mass Spectrometer." *Journal of Chromatography A* 1479: 87-96.
- Kirby, Jo, Catherine Higgitt, and Marika Spring. 2017. "Madder lakes of the 15th–17th centuries: variability of the dyestuff content." In *The diversity of dyes in history and archaeology*, edited by Jo Kirby, 148-161. London: Archetype publications Ltd.
- Kirby, Jo, Maarten van Bommel, and André Verhecken. 2014. *Natural colorants for dyeing and lake pigments : practical recipes and their historical sources*. London: Archetype Publications.
- Kirby, Jo, Marika Spring, and Catherine Higgitt. 2007. "The technology of eighteenth-and nineteenth-century red lake pigments." *National Gallery Technical Bulletin* 28:69.
- Kirby, Jo, and Raymond White. 1996. "The identification of red lake pigment dyestuffs and a discussion of their use." *National Gallery Technical Bulletin* 17:56-80.
- Ormond, Devi, and Catherine Schmidt Patterson. 2019. "The Making of a Parisienne: Manet's Methods and Materials." In *Manet and Modern Beauty: The Artist's Last Years, exh. cat*, edited by Scott Allan, Emily A. Beeny, and Gloria Groom, 147-59. Los Angeles: J. Paul Getty Museum.
- Serrano, Ana, Andre van den Doel, Maarten van Bommel, Jessica Hallett, Ineke Joosten, and Klaas J van den Berg. 2015. "Investigation of crimson-dyed fibres for a new approach on the characterization of cochineal and kermes dyes in historical textiles." *Analytica chimica acta* 897:116-127.

Han et al | May 2019 | AIC's 47th Annual Meeting

Protein Identification in the Technical Analysis of African Art: Successes, Failures, and Lessons Learned

Casey Mallinckrodt, Kathryn Brugioni Gabrielli, Ainslie Harrison, Kristina T. Nelson

The Conservation Initiative in African Art at the Virginia Museum of Fine Arts is a three-year grant-funded project to carry out technical analysis, conservation, and research on the collection. As part of this project, conservators collaborated with curators and scientists to contribute to the knowledge and understanding of the Historic Arts of Africa and the repopulation of object histories lost as a result of colonial collecting practices, aesthetic biases, and social and political pressures. One such partnership was formed with scientists at the Chemical and Proteomic Mass Spectrometry Core Facility at Virginia Commonwealth University to help identify the proteinaceous materials on or incorporated into a selection of objects undergoing study. This effort became a learning experience for both parties, producing compelling results along with instances of ambiguity and some failures. The technique utilized at VCU for protein identification was amino acid sequencing by liquid-chromatography-tandem mass spectrometry (LC-MS/MS), as opposed to peptide mass fingerprinting with mass-spectrometry, which is commonly used in the analysis of cultural heritage objects. This paper will review the differences between these techniques, the types of data generated, the evaluation of results using UNIPROT and other curated and non-curated peptide databases, as well as the possible search parameters. Additionally, we will discuss the potential challenges in data interpretation and the practical considerations for conservators interested in having species-specific protein identification carried out. The results from four objects will be used as case studies: a Yoruba Ógbóni copper-alloy plaque covered with accretions, an Adja Bocio (empowered figure) with layers of ritual applications, a Dinga mask with fur attachments, and a Songye community Nkisi with embedded bone. In addition to the practical considerations related to each assay and the challenges of interpretation, this paper will directly address ethical issues raised by the identification of ritual and power materials and the conservator's responsibilities to protect culturally privileged information.

Proteomics characterization of "organic" metal threads - First results and future directions

Caroline Solazzo[1], Cristina Scibè[2] and Kira Eng-Wilmot[3]

[1]Caroline Solazzo, Research Scientist, Museum Conservation Institute (MCI), Museum Support Center, Smithsonian Institution, 4210 Silver Hill Road, 20746 Suitland, MD, USA. Tel: 301 238 1284. Email: solazzoc@si.edu
[2]Cristina Scibè, PhD Candidate, Faculty of Fine Arts, University of Seville, C./ Laraña 3, 41003 Seville, Spain.
[3]Kira Eng-Wilmot, Textile Conservator, Cooper-Hewitt, Smithsonian Design Museum, 2 East 91st Street, 10128 New York City, NY, USA.

As part of a comprehensive project undertaken by the Museum Conservation Institute to better define and characterize all types of metal threads used in textiles, this work specifically focuses on metal threads made with an animal-based organic substrate. This component of metal threads has been overlooked in the past, due to the lack of appropriate analytical methods to study it. The introduction of proteomics to cultural heritage studies has brought a new set of techniques to characterize protein fibers and other protein-based elements of textiles and is thus particularly well suited for the identification of the protein components in complex and multi-layered organic threads.

Organic metal threads were mainly in use between the 11th and 15th century in weaving and were made by gilding an organic material, such as leather, parchment (vellum), animal membrane or paper, and then cutting the gilded material into narrow strips. These strips were used either flat or wound around a fiber core (such as silk, or linen). The introduction of the "metal-coated organic threads" represents a very important achievement in the development of metal threads technology. They were very popular and preferred to the earlier pure gold threads due to the flexibility of the wrapping materials and the reduced price; indeed, the metal coating was applied in one or multiple thin layers on the organic substrate that made up most of the thickness of the thread. These features led to their extensive use in fabric decoration for a variety of textures and visual effects. Up-to-now there has been no systematic classification of organic metal threads and museums have used a variety of terms to refer to them, such as "leather gold", "skin gold", "silvered/gilded goldbeater's skin", etc. In our research, we were able to distinguish membrane threads (from intestines or other tissues) from skin threads (processed animal skin). Our corpus of samples is mainly composed of medieval threads from textiles of Italian, Spanish, and Middle Eastern/Persian origins (Scibè, in progress). Samples from Northern China and Central Asia complete the corpus for a total of over 70 samples (see acknowledgements for sources of samples). Figure 1 shows two examples of membrane (Italian, 14th C) and skin (Spanish, 13th C) metal wrapped-threads from the Cooper-Hewitt Smithsonian Design Museum.

Figure 1a: 1902-1-257 D, Italy, 14th century Smithsonian Cooper-Hewitt Design Museum and 1b:1943-20-1B, Spain, 13th century, Cathedral de Lerida, Spain, Smithsonian Cooper-Hewitt Design Museum. Images acquired by 3D digital light microscopy with HIROX KH-8700, by Cristina Scibè, Museum Conservation Institute, Smithsonian Institution.

Starting with samples as small as 1x1 mm, the proteomes of each sample were characterized by nanoLC-tandem mass spectrometry (Thermo Scientific Dionex Ultimate 3000 UHPLC system coupled to a Thermo Scientific LTQ Velos Dual Pressure Linear Ion Trap mass spectrometer). Data files were imported into PEAKS studio 8.5 (Bioinformatics Solutions, Inc.) for searching against protein sequence information available in public databases (Uniprot and NCBI). In addition, because domestic sheep (*Ovis aries*), goat (*Capra hircus*), and cow (*Bos taurus*) were found to be the most common species identified, the identification was validated through a series of distinctive markers from collagen type I and type III chains.

Table 1 shows the proteomics results of the Italian membrane thread 1902-1-257 D compared to a reference substrate of bovine intestinal membrane with silver foil.

Table 1 Proteomics results on membrane thread 1902-1-257 D, Italy, 14th century

Collagen proteins		**257-D**		**Cow membrane + silver**	
Accession # in Uniprot	**Protein name**	**%**	**#**	**%**	**#**
sp|P02465|CO1A2_BOVIN	COL1A2	62	74	66	78
sp|P02453|CO1A1_BOVIN	COL1A1	64	93	64	92
tr|Q08E14|Q08E14_BOVIN	COL3A1	48	84	49	67
tr|E1BI98|E1BI98_BOVIN	COL6A1	13	11	31	22
tr|F1MKG2|F1MKG2_BOVIN	COL6A2	10	10	21	18
tr|E1BB91|E1BB91_BOVIN	COL6A3	7	15	21	41
tr|F1MSR8|F1MSR8_BOVIN	COL2A1	12	12	11	10
tr|L8IZS5|L8IZS5_9CETA	COL5A2	9	8	9	11
tr|G3MZI7|G3MZI7_BOVIN	COL5A1			7	11
tr|F1N7Q7|F1N7Q7_BOVIN	COL4A2	1	1	8	7
tr|E1BA17|E1BA17_BOVIN	COL14A1			6	6
sp|Q7SIB2|CO4A1_BOVIN	COL4A1	1	2	3	3
tr|F1MJQ6|F1MJQ6_BOVIN	COL5A3	1	1	1	1
tr|L8IHA8|L8IHA8_9CETA	COL6A5			1	2
tr|F1N0K0|F1N0K0_BOVIN	COL11A1	1	1	3	4
tr|F1MRP6|F1MRP6_BOVIN	COL11A2	1	1	1	2
Non-collagen proteins		**257-D**		**Cow membrane + silver**	

Accession # in Uniprot	Protein name	%	#	%	#
Extracellular matrix proteins					
sp|P21809|PGS1_BOVIN	Biglycan	6	2	3	1
sp|P21793|PGS2_BOVIN	Decorin			41	17
sp|P19427|DERM_BOVIN	Dermatopontin	4	1	9	2
sp|P11116|LEG1_BOVIN	Galectin			42	7
sp|Q05443|LUM_BOVIN	Lumican	11	3	21	7
tr|G3N088|G3N088_BOVIN	Mimecan	5	2	29	11
tr|F1MER7|F1MER7_BOVIN	Heparan sulfate proteoglycan	1	3	5	12
tr|A6QQQ3|A6QQQ3_BOVIN	Prolargin	3	1	36	13
Cytoskeletal proteins					
sp|Q5EA61|KCRB_BOVIN	Creatine kinase B-type			65	24
tr|F1N169|F1N169_BOVIN	Filamin A	2	5	55	106
tr|E1BE25|E1BE25_BOVIN	Filamin C	1	2	20	35
sp|P02584|PROF1_BOVIN	Profilin-1			57	6
tr|E1BIS6|E1BIS6_BOVIN	Synemin	3	6	20	23
tr|F2Z4C1|F2Z4C1_BOVIN	Tubulin alpha chain	6	2	26	8
sp|P48616|VIME_BOVIN	Vimentin			48	20
Smooth muscle proteins					
sp|Q5E9B5|ACTH_BOVIN	Actin, gamma-enteric	32	20	88	44
tr|A4ZZF8|A4ZZF8_BOVIN	Alpha-actinin	2	1	24	16
sp|Q2HJ38|CNN1_BOVIN	Calponin-1	3	1	69	19
sp|O62654|DESM_BOVIN	Desmin	29	13	68	44
tr|F1MYM9|F1MYM9_BOVIN	Myosin heavy chain 11	6	10	42	77
tr|L8I2Q9|L8I2Q9_9CETA	Myosin light polypeptide 6	5	1	69	11
tr|A1L5B0|A1L5B0_BOVIN	Myosin light polypeptide 9	7	1	70	13
sp|Q9TS87|TAGL_BOVIN	Transgelin			51	11
Blood cells and plasma proteins					
tr|D4QBB3|D4QBB3_BOVIN	Hemoglobin beta			48	5
sp|P01966|HBA_BOVIN	Hemoglobin subunit alpha			42	3
Others					
tr|Q58DP7|Q58DP7_BOVIN	Heat shock 27kDa	9	2	74	11
tr|F2Z4J1|F2Z4J1_BOVIN	Histone H2A			28	4
tr|F1N453|F1N453_BOVIN	Histone H2B	7	1	33	4
sp|Q5E9F8|H33_BOVIN	Histone H3			41	6
tr|E1BLC2|E1BLC2_BOVIN	Histone H4	8	1	29	3
tr|Q2KJC7|Q2KJC7_BOVIN	Periostin	2	1	15	6

All proteins identified in the textile sample are shown and separated in collagen and non-collagen proteins. Additional proteins were identified in the reference sample, some of which are shown in Table 1. The proteins identified with the highest protein coverage (%) and number of peptides (#) were the collagen type I chains alpha-1 and alpha-2 (Col1A1 and Col1A2) and collagen type III alpha-1 chain (Col3A1). These three collagen chains were identified as having very similar coverage as the reference sample. Other collagen chains from type IV, V, VI, XI and XIV were identified in the reference membrane, with some of them also identified in the textile sample, but usually with lower coverage. The walls of organs from the digestive and urinary tracts are also made of non-collagenous proteins such as extracellular matrix proteins, cytoskeletal proteins, and smooth muscle proteins, some of which are indicated in Table 1. The smooth muscle proteins, in particular, are contractile proteins found in the muscles that line the internal organs of the body, including the blood vessels, stomach, intestines, urinary bladder, and uterus. As observed in the previous study of a 14th C Italian textile (Popowich, Cleland, and Solazzo, 2018), the analysis of sample 1902-1-257 D showed the presence of smooth muscle proteins of which actin, desmin, and myosin heavy chain 11 were identified with the highest confidence. In the reference membrane, the actin protein was precisely identified as “Actin, gamma-enteric smooth muscle” or ACTG2, characteristic of intestinal muscles, with an 88% coverage and two peptides (WISKPEYDEAGPSIVHR and EEETTALVCDNGSGLCK) unique to the intestinal actin. The less complete identification of actin in 1902-1-257 D, on the other hand, yielded a series of peptides that were also present in actin from skeletal muscles (ACTA1), aortic smooth muscle (ACTA2), cardiac muscle (ACTC1), so that it is not possible to further specify the tissue of origin based on this protein. Desmin is also unspecific as it is found in the intermediate filaments of cardiac muscle, skeletal muscle, and smooth muscle. However, the identification of myosin heavy chain 11, a protein found in smooth muscle only, confirms that an internal organ such as stomach, intestines or bladder is the source of the membrane.

Table 2 shows the proteomics results on the Spanish skin thread 1943-20-1B.

Table 2. Proteomics results on membrane thread 1943-20-1B, Spain, 13th century

Collagen proteins		**20-1B**	
Accession # in NCBI	**Protein name**	**%**	**#**
XP_017920382.1 PREDICTED: isoform X1 [Capra hircus]	COL1A1	57	99
XP_005678993.1 PREDICTED [Capra hircus]	COL1A2	56	65
XP_005675926.1 PREDICTED [Capra hircus]	COL3A1	41	48
Non-collagen proteins		**20-1B**	
Accession # in Uniprot	**Protein name**	**%**	**#**
sp|P00698|LYSC_CHICK OS=Gallus gallus	Lysozyme C	32	4
tr|A0A2H4Y814|A0A2H4Y814_CHICK OS=Gallus gallus	Ovalbumin	74	42
tr|A0A2H4Y7V4|A0A2H4Y7V4_CHICK OS=Gallus gallus	Ovalbumin	74	39
tr|A0A2H4Y816|A0A2H4Y816_CHICK OS=Gallus gallus	Ovalbumin	69	35
tr|A0A2H4Y8F0|A0A2H4Y8F0_CHICK OS=Gallus gallus	Ovalbumin	74	37
tr|A0A2H4Y7W1|A0A2H4Y7W1_CHICK OS=Gallus gallus	Ovalbumin	70	36
tr|A0A2H4Y7U4|A0A2H4Y7U4_CHICK OS=Gallus gallus	Ovalbumin	70	36
tr|A0A2H4Y8D1|A0A2H4Y8D1_CHICK OS=Gallus gallus	Ovalbumin	67	39
tr|A0A2H4Y8G2|A0A2H4Y8G2_CHICK OS=Gallus gallus	Ovalbumin	62	36
tr|A0A2H4Y882|A0A2H4Y882_CHICK OS=Gallus gallus	Ovalbumin	68	39
tr|I0J178|I0J178_CHICK OS=Gallus gallus	Ovalbumin	5	3
tr|A0A1D5P4L7|A0A1D5P4L7_CHICK OS=Gallus gallus	Ovotransferrin	6	4
tr|I0J171|I0J171_CHICK OS=Gallus gallus	Ovoglobulin	8	3

The identification of collagen chains in this sample is limited to Col1A1, Col1A2, and Col3A1, typical of skin-based objects. Other collagen and non-collagenous proteins are eliminated during preparation when the skin is turned into parchment, vellum or leather. The skin was best matched to *Capra hircus* (domestic goat) and contained, in addition, the peptide GPSGEPGTAGPPGTPGPQGFLGPPGFLGLPGSR that has been characterized as unique to goat (Buckley et al. 2010). Skin threads are usually made with an adhesive that can be visualized by UV-reflected microscopy on cross-sections of the threads. The search for a protein-based adhesive revealed the presence of the egg white proteins ovalbumin (most abundant protein in egg white), ovotransferrin, ovoglobulin, and lysozyme from chicken. Threads made with sheep skin and adhesives based on collagen glue, including fish glue, have also been found in threads of different origins, showing a variety of techniques used to make the metal threads.

The information obtained from proteomics has revealed distinct methods of fabrication that will refine our classification of metal-coated organic threads as well as the provenancing of textiles of uncertain origin. Future work will focus on better characterizing the protein adhesives, especially the ones made with fish glue, and understanding the processing method of skin-based threads (parchment vs vellum vs leather).

ACKNOWLEDGEMENTS

The present work has been developed as part of the Smithsonian's Museum Conservation Institute's project "Golden textiles: technology, mobility, and exchange", and Cristina Scibè's doctoral research "Metal threads in 11th-15th century Hispano-Islamic and Italian textiles: methodological approach for the investigation of materials and manufacturing techniques".

Kindly acknowledged for their permission to study the textile fragments and their collaboration in sampling metal threads are Lorenzo Lorenzini (Curator of the Gandini Collection, Museum of Civic Art, Modena), Silvia Saladrigas Cheng (Documentalist, Textile Museum and Documentation Center, Terrassa), Daniela degl'Innocenti (Textile Conservator and Head of the Scientific Department, Textile Museum, Prato), Geertje Gerhold (Brandenburg Textile Treasury), Maren Heun (Stralsund Museum), and Angela Cheung (Conservation Office, Hong Kong). For their support on the project at the Smithsonian's Museum Conservation Institute (MCI) we thank Drs. Thomas Lam (3D microscopy), Timothy Cleland and Asher Newsome (proteomics and mass spectrometry), Mary Ballard (textile conservation), Robert J. Koestler (Director) and Paula DePriest (Deputy Director). The proteomics analyses were carried at MCI's Proteomics and Molecular Mass Spectrometry Laboratory, and supported by MCI's Federal and Trust Funds and the Andrew W. Mellon Foundation – Directorship Endowment.

REFERENCES

Popowich Aleksandra K., Timothy P. Cleland, and Caroline Solazzo. 2018. "Characterization of membrane metal threads by proteomics and analysis of a 14th c. thread from an Italian textile", *Journal of Cultural Heritage*, 33: 10-17.

Scibè Cristina. In progress. Metal threads in 11th-15th century Hispano-Islamic and Italian textiles: methodological approach for the investigation of materials and manufacturing techniques. (Acronym: METHIT). Ph.D. diss., University of Seville, Spain.

Buckley Mike, Sarah Whitcher Kansa, Sarah Howard, Stuart Campbell, Jane Thomas-Oates, and Matthew Collins. 2010. "Distinguishing between archaeological sheep and goat bones using a single collagen peptide." *Journal of Archaeological Science* 37: 13–20

The Application of Surface Enhanced Raman Spectroscopy (SERS) and Gel-Sampling to Identify Synthetic Dyes Used on Hand-Colored Photographs

Han Neevel, Inez van der Werf, Katrien Keune, Veronica Biolcati

Until the commercially successful introduction of chromogenic color prints by Kodak in 1935, colored photographic pictures mainly were produced by hand-coloring B. & W.-photographs, e.g. Daguerreotypes, albumen and gelatin-based prints (1). This was common practice with portraits on postcards (Figure 1). Until 1860, inorganic and natural organic pigments in a binding medium were applied. Later, inks, containing synthetic dyes were introduced. As many of these dyes are very light-sensitive, caution must be taken when exhibiting these artefacts. Little is known about the practice of hand-coloring. Therefore, a proper identification of these dyes would help to understand the coloration process and assess the risk of fading. Hydrogels, e.g. the "Nanorestore Gel", or an agar gel, can be used to gently extract water-soluble dyes from the gelatin layer of a photograph, e.g. for cleaning purposes (2, 3). These gels could be useful for micro-sampling. Surface Enhanced Raman Spectroscopy (SERS) is a very powerful technique for dye identification, especially for synthetic dyes (4). The silver colloid, added to the sample taken from the object, can enhance the Raman signal up to a factor of 109, making it even possible to detect single molecules, e.g. crystal violet (5). According to research done by Doherty et al., methylcellulose films, doped with a silver colloid can be used to extract dyes from the artefact's surface for analysis by SERS (6). In our research, this principle has been applied by doping the "Nanorestore Gel" and an agar gel, with colloidal silver (prepd. according to a description by Lee & Meisel (7). A small piece of the gel is immersed into the colloid and left there for a while to be impregnated by the colloid. During the short contact time (minutes) of a very small cube (area: c. 1 mm2) of the hydrogel, water-soluble dyes migrate into the gel and come into contact with the colloid. They then can be analyzed by SERS. This way, dyes on 4 hand-colored photographs from a private collection could be extracted and successfully identified by SERS. The spectra were measured with a Renishaw RAMAN microscope with a 785 nm Laser. In order to identify the dyes, their Raman spectra were compared with spectra taken from the RCE's large reference collection of synthetic dyes. The red dye in the roses on the postcard in Figure 1 turned out to be eosin. *Corresponding author Many historic gelatin-based photographs show silver mirroring, the formation of colloidal silver at the surface, caused by redox cycling of silver in the gelatin layer (8). The silver mirroring on some of these photographs was shown to function as a SERS-active substrate, enhancing the Raman signal of the dye in contact with it.

Understanding Air-Tight Case Environments at the National Museum of the American Indian (Smithsonian Institutions) by SPME-GC-MS

Alba Alvarez Martin, Cali Martin, Gwénaëlle Kavich, Kelly McHugh, Rebecca Kaczkowski

The National Museum of the American Indian opened the exhibition Americans in January 2018. The exhibition highlights the deep connections between Americans and American Indians as illustrated through history, pop culture, and the identity of the United States. The minimalistic design of the cases containing Lakota, Northern Cheyenne, and Arapaho war shirts and an eagle feather headdress from the Sicangu Lakota displayed in the Battle of Little Bighorn gallery was achieved through frameless case construction. The cases allow the visitor to feel as though they are standing in the midst of warriors. These cases are described as air tight and are marketed as such by the fabricator. One week after the exhibition opening, the cases were opened to address some locking mechanism issues. When opening the cases, they emitted a strong and distinct chemical odor from the interior. This raised immediate concern for the objects. At the request of the collections manager and conservator, exhibition project managers contacted the case fabricators to confirm what case materials were used in order to better understand the potential source of the odor. Concurrently, the collections manager opened the cases weekly to allow for the escape of built-up volatile organic compounds in the hopes that the newly constructed cases would sufficiently off-gas. Additionally, sorbent materials were placed in some of the exhibition cases in order to help with the issue. Unfortunately, the problem persisted. The case fabricators were forthcoming with information and were just as keen to understand what was occurring in the case environment, however, there was some dispute as to the source of the odor. In order to find the source of smell, conservation scientists at the Smithsonian Institution's Museum Conservation Institute carried out a comprehensive analysis of the volatile organic compounds (VOCs) emitted by the exhibition case and by the object itself. Solid phase microextraction (SPME) coupled with gas chromatography-mass spectrometry (GC-MS) is starting to be widely applied in museum institutions as a screening method for the evaluation of the off-gassing process of construction materials and historical objects. In this case, SPME-GC-MS analysis was performed during the exhibition with the aim to find the origin of the smell. The detection and identification of VOCs were carried out simultaneously in: (i) two exhibition cases, (ii) all the individual construction materials and (iii) similar historical object. This analysis showed with confidence that the odorous/fragrant compounds were released by the construction materials and not by the historical objects placed within the exhibition cases. In addition, due to the measurements taken in different positions around the exhibition case, results were useful to point out the range of efficiency of the sorbent material placed in some of the exhibition cases. Since the SPME setup does not require any modification in the exhibition display, the testing remained invisible to the museum visitors. This aspect, in combination with the fast analysis that this technique involves, allowed the collections manager and conservator to take a prompt response in order to preserve the integrity of the collection.

Wood You Rather? Exploring the Complementarity of Chemotaxonomic Approaches to Mahogany Identification

Katherine Schilling, Arlen Heginbotham, Edward R. Sisco, Michael R. Schilling, Randy S. Wilkinson, Richard R. Hark

Wood identification, specifically mahogany (Swietenia) species identification, through chemotaxonomy is a re-emerging research area that has sprouted primarily from thermal desorption gas chromatograph/mass spectrometry (TD-GC/MS) and direct analysis in real time mass spectrometry (DART-MS). The practical question arising from these exciting and innovative research veins is: Do objects conservators need to find a collaborator with a DART-MS or can they work with a conservation scientist to do TD-GC/MS? This talk explores the interaction of each technique with wood samples by characterizing the marker compounds, their distribution throughout the parent tree, and their importance to the final identification. Recent research at the Getty Conservation Institute (GCI) and at the Institute for the Preservation of Cultural Heritage (IPCH) has converged over the identification of wood species used in decorative arts objects using a chemotaxonomic approach when a traditional anatomical approach is not feasible. The GCI has spearheaded the MOXI project (Molecular Xylem Identification), which is an innovative application of TD-GC/MS and the creation of an INT-SUM mass spectral "fingerprint" library using F-Search (Frontier Laboratories, LTD). IPCH has partnered with the GCI for a cross-lab method validation, and has applied the method to the analysis of mahogany pieces in the Rhode Island furniture collection at the Yale University Art Gallery (YUAG). Additional research at IPCH and the National Institute of Standards and Technology has attempted to isolate and identify the marker compounds, and assess their robustness with respect to anatomical point of origin in the tree. DART-MS is a way to analyze slivered or powdered wood samples using an ionizing stream under ambient conditions. DART-MS analysis revealed the presence of high molecular weight ions that were statistically important to the identification of mahogany species, TD-GC/MS analyses with and without chemical derivatization do not suggest these compounds are detectable in their intact or decomposed forms by this method. Heating in ampules filled with argon followed by solvent extraction of residue and subsequent analysis by liquid chromatography/mass spectrometry were performed to ascertain if these high molecular weight compounds are liberated by thermal desorption from the wood and are detectable by DART-MS but not by GC/MS. Initial results show that these compounds are indeed liberated by thermal desorption, and research into the identity of these compounds is still ongoing. Additional discussion will focus on the statistical value of these compounds to the differentiation of mahogany species from one another, and the application of TD-GC/MS to species identification.

Research and Technical Studies and Objects Specialty Groups Presentations

Decision-Making in Context: Conservation of Gold and Magnesium Alloy Components on a Surveyor Spacecraft

Jacqueline Riddle, Elizabeth Beesley, Lisa Young, Malcolm Collum

In preparation for the first lunar landing, NASA created the Surveyor Program which sent seven robotic spacecraft to the Moon between June 1966 and January 1968. These spacecraft provided crucial information to the Apollo 11 mission which put the first humans on the Moon in July 1969. The Smithsonian acquired a full-scale engineering model of a Surveyor spacecraft in 1968, and it has been on continuous display since then. Amongst other components, the spacecraft has a mechanical scoop, designed to dig trenches in the lunar soil, a TV camera, designed to send live video feed back to Earth, and an alpha-scattering surface analyzer, designed to conduct the first elemental analyses of the lunar soil. The alpha-scattering instrument is housed in a gold-plated copper box secured to a magnesium alloy base. Extensive magnesium corrosion was discovered on the base and subsequently treated in 2013, when the instrument was temporarily removed due to damage caused by a leaking pipe. In 2017, the entire spacecraft was removed from display in preparation for the upcoming renovation of the Smithsonian National Air and Space Museum. For the first time in almost 50 years, conservators were able to conduct a thorough examination, technical analysis and treatment of the spacecraft. This included analysis using X-ray fluorescence spectrometry (XRF) and Fourier-transform infrared spectroscopy (FTIR), extensive cleaning and iron stain reduction, consolidation of paint and plastics, in-painting, and corrosion mitigation. The 2017 examination revealed that the magnesium treatment performed in 2013 was ineffective. Galvanic corrosion had further developed between the magnesium base and the gold-plated component, indicating that the initial treatment strategies would not be sufficient for its long-term display. Conservators walk an ethical tight rope where several factors are balanced: the principle of reversibility countered with the challenges of preserving fugitive materials, the principle of minimal intervention with the need for an enduring treatment solution. The presence of unusual modern materials with no established conservation treatment methodologies adds a layer of uncertainty in the decision-making process. In the conservation of large technological artifacts, treatment frequently requires complete or partial disassembly of the artifact. At the Smithsonian National Air and Space Museum, large artifacts are often suspended from the ceiling for long-term display, where they remain practically inaccessible for years. When suspending artifacts above the public, conservation treatments—particularly to structural components—cannot fail. All of these factors can drive treatment decisions towards more restorative techniques. This paper will present the decision-making process and ultimate outcome of the conservation treatment on the Surveyor spacecraft. It will focus on the treatment of the alpha-scattering surface analyzer, which contained persistent corrosion of magnesium alloy parts in contact with gold-plated components. Tactics for treating galvanic corrosion, as well as new tools and techniques adapted from the aerospace industry will be presented.

Examining the Use of Ozone Test Strips to Detect PVC Plastics in Museums

Mary Coughlin, G. Asher Newsome, Gwénaëlle Kavich, Qiuhui Wang

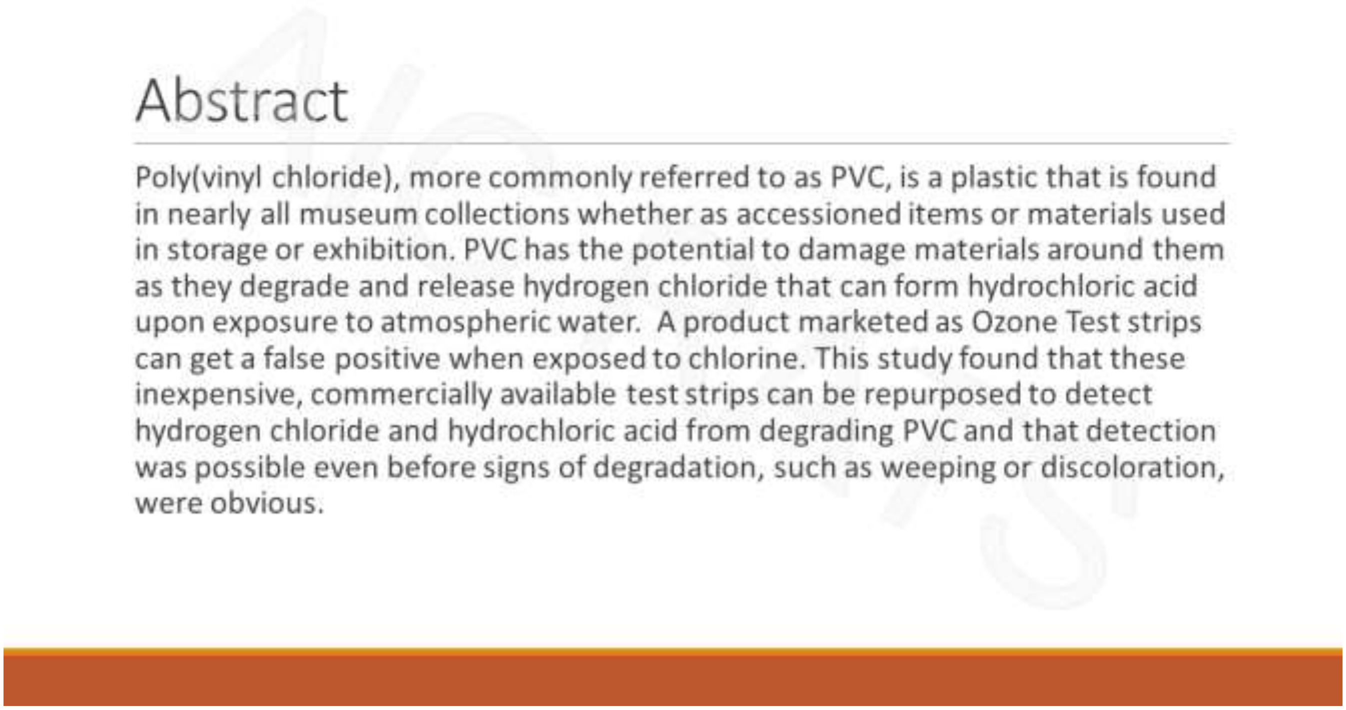

Abstract

Poly(vinyl chloride), more commonly referred to as PVC, is a plastic that is found in nearly all museum collections whether as accessioned items or materials used in storage or exhibition. PVC has the potential to damage materials around them as they degrade and release hydrogen chloride that can form hydrochloric acid upon exposure to atmospheric water. A product marketed as Ozone Test strips can get a false positive when exposed to chlorine. This study found that these inexpensive, commercially available test strips can be repurposed to detect hydrogen chloride and hydrochloric acid from degrading PVC and that detection was possible even before signs of degradation, such as weeping or discoloration, were obvious.

For the past 80 years, Poly(vinyl chloride) or PVC has been one of the most commonly used plastics in the world. PVC's popularity means that it is found in the vast majority of museum whether as works of art, examples of contemporary material culture, or as storage and exhibition products. As some PVC degrades, plasticizer migration and/or the release of acids and oxidants such as chlorine may accelerate degradation of nearby materials. Therefore, it is advantageous to identify PVC in collections. However, identifying a specific type of plastic is not easy. In the past, identification has relied on visual clues, maker's marks, and burn tests. More concrete analysis is possible with the use of analytical equipment such as pyrolysis gas chromatography –mass spectrometry (Py-GCMS), Fourier transform infrared spectroscopy (FTIR), and Raman spectroscopy. However, access to such equipment and expertise to use it is typically the domain of larger, well-funded museums. Since the majority of museums are small, understaffed, and underfunded institutions, access to scientific analysis is limited. Having an easy-to-use, inexpensive method of detecting chlorine that may be emitted from PVC would greatly benefit many museums because knowing if a plastic is emitting an oxidant could influence storage, display, and deaccessioning decisions. In spring 2018, Mary Coughlin, Assistant Professor in Museum Studies at The George Washington University, G. Asher Newsome, PhD, Physical Scientist at the Smithsonian Museum Conservation Institute, Gwénaëlle Kavich, Conservation

Scientist at the Smithsonian Museum Conservation Institute, and Qiuhui Wang, graduate student in Environmental and Green Chemistry from The George Washington University, tested commercially available Ozone Test Strips that are marketed as detectors for the presence of ozone in the environment but, according to the instructions, can get a false positive for chlorine. This project aimed to determine if Ozone Test Strips could be repurposed to detect chlorine that may be emitted from PVC. The study found that The Ozone Test strips will react to chlorine, as demonstrated by testing with hydrochloric acid solution as well as testing with a chlorine gas wafer and a hydrochloric acid permeation tube in a dynacalibrator pollutant generator. The Ozone Strips reacted to severely degrading PVC samples and to a few PVC items that still looked to be in good condition (all identified with FTIR and XRF). However because the Ozone Test Strips reacted to one non-PVC item (acrylic identified with FTIR), questions are raised about how useful the Ozone Strips are for identifying PVC and whether it is enough to use them as an indicator for oxidants coming from plastics in general. More work is planned for the fall and winter in setting up low-tech testing of plastic samples in sealed glass beakers and monitoring with the Ozone Strips. The goal of presenting at the Annual Meeting is to present results and to gather ideas for what the strips are reacting to in order to better understand the chemistry involved in these interactions and if these strips can be utilized in museum collections.

It all started with an Appendix...

Ellen Pearlstein (2017) Teaching Sustainable Collection Care, Journal of the American Institute for Conservation, 56:2, 113-125

In the JAIC special issue on Collection Care, Ellen Pearlstein noted in her article that "Ozone test strips were employed. Upon exposure to ozone, the strip turns from white to brown. The test is simple and quick (10 min) to use. However, it should be noted that the presence of other oxidative reagents, such as chlorine, may cause a false positive."

Knowing that most PVC plastics contains a high level of chlorine as part of its manufacture and that hydrogen chloride can be emitted as it degrades, got me thinking that perhaps the ozone strips could be re-purposed for the use of detecting deteriorating PVC in museum collections.

Poly(vinyl chloride) - PVC

Poly(vinyl chloride) or PVC is one of the most commonly used thermoplastic polymers in the world. Unplasticized, rigid PVC tends to be more stable than flexible PVC whose plasticizers can leach out as it degrades resulting in weeping and deformation. Pictured here you see examples of plasticized PVC that were evaluated as part of this study.

Dehydrochlorination, a reaction in which hydrogen chloride is removed is the primary degradation pathway for PVC. This is an autocatalytic reaction so if hydrogen chloride remains in the surrounding environment, the rate of degradation is accelerated. The gaseous hydrogen chloride forms hydrochloric acid with atmospheric water.

Therefore, in a museum context, knowing if PVC is emitting an oxidant such as hydrogen chloride could provide insight into how collections are aging and influence storage and display decisions.

Having an easy-to-use, inexpensive method of detection would greatly benefit the many museums who do not have access to analytical equipment for identification of plastics and their associated risks.

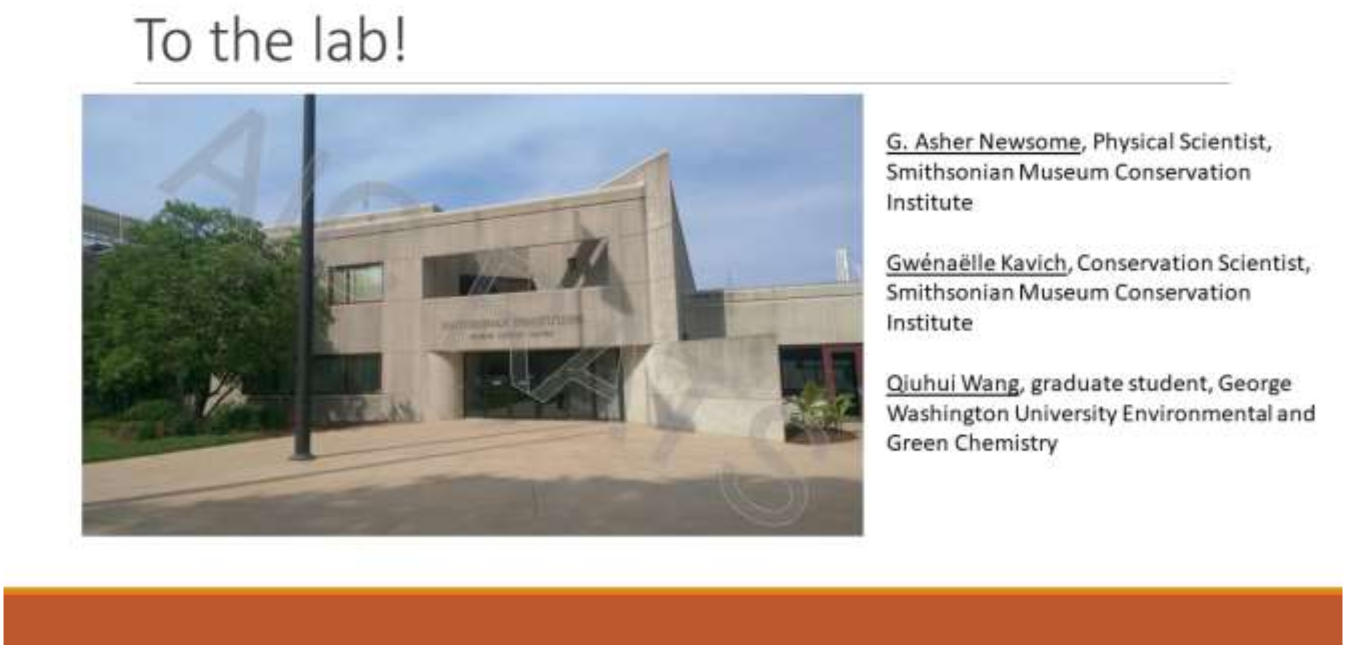

To the lab!

G. Asher Newsome, Physical Scientist, Smithsonian Museum Conservation Institute

Gwénaëlle Kavich, Conservation Scientist, Smithsonian Museum Conservation Institute

Qiuhui Wang, graduate student, George Washington University Environmental and Green Chemistry

With funding from the George Washington University's Columbian College Facilitating Fund and the assistance of scientists from the Smithsonian's Museum Conservation Institute, myself and a graduate student from the Environmental and Green Chemistry program at the university spent the winter and spring of 2018 exploring the application of Ozone Strips for plastics monitoring.

Test Strips by Macherey-Nagel

Ozone Test Strip

white → yellow → brown

potassium iodide starch paper

marketed for ozone

sensitive to other oxidants such as chlorine

Potassium Iodide Starch paper

white → blue-violet

Macherey-Nagel produces commercially available Ozone Test Strips that turn through shades of light yellowish beige to brown depending on the concentration of oxidant present. You'll notice the color scale on the side of the packaging, with the darker the reaction, the higher the concentration of oxidant.

According to the manufacturer, Ozone Test Strips are made with potassium iodide starch paper. Traditionally, potassium iodide starch produces a violet colored reaction. Since Macherey-Nagel confirmed that the Ozone Test Strips are basically potassium iodide starch, a product marketed as Potassium Iodide Starch Paper by Macherey-Nagel was purchased.

A new Potassium Iodide Starch Paper strip was analyzed with XRF and had similar peaks to a new, unreacted Ozone Test strip, however, the peaks were a smaller intensity and did not show the presence of chlorine as was seen on the Ozone strip. So, while the manufacturer indicated that the ozone strips are potassium iodide starch paper, the two products have some differences.

In testing with PVC samples, they did not perform similarly and the potassium iodide starch papers were trickier to use because they need to be wetted. Because of that and their lack of reaction, they were only briefly studied as part of this project.

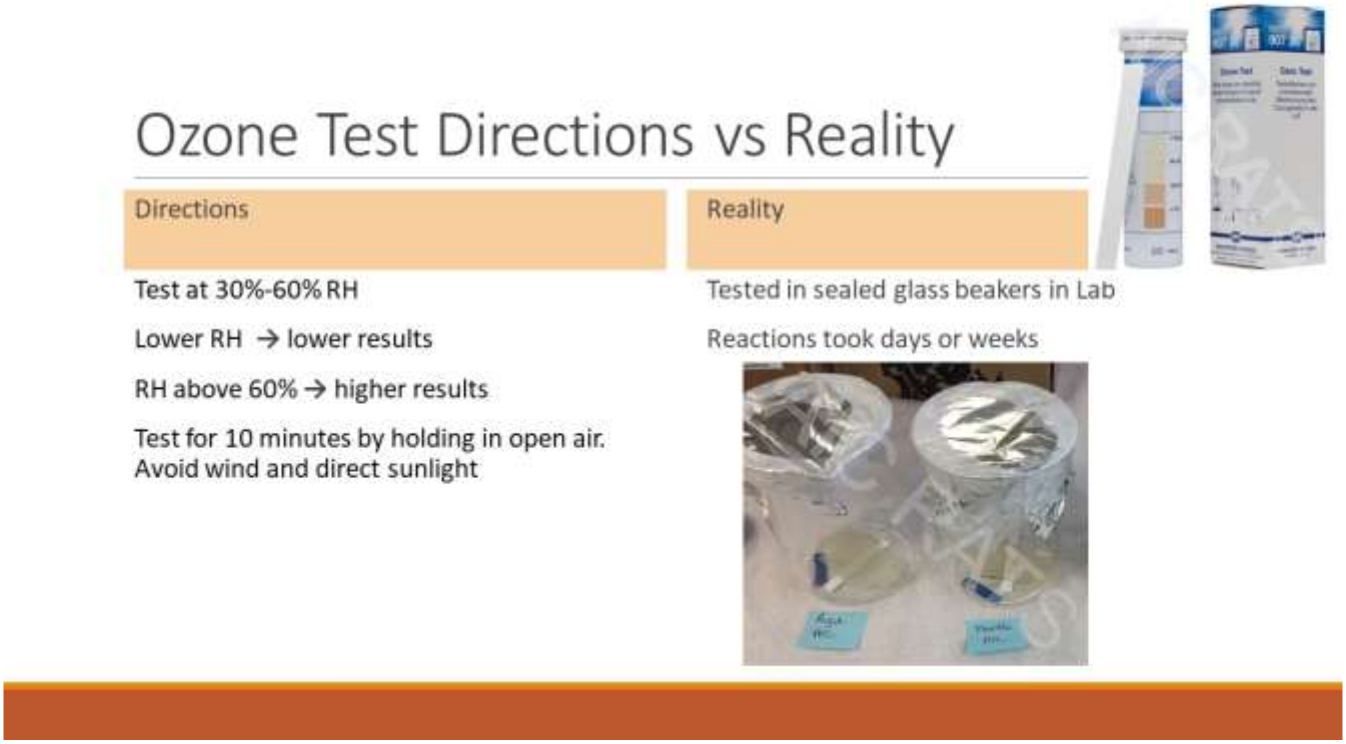

Ozone Test Directions vs Reality

Directions	Reality
Test at 30%-60% RH	Tested in sealed glass beakers in Lab
Lower RH → lower results	Reactions took days or weeks
RH above 60% → higher results	
Test for 10 minutes by holding in open air. Avoid wind and direct sunlight	

According to the directions, Ozone Strip testing should occur at 30%-60% RH with lower RH values leading to lower test results and RH above 60% resulting in higher results than are present. The test is designed to work in 10 minutes by holding in open air but avoiding wind and direct sunlight.

For purposes of our experiment, testing was conducted in glass beakers sealed with aluminum foil with Parafilm wrapped around the edges to ensure that the plastic samples were well sealed since testing showed the larger lab environment had enough oxidants present to achieve a dark brown reaction within a few hours. The RH in the lab over the winter was quite low at 8 - 15%, which is well below the ideal testing range and likely slowed the reaction when tested in the ambient environment.

For the plastic samples tested, it took a few days or even weeks to see positive results.

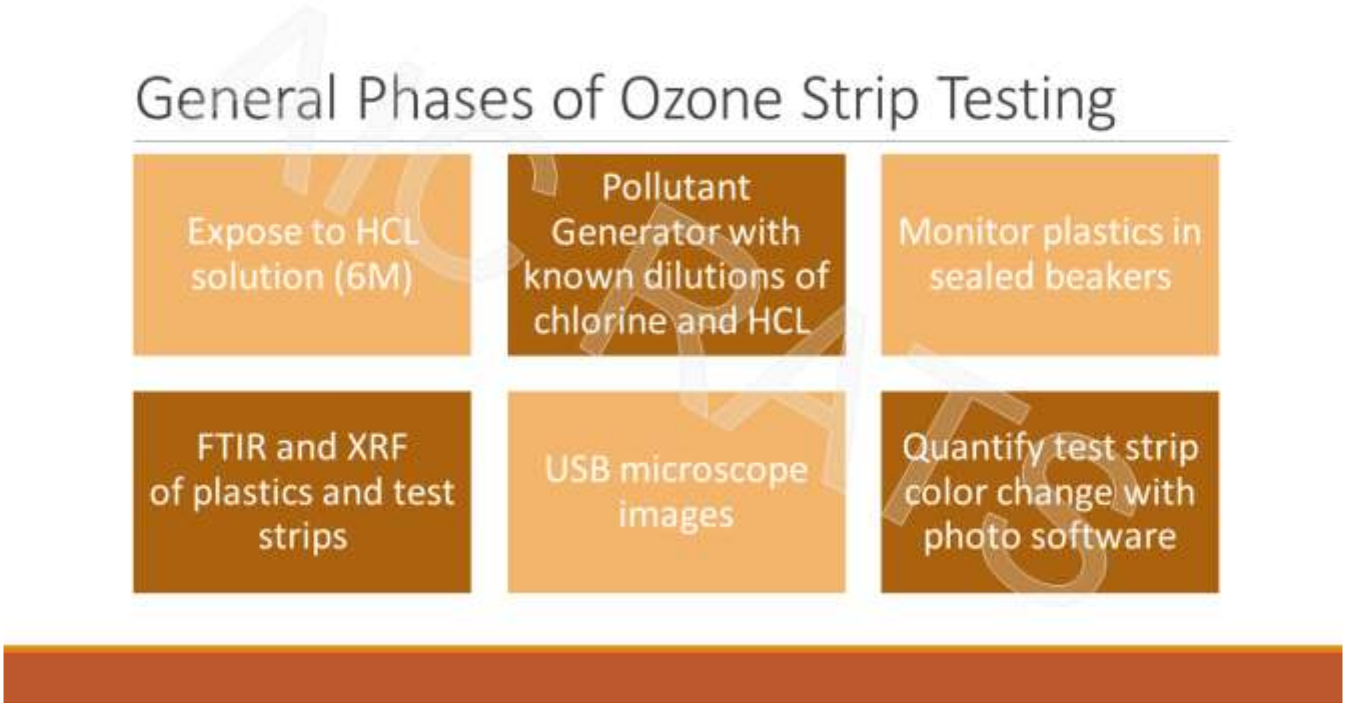

General Phases of Ozone Strip Testing

- Expose to HCL solution (6M)
- Pollutant Generator with known dilutions of chlorine and HCL
- Monitor plastics in sealed beakers
- FTIR and XRF of plastics and test strips
- USB microscope images
- Quantify test strip color change with photo software

Here are the general phases of the testing that we carried out. I won't go into details of them all today.

We wanted to make sure the Ozone strips reacted so first tested by exposing them to hydrochloric acid.

We then used a pollutant generator to evaluate the sensitivity of the stirps to chlorine.

Next we evaluated the reaction of Ozone Strips sealed in glass beakers with plastics identified with FTIR and XRF.

Images of reacted Ozone Strips were taken using a USB microscope to better see reaction locations on the strips.

Images of strips were then taken on a flatbed scanner then looked at with a raster graphics editor to loosely quantify the Red, Green, Blue color changes.

Now for more details about the testing phases…

Ozone Test Strip exposure to HCl solution (6M)

Ozone Test Strips cut to various sizes (whole, ½, ¼) and vertically hung in HCl solution bottle for 10 minutes

- After 5 minutes, see reaction around edges
- After 10 minutes, reactive square is yellow but darker at edges
- Smaller the size of the strip, quicker/darker reaction

Strips put horizontally on the opening of the bottle

- Strips reacted but lighter yellow color than those closer to HCL solution

Darker reaction at edges because of more surface area

When ozone test strips were put vertically inside a bottle of hydrochloric acid, all of the strips changed color around the edges within 5 minutes. Over time, the color reaction occurred in the center but remained darkest at edges.

Strips that were cut smaller had quicker, darker reactions likely because of the increased surface area.

When strips were placed ON the opening of the bottle rather than hanging down inside, the reaction took longer and was more subtle; confirming that the more concentrated the oxidant, the quicker and darker the reaction on the test strip.

Pollutant Generator

Dynacalibrator pollutant generator, model 230 with **acetic acid permeation tube and A-D strips**

- Set-up works!

To try to determine the sensitivity of the strips, we tested with known dilutions of chlorine and HCL acid using a pollutant generator.

The pollutant generator setup was first tested using acetic acid and A-D strips since that reaction is well established. This testing confirmed that the test design with the pollutant generator worked!

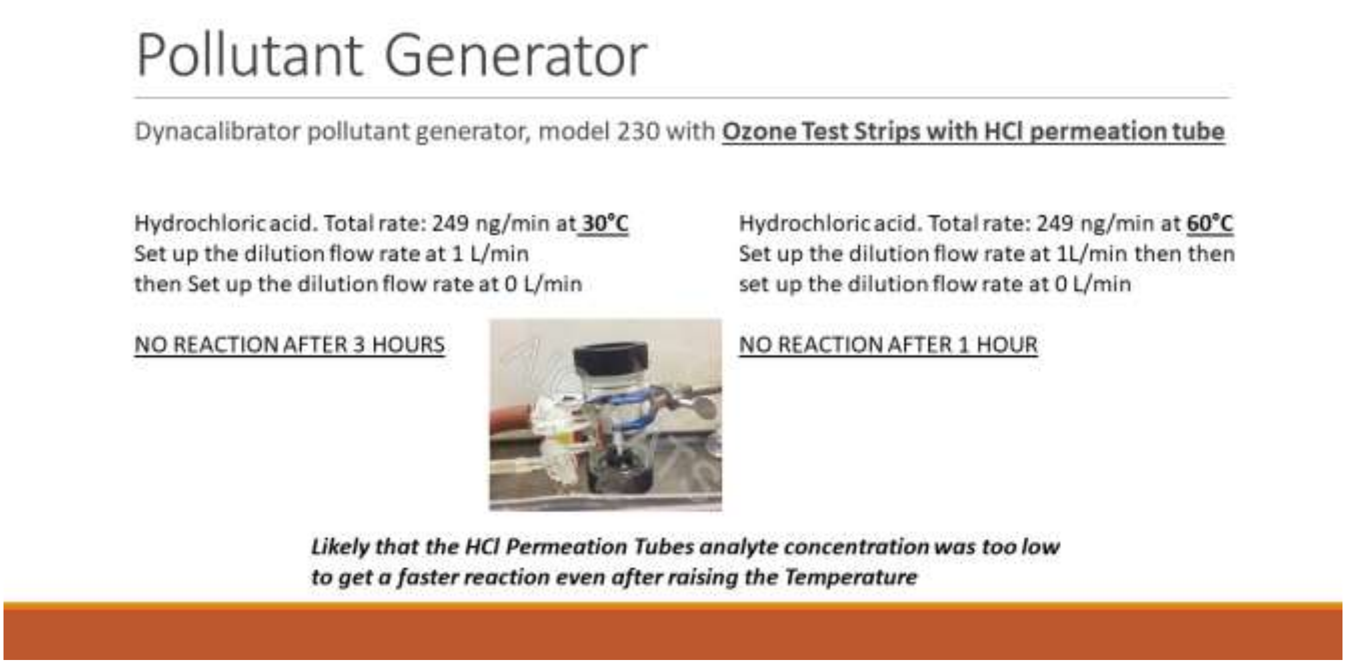

Pollutant Generator

Dynacalibrator pollutant generator, model 230 with Ozone Test Strips with HCl permeation tube

Hydrochloric acid. Total rate: 249 ng/min at 30°C
Set up the dilution flow rate at 1 L/min
then Set up the dilution flow rate at 0 L/min

NO REACTION AFTER 3 HOURS

Hydrochloric acid. Total rate: 249 ng/min at 60°C
Set up the dilution flow rate at 1L/min then then
set up the dilution flow rate at 0 L/min

NO REACTION AFTER 1 HOUR

Likely that the HCl Permeation Tubes analyte concentration was too low to get a faster reaction even after raising the Temperature

We then moved onto testing Ozone Strips with a hydrochloric acid permeation tube in the pollutant generator. However, we could not achieve a reaction.

After speaking with a chemist from the company, it seems likely that the hydrochloric acid permeation tube analyte concentration was too low to get a reaction that was quick enough for us to observe, even after raising the temperature in an effort to drive the reaction.

For me, this was a lesson learned to ask to talk to a chemist rather than the sales rep when ordering! I just didn't ask the right questions. But thankfully, the chemist guided me towards an option that yielded results.

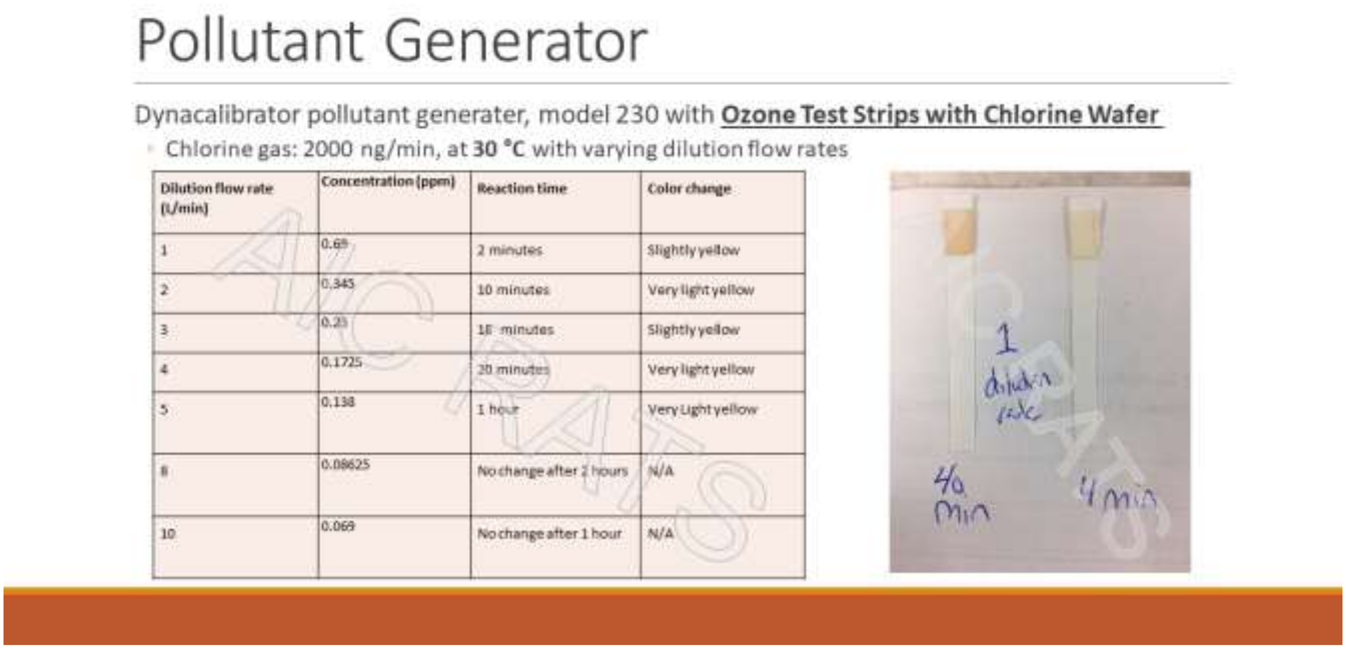

Pollutant Generator

Dynacalibrator pollutant generater, model 230 with **Ozone Test Strips with Chlorine Wafer**

- Chlorine gas: 2000 ng/min, at **30 °C** with varying dilution flow rates

Dilution flow rate (L/min)	Concentration (ppm)	Reaction time	Color change
1	0.69	2 minutes	Slightly yellow
2	0.345	10 minutes	Very light yellow
3	0.23	18 minutes	Slightly yellow
4	0.1725	20 minutes	Very light yellow
5	0.138	1 hour	Very Light yellow
8	0.08625	No change after 2 hours	N/A
10	0.069	No change after 1 hour	N/A

We then tested the strips in the pollutant generator with a chlorine wafer.

This showed that the ozone test strips are reactive to chlorine and that the higher the concentration, the faster the reaction. And the longer the testing time at a high concentration, the darker the reaction.

These results again showed that the edges of the strip are more reactive likely because of the increased surface area.

For the results in the table, the testing was stopped as soon as a visible reaction was noticed which is why all the of the color changes are noted as slightly yellow or very light yellow. The testing of lower concentrations were abandoned after a few hours but it could be that reactions would occur if testing had continued.

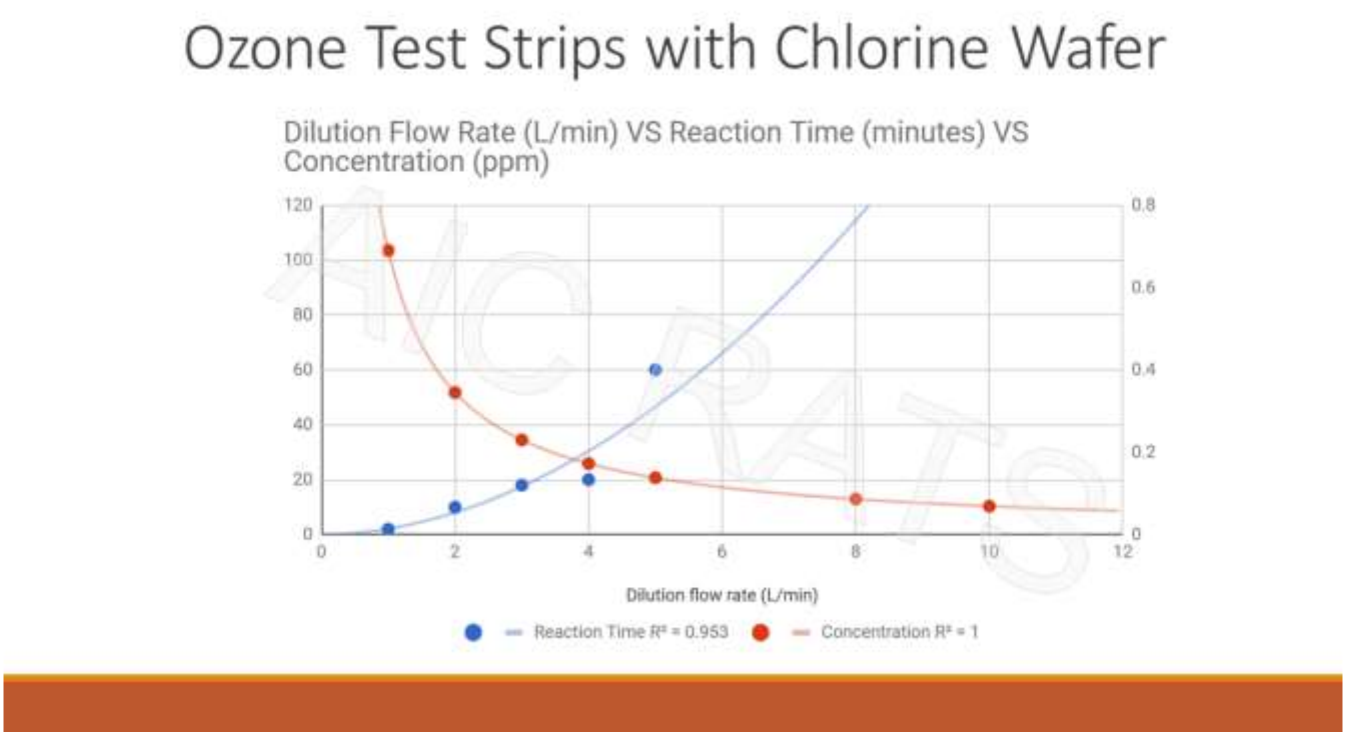

Ozone Test Strips with Chlorine Wafer

Here is a graph showing the results from the previous chart. Again, the more concentrated the chlorine, the faster the reaction.

Note that the reaction time listed for the chlorine gas may not be exactly accurate because of non-continuous visual monitoring. The Reaction Time value of 0.953 is pretty good for visual inspection which for us indicated that the strips have potential in real world monitoring.

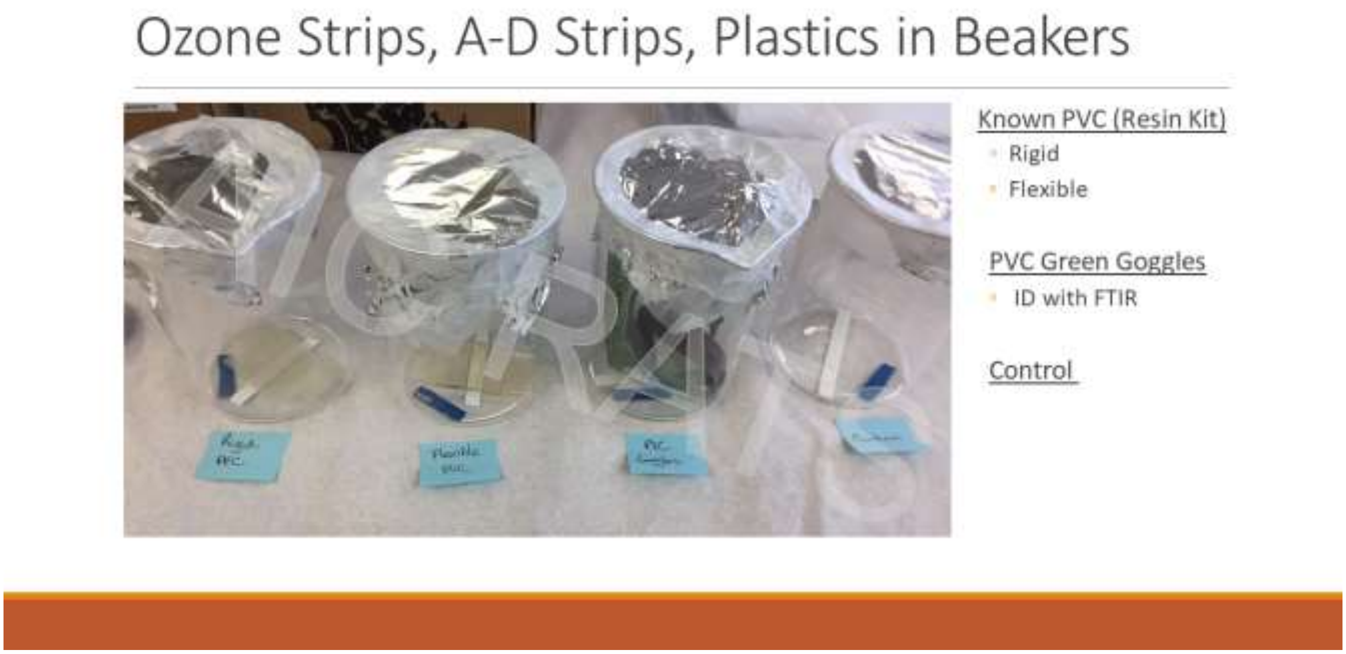

Ozone Strips, A-D Strips, Plastics in Beakers

Known PVC (Resin Kit)
- Rigid
- Flexible

PVC Green Goggles
- ID with FTIR

Control

We started testing in glass beakers with 3 known samples of PVC as well as a control. All beakers were sealed with aluminum foil wrapped in parafilm around the edges. Ozone test strips and A-D strips were placed in each beaker.

Rigid and Flexible PVC from the Resin Kit of known plastic samples as well as green safety goggles identified with FTIR as having flexible PVC sides were chosen for the first round of testing that lasted for 2 weeks.

Ozone Strips, A-D Strips, Plastics in Beakers

2 weeks testing

Equal results at top and bottom

Since Chlorine is denser than air, in initial testing, test strips were placed at the top and bottom of the beakers to see if there would be a difference in the results

As you can see, there was no difference so testing proceeded with monitoring strips on the bottom only.

Ozone Strips, A-D Strips, Plastics in Beakers

Control

No reaction

Seal edges of aluminum foil with Parafilm

For the control, there was no reaction for the Ozone Strips or A-D strips.

The lack of reaction of the Ozone Strips confirms that the tests were well sealed because the strips reacted within hours to the ambient environment in the lab. Earlier tests that did not seal the edges of the aluminum foil with parafilm resulted in reacted Ozone Strips.

Ozone Strips, A-D Strips, Plastics in Beakers

Rigid PVC from 20 year old Resin Kit

No reaction of Ozone Strip or A-D strip

Rigid, unplasticized PVC is more stable than flexible, plasticized PVC

Rigid PVC from the Resin Kit of known plastics did not react - which is not surprising since rigid, unplasticized PVC is more stable than flexible PVC

Ozone Strips, A-D Strips, Plastics in Beakers

Flexible PVC from 20 year old Resin Kit (confirmed with FTIR), weeping, warped

Slight reaction of Ozone Strips after one day

Increased reaction after 4 days and 7 days

A-D strips no reaction

Flexible, plasticized PVC from the Resin Kit was weeping and warped, which are visual signs of deterioration.

The Ozone Strip slightly reacted after one day, seen here, and the reaction increased after 4 days and one week.

Ozone Strips, A-D Strips, Plastics in Beakers

PVC Green Goggles (FTIR), weeping

Reaction of Ozone Strips after one day

Increased reaction after 4 days and 7 days

A-D strips no reaction

Green safety goggles with PVC sides that were weeping and tacky were also monitored.

There was a positive reaction of the ozone strip noticeable after one day, seen here, and a slight increase in change at day 4 and day 7

The A-D strips did not change which may indicate that acidic off-gassing is not occurring or is below the detection limit.

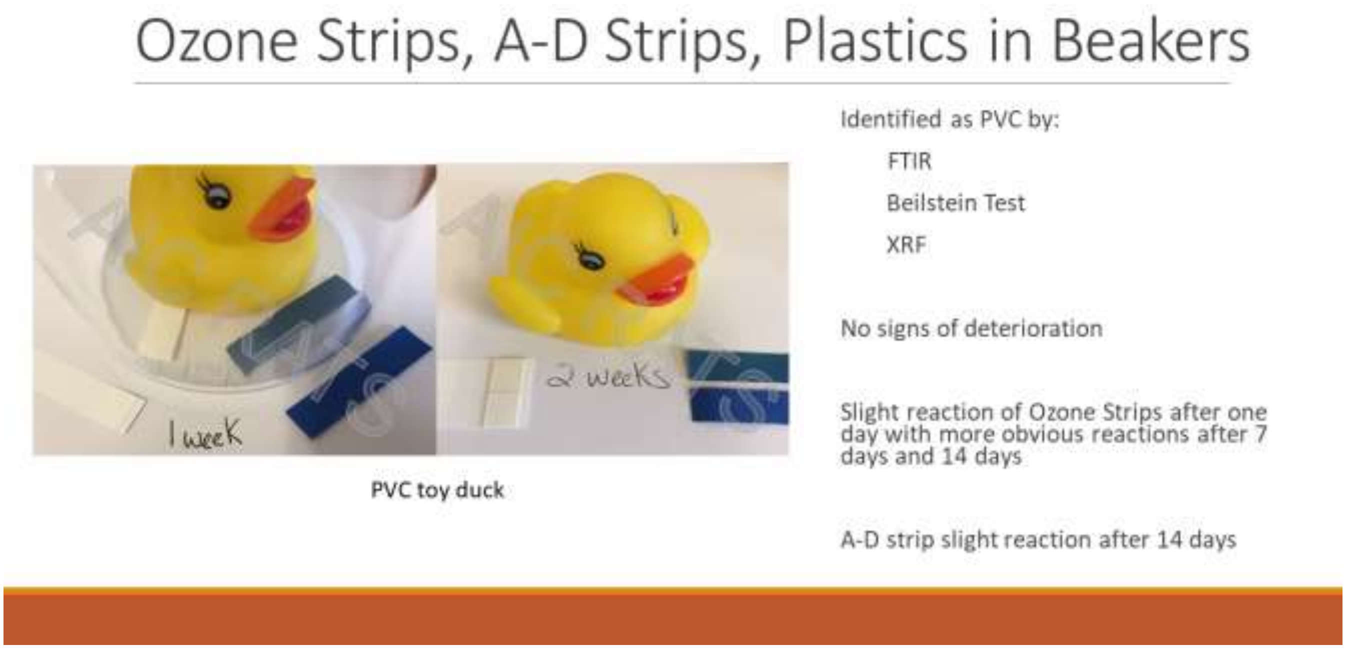

Ozone Strips, A-D Strips, Plastics in Beakers

PVC toy duck

Identified as PVC by:

- FTIR
- Beilstein Test
- XRF

No signs of deterioration

Slight reaction of Ozone Strips after one day with more obvious reactions after 7 days and 14 days

A-D strip slight reaction after 14 days

This duck bath toy had no observable signs of deterioration. It was not weeping, tacky, distorted, and there was no noticeable odor.

It was previously identified as PVC using the Beilstein burn test for halogens and XRF detected the presence of chlorine. FTIR confirmed the duck as PVC.

The Ozone strip reacted after one day and the color change increased over the course of 2 weeks.

The A-D strips did not appear to change until 2 weeks though this could have been caused by light exposure.

PVC Duck
Ozone Strips, 220x magnification

PVC yellow duck, 1 week exposure

Control

Here you see images of ozone test strips exposed to the yellow duck taken with a USB microscope. It is interesting that unaided, the reaction of the strip after one week seemed more subtle but when viewed with magnification, the reaction is more obvious. The reaction is darker around the edges, as expected.

For those keen and observant folks in the audience, you may be wondering how I took images at one week when I just told you I monitored the toy duck for two weeks. Well, rest assured, there were several rounds of monitoring to make sure I could be confident in the results and the two week test was not compromised to get these images!

Ozone Test Strip Scans

CONTROL

Hue: 160 Sat: 0 Lum: 240 Red: 255 Green: 255 Blue: 255

DUCK 1 WEEK

Hue: 34 Sat: 153 Lum: 230 Red: 251 Green: 249 Blue: 237

Microsoft Paint raster graphics editor RGB results

I then scanned the strips on a flatbed scanner at 600 dpi and used Microsoft Paint raster graphics editor to compare the Red, Green, Blue color results of reacted strips to brand new, control strips in order to quantify the reactions.

The greater the degree of reactions observed under normal viewing, meaning the more yellow they were, the greater the deviation from the RGB designation of 255 on the control strip.

I also played around with the scans in Photoshop and generated histograms but I preferred the simplicity of the color visuals from the Microsoft Paint software.

Ozone Strips, A-D Strips, Plastics in Beakers

PVC Clear Goggles (FTIR and XRF), weeping, discolored

Reaction of Ozone Strip after 1 day

Increased reaction after 4 days and 7 days (image)

A-D strip had slight reaction (turquoise).

Reactions after 7 days in 2018

Clear goggles with flexible, weeping, discolored sides that were identified as PVC with FTIR, and the presence of chlorine was detected with XRF, were monitored with Ozone strips and A-D strips.

The ozone strip noticeably reacted after one day and the reaction progressed over the course of the week to the level you see here. The darker reaction along the edges is particularly obvious.

After 7 days, the A-D strip shifted from the original dark blue to be more turquoise indicating that acidic off-gassing is present.

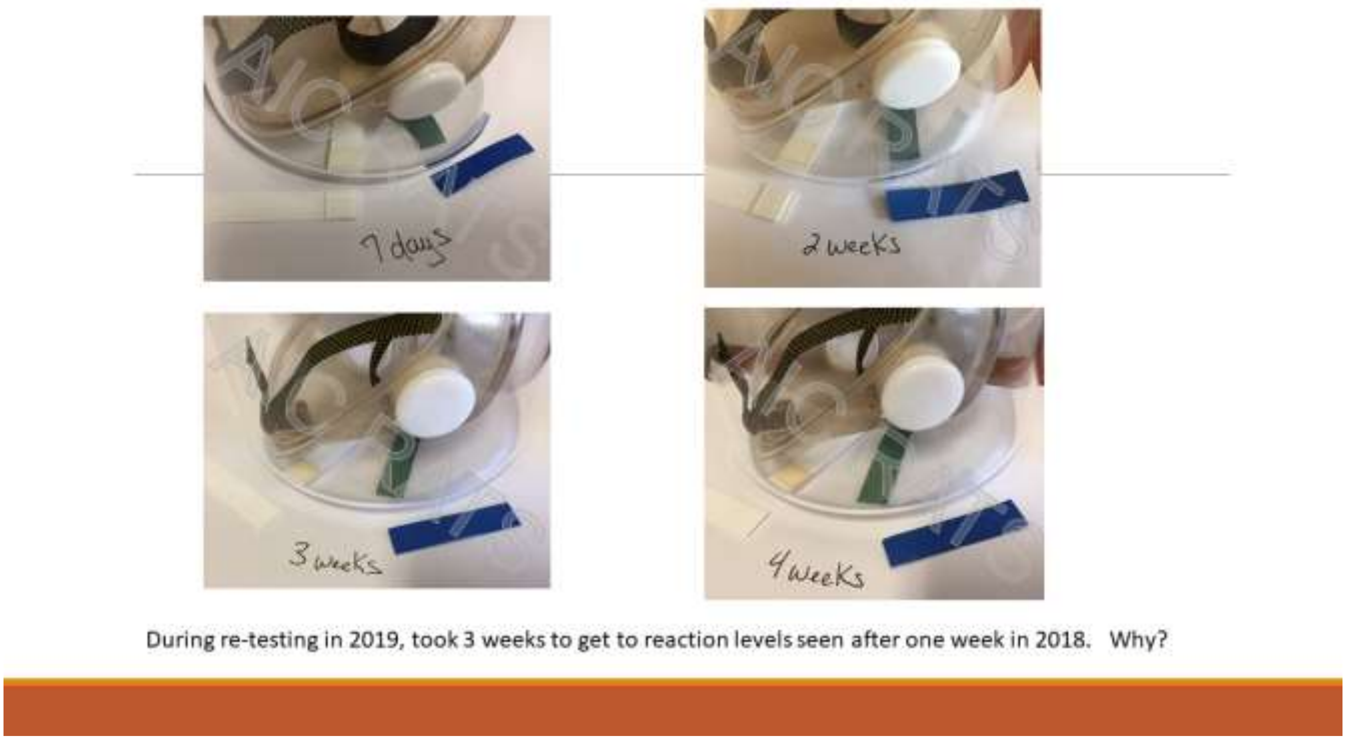

During re-testing in 2019, took 3 weeks to get to reaction levels seen after one week in 2018. Why?

In a second phase of testing this past winter and spring, about a year after the testing results you just saw, the reaction of the Ozone Strip was less obvious and it took 3 weeks to get to the same color reaction that had been previously noted after just one week.

Why was this?!

It should be noted that the A-D strip mimicked the results of the previous year at the one week point and turned greener as testing continued over the month.

Ozone Strips, A-D Strips, Plastics in Beakers

Ventilation for about 6 months before first retesting in 2019.

Did ventilation reduce oxidant concentration? Did this slow reaction of the ozone strip?

Re-tested again: Wrapped up in aluminum foil for 4 months. Results mimicked original reactions observed in 2018.

2018, 7 days

2019 1st test

2019 2nd test, 7 days

In order to understand the different results of the Ozone Strip, I reflected on what I did with the clear goggles after the initial testing last year. After I packed up from testing in the MCI lab, I left the goggles in the open for about 6 months before retesting in 2019.

I speculate that the ventilation reduced the oxidant concentration and slowed the reaction of the ozone strip. Which, seems to support general recommendations that ventilation can be beneficial for many deteriorating plastics.

I then wrapped the goggles in aluminum foil for 4 months and tested again. Sure enough, these results mimicked the original dark reaction observed after 7 days. And actually appeared to be a bit darker!

So, for moving forward, I need to figure out how this impacts testing duration recommendations and if it is advisable to wrap plastics for a period of time to concentrate any oxidants that may be present to expedite testing.

Ozone Strip Scans

CONTROL

GOGGLES 1 WEEK

GOGGLES 8 WEEKS

Microsoft Paint raster graphics editor RGB results

And here are scans of the ozone strips used to test the clear goggles after one week and after two months.

Remember that the RGB allocation for the control strip is 255 and you can see how the red, green, and blue divergence from that is greater as the reaction got darker.

Over time, the reaction of the strip became more even. It should be noted that the color readings for the scans were taken in the upper left corner rather than in the center because the edges of the strips are more reactive.

PVC Clear Goggles
Ozone Strips, 220 magnification

Clear Goggles, 1 week

Clear Goggles, 8 weeks

Here under magnification, you can also see that the reaction became more uniform over time.

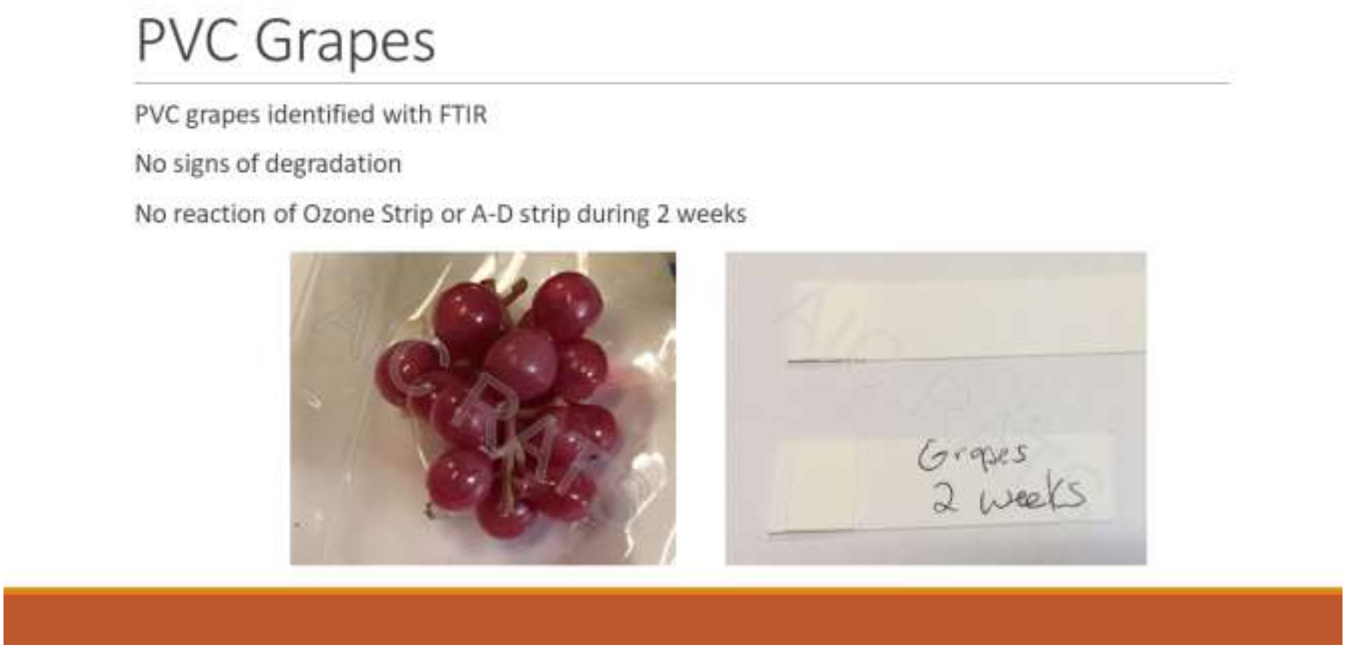

PVC Grapes

PVC grapes identified with FTIR

No signs of degradation

No reaction of Ozone Strip or A-D strip during 2 weeks

A cluster of PVC grapes purchased from a craft store over 10 years ago were tested. The grapes are still in good condition with no obvious signs of degradation.

Neither the A-D strip nor the Ozone Strip reacted after 2 weeks of testing.

To me, this indicates that ozone strips can't be used to identify PVC in general but rather can be used to identify degrading PVC that is releasing an oxidant

This is an important distinction.

Ozone Strips, A-D Strips, Plastics in Beakers

Red Foam (Polyurethane?)

Degrading – doesn't bounce back

Strong Odor

A-D strip turned turquoise after 2 days

No reaction with Ozone Strip after 7 days

In December when I was unpacking Christmas ornaments with my family, I smelled an acrid smell that I was pretty sure was degrading polyurethane. I then found the culprit: this piece of red foam that was part of packaging from an ornament dated as 2001. It is not surprising that a piece of almost 20 year old foam would be having issues!

When I pushed on the foam, it no longer bounced back, which is another common sign of polyurethane foam deterioration.

I then decided to take the foam and test it in a glass beaker with an A-D strip and an Ozone Strip. The A-D strip turned turquoise after 2 days and after one week, the ozone strip still did not react at all.

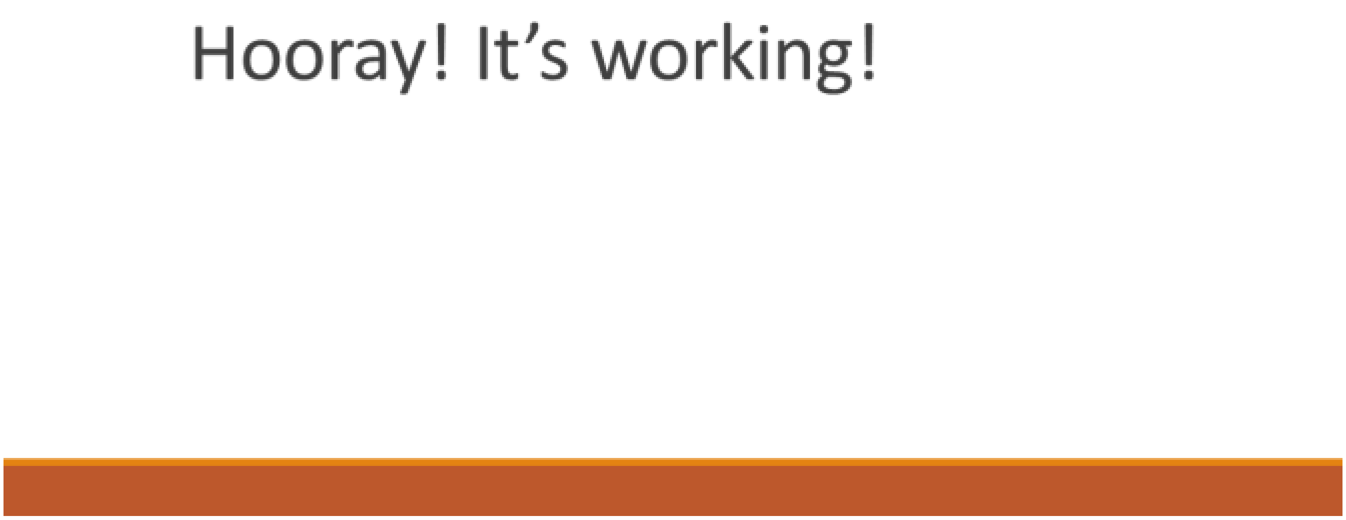

Hooray! It’s working!

To me this was exciting because it meant that the ozone strips seem to be sensitive to oxidizers that can be emitted from PVC rather than sensitive to all deteriorating plastics.

So, the strips could have a role in identifying degrading PVC even before visual signs of deterioration are obvious, as was seen with the yellow duck.

Or is it….

And then I tested a butter dish…

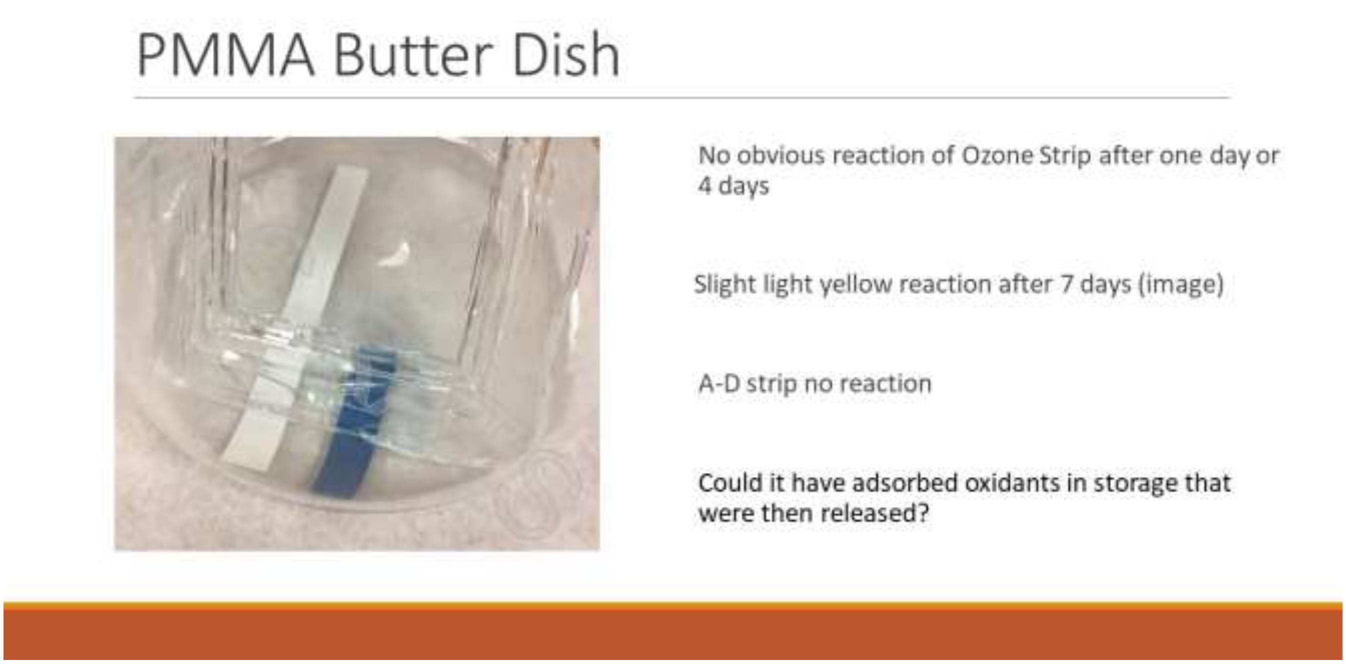

PMMA Butter Dish

No obvious reaction of Ozone Strip after one day or 4 days

Slight light yellow reaction after 7 days (image)

A-D strip no reaction

Could it have adsorbed oxidants in storage that were then released?

The butter dish was identified with FTIR as Poly(methyl methacrylate) more commonly referred to as acrylic. It made its way into my plastic study collection because my husband put it into the dishwasher and an impressive network of cracks formed in it.

During testing, the A-D strip never reacted which is encouraging because we consider acrylic to be stable.

However, after one week there seemed to be a very slight reaction of the Ozone Strip. Could it be that it adsorbed oxidants from my haphazard method of storing mixed plastics in a single box over the course of a decade? Could the increased surface area from the extensive cracking enabled it to adsorb oxidants?

At that point we pulled it out from testing and analyzed it with XRF but no chlorine was detected nor was anything unexpected present.

PMMA Butter Dish

1 week 2 weeks 3 weeks
5 weeks

In the original 2018 tests, the acrylic butter dish went from being stored with a mixture of plastics (including degrading PVC) to directly being sealed in the beaker for testing.

In 2019, the butter dish was left in the open for one week before testing.

Retesting did not have noticeable results in the Ozone strip or A-D strips until 5 weeks and even then I was questioning if there was a color change in the ozone strip.

It is assumed that the A-D strip reaction could have more to do with light fading than an actual positive reaction for acidic off-gassing.

PMMA Butter Dish
Ozone Strips, 220x magnification

Butter dish, 5 weeks

Control

Here is the magnified ozone strip exposed to the acrylic butter dish for 5 weeks compared to a control. You can see that even at the more reactive edges, there does not seem to be a positive reaction.

Ozone Strip Scans

Hue: 160 Sat: 0 Lum: 237 Red: 252 Green: 252 Blue: 252

Hue: 160 Sat: 0 Lum: 240 Red: 255 Green: 255 Blue: 255

Microsoft Paint raster graphics editor RGB results

I then scanned the strip to get the RGB color readings. The RGB readings for the strip exposed to the acrylic butter dish for 5 weeks had values of 252 for red, green, and blue. This is a deviation from the 255 RGB readings from the control strip.

Is this a change?

Microsoft Paint raster graphics editor RGB results

But in taking various readings on different control strips, I could get some variety in the RGB color scale as you see here.

So, did this strip change? Is a reaction this subtle or questionable a positive reaction?

And if it is, what does a positive reaction of the ozone strip to acrylic say for the applicability of these test strips in museums?

Does it reiterate the importance of monitoring plastics in collections for signs of degradation? Then isolating them when possible? Does ventilation have a key role in preventing the build up of acidic off-gassing and oxidants from degrading plastics that can then be adsorbed by other materials in the vicinity?

For me, those are the takeaways.

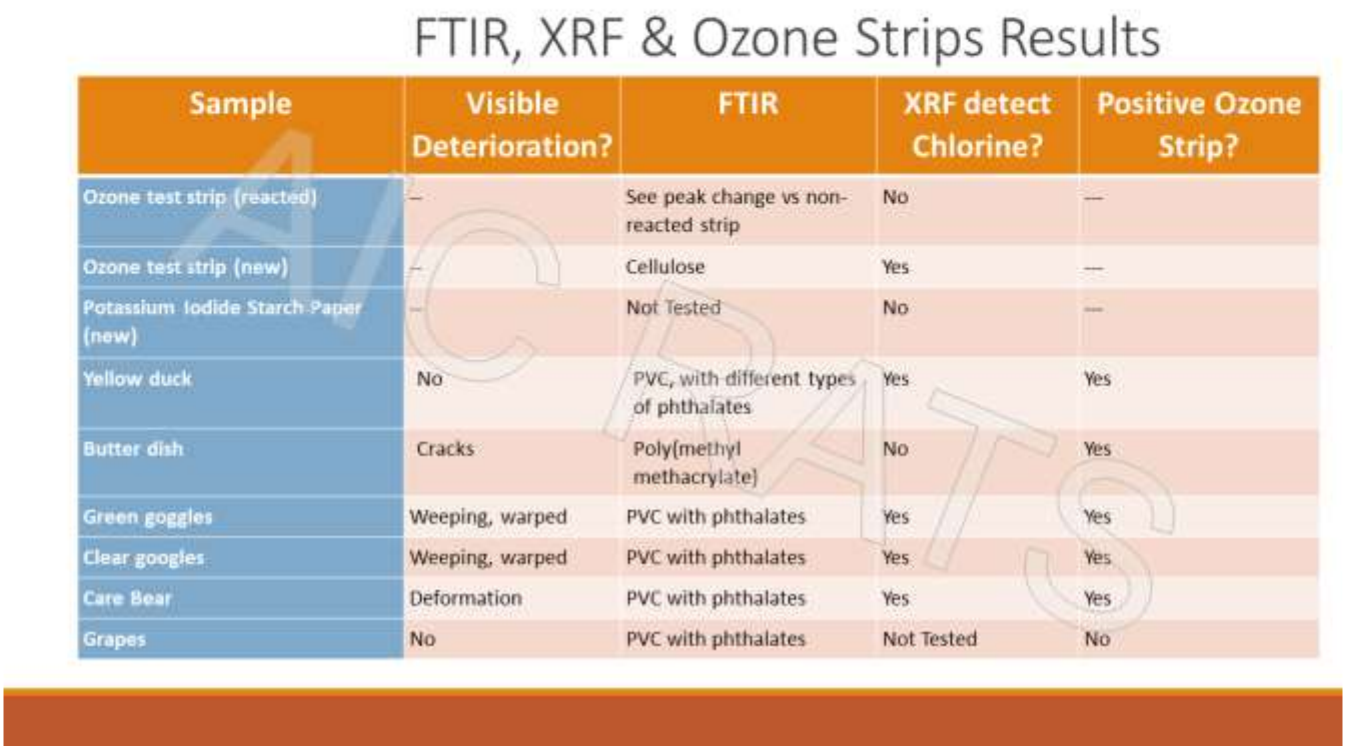

FTIR, XRF & Ozone Strips Results

Sample	Visible Deterioration?	FTIR	XRF detect Chlorine?	Positive Ozone Strip?
Ozone test strip (reacted)	—	See peak change vs non-reacted strip	No	—
Ozone test strip (new)	—	Cellulose	Yes	—
Potassium Iodide Starch Paper (new)	—	Not Tested	No	—
Yellow duck	No	PVC, with different types of phthalates	Yes	Yes
Butter dish	Cracks	Poly(methyl methacrylate)	No	Yes
Green goggles	Weeping, warped	PVC with phthalates	Yes	Yes
Clear googles	Weeping, warped	PVC with phthalates	Yes	Yes
Care Bear	Deformation	PVC with phthalates	Yes	Yes
Grapes	No	PVC with phthalates	Not Tested	No

I thought it would be helpful at this point to review testing results on various plastic samples utilized in this study.

This table lists each sample object, FTIR identification, whether chlorine was detected with XRF, and if the ozone strip had a positive reaction.

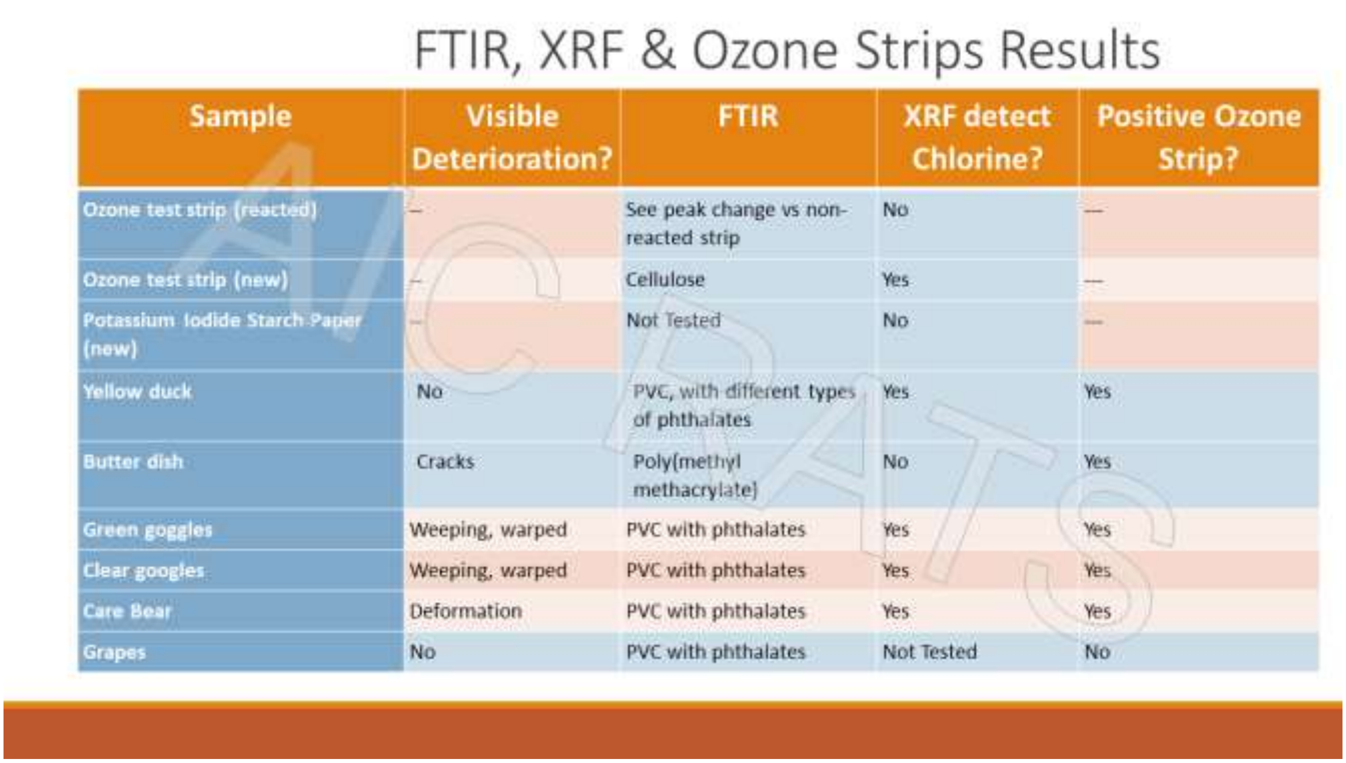

FTIR, XRF & Ozone Strips Results

Sample	Visible Deterioration?	FTIR	XRF detect Chlorine?	Positive Ozone Strip?
Ozone test strip (reacted)	—	See peak change vs non-reacted strip	No	—
Ozone test strip (new)	—	Cellulose	Yes	—
Potassium Iodide Starch Paper (new)	—	Not Tested	No	—
Yellow duck	No	PVC, with different types of phthalates	Yes	Yes
Butter dish	Cracks	Poly(methyl methacrylate)	No	Yes
Green goggles	Weeping, warped	PVC with phthalates	Yes	Yes
Clear googles	Weeping, warped	PVC with phthalates	Yes	Yes
Care Bear	Deformation	PVC with phthalates	Yes	Yes
Grapes	No	PVC with phthalates	Not Tested	No

XRF of the test strips led to some questions. Why do new Ozone Test Strips have chlorine but it is not present in the reacted strips? What is the chemistry of the positive reaction on the strip?

Why did the new Potassium Iodide Starch Paper not show chlorine if the Ozone Test Strips are also potassium iodide starch? What is the difference in their manufacture? Since testing of the papers did not mimic each other, there is clearly a difference between the ozone test strip and Potassium Iodide Starch Paper even if the manufacturer indicated that the ozone strips are potassium iodide starch papers.

It was surprising that the acrylic butter dish had a slight reaction to the ozone strip but it could be that the reaction had more to do with increased surface area from the cracks and long-term exposure to deteriorating PVC. It seems possible that the acrylic dish adsorbed enough oxidants to cause a reaction of the strip. Ventilation reduced the reaction of the test strip to the point where it was not even clear if it did react. This seems to support ventilation as a recommended practice for many deteriorating plastics in museum collections.

The PVC grapes did not have a positive reaction with the Ozone test strips after 2 weeks of testing. So, the strips can't be counted on to identify PVC but rather can be used to detect the presence of an oxidant released from deteriorating PVC. As seen with the yellow duck, the presence of an oxidant that is detectable with the strips is possible even before other signs of PVC deterioration are obvious, which is pretty exciting.

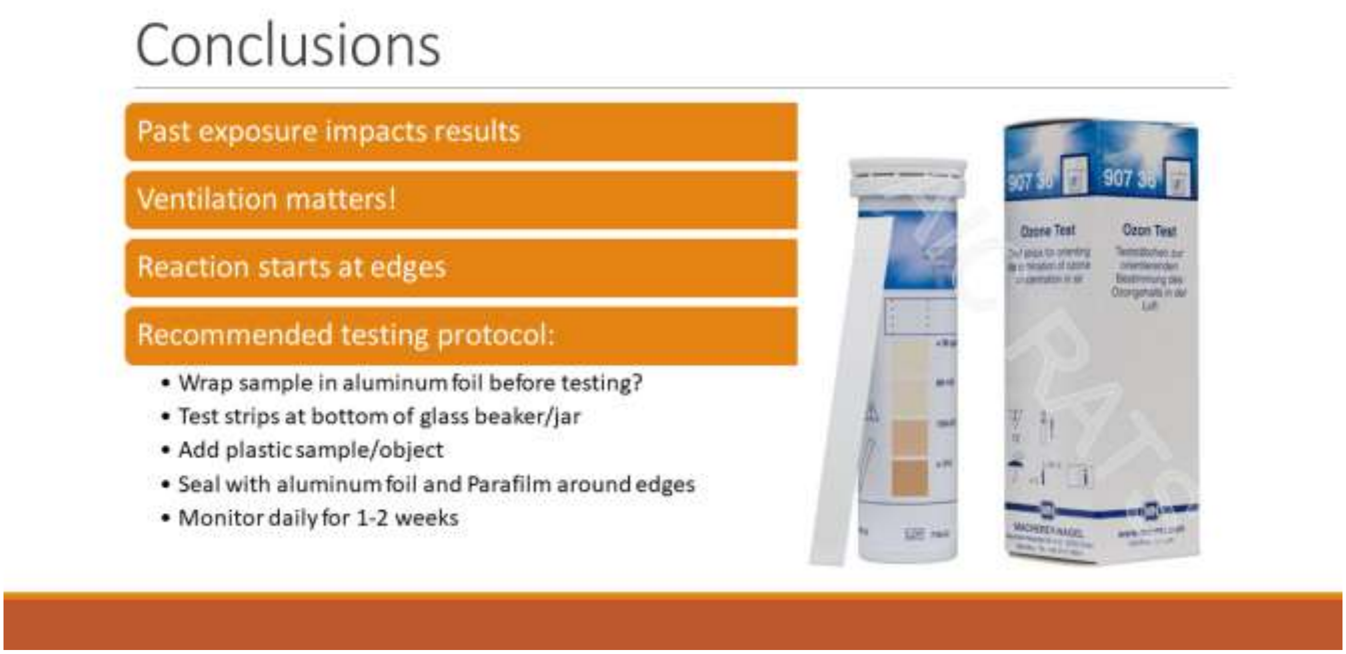

Conclusions

Past exposure impacts results

Ventilation matters!

Reaction starts at edges

Recommended testing protocol:

- Wrap sample in aluminum foil before testing?
- Test strips at bottom of glass beaker/jar
- Add plastic sample/object
- Seal with aluminum foil and Parafilm around edges
- Monitor daily for 1-2 weeks

So, to summarize:

Plastics or other adsorbent materials that were exposed to oxidizing agents, such as those released from degrading PVC, can get a positive reaction on ozone strips. This reinforces the need to identify plastic types in museum collections to understand their vulnerabilities and the risks they pose to nearby materials.

As observed in this testing, ventilation reduces the concentration of oxidizers and acids and, therefore, can be an impactful option for the storage and display of plastics.

The Ozone Strips are more reactive around the edges because of greater surface area so this is where you would first see a change from white to yellowish beige to brown. The longer the monitoring, the more even the color change on the strip. It may help to concentrate potential oxidants by wrapping the test sample in aluminum foil for a few days before testing.

One week should be the minimal time for monitoring but you will want to do daily checks. And make sure to seal the beaker so you don't get a false positive from ambient conditions. In our testing, sealing with aluminum foil and parafilm worked well.

Comparing a used test strip with a new one can help determine if a change occurred. Looking at the strips under magnification can help confirm unaided visual observations but for the most part, a change was obvious without magnification.

In conclusion, ozone strips seem promising as a low-tech, accessible monitor for identifying PVC that is emitting an oxidant but if PVC degradation has not started, a reaction will not occur. But that does NOT mean that those are stable plastics that you don't have to worry about! It just means you should periodically monitor them over time.

As we have seen and as we know, PVC is a malignant plastic that should not be ignored!

Thank you!

Smithsonian

G. Asher Newsome, Physical Scientist, Smithsonian Museum Conservation Institute

Gwénaëlle Kavich, Conservation Scientist, Smithsonian Museum Conservation Institute

GW

Qiuhui Wang, graduate student, George Washington University Environmental and Green Chemistry

George Washington University's Columbian College Facilitating Fund

I want to again acknowledge the help and work of Asher Newsome and Gwen Kavich from MCI as well as Lucy Wang who graduated from the Environmental and Green Chemistry graduate program at GW

Sources of Materials

A-D Strips, Image Permanence Institute
https://www.imagepermanenceinstitute.org/imaging/ad-strips

Ozone Test strips: https://www.mn-net.com/tabid/10494/default.aspx Available from Amazon.

Potassium Iodide Starch Paper MN 616 T: https://www.mn-net.com/tabid/10444/default.aspx Available from Amazon

Emission of New Plasticizers from Polymers: Evaluation of the Degradation and Life-Time Prediction of Soft-PVC Objects in Museums Collections

Patricia Schossler

Introduction Due to its economical and technical importance, poly vinyl chloride (PVC) is one of the most produced and consumed plastics since the 1950s. Recent surveys pointed out the consequent increasing presence of soft-PVC in museums collections, as well as the fast and remarkable degradation of objects made from or containing soft-PVC. The degradation of plasticized PVC is directly related to dehydrochlorination accompanied by diffusion of the plasticizer through the polymer matrix, deposit at the surface of the object and further emission in the environment. This results in tacky surface, stiffening, tearing, embrittlement and discoloration of the soft-PVC object. Esters of phtalic acids were widely used as plasticizers until the beginning of the 1980s, when "alternative or non-phthalate plasticizers" were introduced in the market as substitutes for the controversial mutagenic phthalates. In this work the long term emission profile of three alternative plasticizers from soft-PVC samples was measured, in order to verify the quantity of plasticizer emitted over a long period of time as well as to monitor of changes in optical and mechanical properties of the soft-PVC samples under study. Experimental Results Three soft-PVC samples were provided by artists: sample PVC1 was plasticized with diisononylphthalate (DiNP), sample PVC2 presented 1,2-cyclohexane dicarboxylic acid diisononyl ester (DINCH) as plasticizer and in the sample PVC3, diethyl citrate (DEC) was identified as plasticizer. The plasticizers emission measurements were realized using a Field and Flow Emission Cell (FLEC) with an air exchange rate of 269 h-1. The sampling took place every week during 5 months and was accomplished using glass wool absorption tubes. The measurement of the loaded collecting phase was done by thermal desorption and GC/MS. The plasticizers presented a similar long-term emission profile with an increasing loss of plasticizer during the first 4 weeks, after which the steady-state was reached and the constant plasticizer loss rate observed was in accordance with the vapor pressure of the compounds under study. After accelerated ageing, tacky surfaces and stiffening were observed in all the samples. PVC3 presented the major yellowing among the samples, which could be justified by the presence of DEC as biodegradable plasticizer. At the aesthetic change corresponded a structural degradation, as it was confirmed by an increase in stiffness and a decrease in the strain at break of all the samples. Sample PVC3 was the most degraded, while samples PVC2 and PVC1 presented similar degradation profile after the accelerated thermal ageing. Conclusions The results showed a major and considerable susceptibility to degradation of sample PVC3, if compared to samples PVC2 and PVC1. Considering previous researches related to the emission of the banned plasticizer di-2-ethylhexyl phthalate (DEHP) from soft-PVC samples, only the sample plasticized with DiNP presented a lower emission potential. Consequently, it is to expect a faster degradation and consequent shorter lifetime of PVC objects plasticized with DINCH and DEC. Since the samples under study were provided by artists, they will be advised about the degradation susceptibility of the materials, as well as a valuation of other possible plasticizers will be provided.

Getting to the Gut of the Matter: The Conservation of Siberian Yupik Winter Gut Parkas

Amy Tjiong, Gabrielle Tieu, Judith Levinson, Samantha Alderson

In 2014, objects conservators at the American Museum of Natural History (AMNH) undertook a two-year project to treat and rehouse portions of its Siberian ethnographic collection. These pieces are frequently requested for study by native knowledge-holders, traditional artisans and researchers. Among the 100 objects chosen for treatment were 14 gut skin parkas attributed to the Siberian Yupik people. The parkas were fabricated from the intestines of marine mammals to produce materials termed ‘summer gut’ and ‘winter gut’. When wet, summer gut is translucent, easily conforms to the wearer’s body, and is waterproof. When dry, however, it is very brittle and easily prone to tearing. Winter gut, on the other hand, is opaque white in color, soft and supple when dry, but can have a negative reaction to contact with moisture. Limited information exists in the anthropological and conservation literature regarding the manufacture and treatment of winter gut and how it differs from summer gut in appearance and functional qualities. In fact, current conservation treatment approaches for winter gut tend to rely on strategies designed for hide or summer gut. Experimentation to produce winter and summer gut was undertaken and ultimately provided enough material to test treatment protocols and materials. Accompanying and supporting treatment, this project involved extensive scientific analysis and native consultation. Peptide mass fingerprinting (PMF) analysis was performed to determine species of the source animals and to shed light on fabrication practices and differences among the Yupik of eastern Siberia and those of St. Lawrence Island. Additionally, histological study was performed to examine microscopic differences between winter and summer gut, which clarified their differing sensitivity to moisture. Extensive native collaboration, such as web-enabled video conferencing, visits by native scholars and craftsmen to the museum, and travel by conservators to both sides of the Bering Strait took place throughout the project. The information gained from scientific analyses and collaboration with descendant communities offers an expanded view of the technical qualities and cultural uses of winter gut and a reconsideration of current conservation approaches to objects manufactured from this unique material.

Miniature Wax Sculptures at the Philadelphia Museum of Art: A Technical Study, Treatment, and Gallery Presentation

Nicole M Passerotti, Alexandra Letvin, Beth A. Price, Cathleen Duffy, Melissa Meighan

The Philadelphia Museum of Art (PMA) has one of the largest and most distinguished European portrait miniature collections in America. The collection comprises painted miniatures and waxes, both low relief and small sculptures, dating from the 16th to the 20th centuries. As part of a ten-month Samuel H. Kress Fellowship, the conservator worked closely with curators in order to establish joint priorities, to define consistent terminology, and to survey 190 waxes in the collection. In addition to the survey, exchange with colleagues, and visits to collections including the V&A and the Wallace Collection among others, the project culminated in the technical study, treatment, and recommendations for the long-term care of the wax collection. Eleven waxes were chosen to investigate materials, fabrication, and condition. The group selected for analysis included waxes from England, France, Germany, and Italy, manufactured between the 16th and 19th centuries. Samples from each of the eleven objects were analyzed using Fourier transform infrared microspectroscopy, scanning electron microscopy with energy dispersive spectroscopy, and pyrolysis-gas chromatography-mass spectrometry to characterize the waxes and the colorants used in the creation of these objects. From the eleven objects analyzed, seven waxes then were selected for treatment. The objects represented a range of treatments that will provide guidelines and methodologies for future conservation of the collection. Conservation treatment included structural repairs, compensation, and cleaning informed by the Modular Cleaning Program. The conservator and the curator worked in concert to prepare a focused installation, repurposing a free-standing floor case in a dedicated miniatures gallery. The case features recently treated waxes with their respective x-radiograph images, encouraging visitors to look more closely and consider how these delightful objects were made. The objects chosen for display highlight three major methods of manufacture: hand- built on metal armature, mold made with known multiples, and a prefabricated mold designed for amateur artists. This study is a model for collaboration between curators, conservators, and scientists. The result of the project has been a contribution to the wax miniature scholarship, specifically to the materials used and the methods of fabrication. The study also has informed the treatment of these delicate objects in a sensitive and confident manner.

A Preliminary Investigation into the Use of Laser Cleaning to Stabilize Bronze Disease

Emily Frank, Michaela Paulson, Carol E. Snow, Pablo Londero

A Preliminary Investigation into the Use of Laser Cleaning to Stabilize Bronze Disease

Emily Frank, Michaela Paulson, Pablo Londero, & Carol Snow

American Institute for Conservation | 47th Annual Meeting

Joint Objects and Research and Technical Studies Session | May 16, 2019

Abstract

This paper documents a preliminary study on the use of an externally modified laser to remove active chloride corrosion on copper alloys. Previous use of lasers in metals conservation has included removing coatings, unwanted patinas, and surface accretions, but laser spot treatment of bronze disease has yet to be tested systematically. This paper describes our methodology and reports initial findings. We investigate how laser cleaning might enhance existing treatment methods, allowing for increased efficiency and improved long-term preservation.

To be a flexible tool for the treatment of bronze disease, laser spot size must be independent of energy output, allowing the conservator to target only the afflicted area at the optimal fluence. Thus, our approach requires fine tuning fluence in relation to corrosion properties and surface preparation. For this study, we manipulated the fixed energy output of a Compact Phoenix Laser, without altering the handheld unit, through a series of lenses and a polarizer. The modified 1064 nm laser successfully micro-excavated pits of bronze disease. Examination of the treated samples

with stereomicroscopy, scanning electron microscopy, and Raman spectroscopy appears promising. Micromelting at the micron and sub-micron level on some samples requires further study.

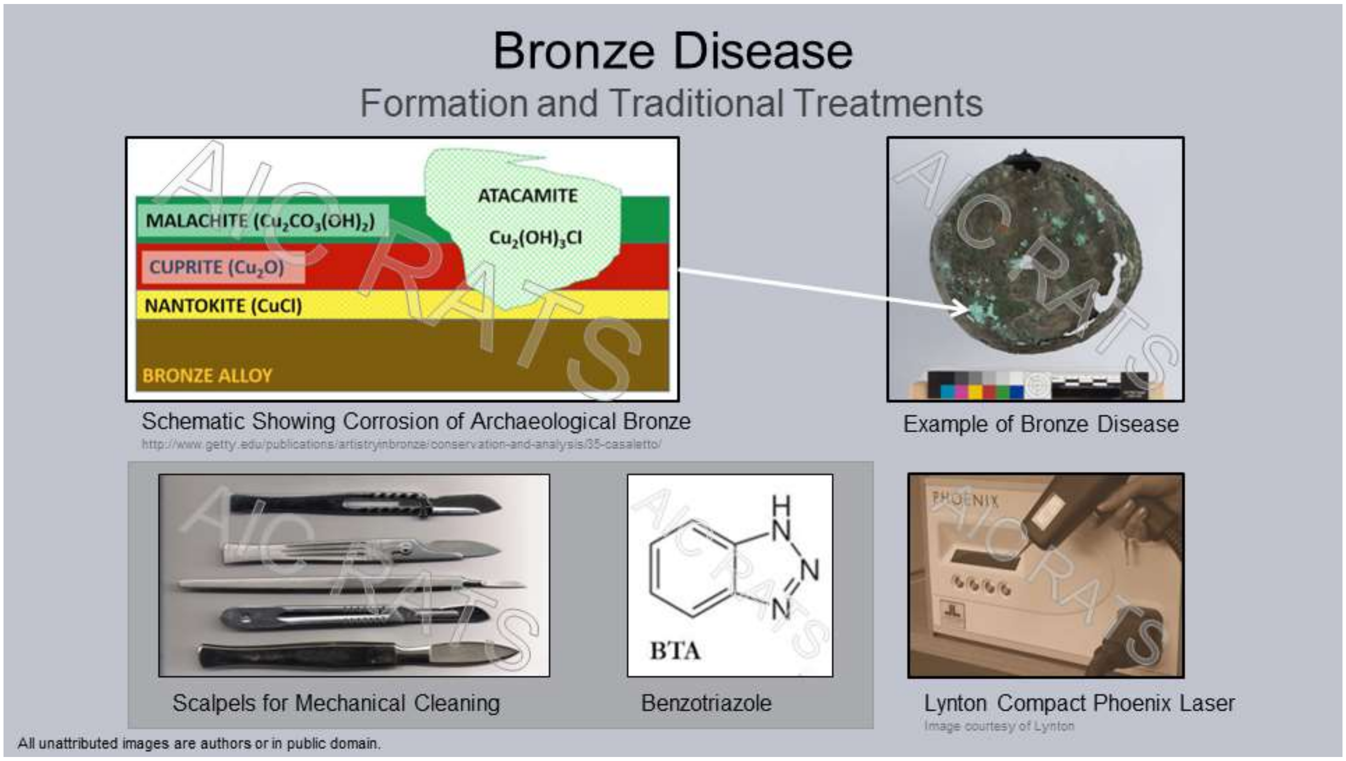

Bronze Disease

Formation and Traditional Treatments

Schematic Showing Corrosion of Archaeological Bronze

http://www.getty.edu/publications/artistryinbronze/conservation-and-analysis/35-casaletto/

Example of Bronze Disease

Scalpels for Mechanical Cleaning

Benzotriazole

Lynton Compact Phoenix Laser

Image courtesy of Lynton

All unattributed images are authors or in public domain.

Introduction

The stabilization of active copper chloride corrosion, or bronze disease, has been a challenge since the earliest days of conservation (Weisser 1994, 141-152). Visible, light-green, powdery copper trihydroxychlorides—such as atacamite, clinoatacamite, and paratacamite—and underlying waxy cuprous chloride—nantokite—are part of an autocatalytic cycle of corrosion, which results in complete powdering of metallic copper alloy objects (Scott 2002, 127). Traditionally, a wide range of treatment methods have been used to address bronze disease, such as mechanical excavation of corrosion; chemical pretreatment/treatment with sodium carbonate, benzotriazole (BTA), silver oxide paste, sodium sesquicarbonate, alkaline Rochelle salts, etc.; and tight control of storage and display environments. Electrolytic and electrochemical stripping have also been used to remove and/or stabilize corrosion. Contemporary treatment options must consider a wide range of variables, including but not limited to alloy composition, manufacturing technique, pre-burial wear/use, burial environment, excavation method, post-burial stabilization, on-site conservation, storage method/environment, and subsequent treatment/retreatment. The treatment methodologies conservators have used over the years to stabilize this class of objects have had variable success with regards to long-term preservation, especially when control of the relative humidity is problematic (Scott 1990, 193).

The use of lasers in the treatment of metals has been documented for the removal of coatings, unwanted patinas, and surface accretions (Drakakki et al. 2010, Siano et al. 2012, Sansonetti et al. 2015, etc.). The cleaning of silver coins from an archaeological site in Najran (Saudi Arabia) using a Q-switched Nd:YAG laser at 1064 nm (5 ns, 100 mJ) resulted in the removal of a variety of corrosion products, some notably chloride containing (Abdel-Karrem et al. 2016, 135 and 137). The researchers used a fluence of 1.6 J/cm2, delivering five laser pulses to clean thin corrosion layers and fifteen for the thickest ones. Analysis with scanning electron microscopy/energy dispersive X-ray spectroscopy (SEM/EDS) of the treated surfaces demonstrated that their procedure removed the elements Copper, Oxygen, Carbon, Aluminum, Silicon, Sulfur, Chlorine, Potassium, Calcium, and Iron. Though targeting bronze disease was not their aim, their results suggest the successful removal of bronze disease products (atacamite/paratacamite) (Abdel-Karrem et al. 2016, 139).

Many conservation departments own or use lasers with fixed pulse energies, such as the Compact Phoenix™ produced by Lynton Lasers Ltd., to carry out a range of treatments on a wide variety of objects. Increasing and decreasing the spot size on these laser units, i.e. the distance from the handheld unit to the surface to be treated, is the only way to manipulate the fluence, or the optical energy delivered per unit area. For such a laser to be a viable tool for the treatment of bronze disease, the laser spot size must remain small enough to target the afflicted area and avoid the surrounding metal and any nearby stable corrosion products. To achieve a small spot size at a low enough energy to remain under the specific heat capacity of the metal, the energy output of the laser must be manipulatable.

Through a series of external modifications that do not alter the hardware, it is possible to reduce the energy of the beam while maintaining a constant small spot size, thus reducing the fluence and allowing for targeted treatment of small areas on copper alloy archaeological fragments afflicted with bronze disease.

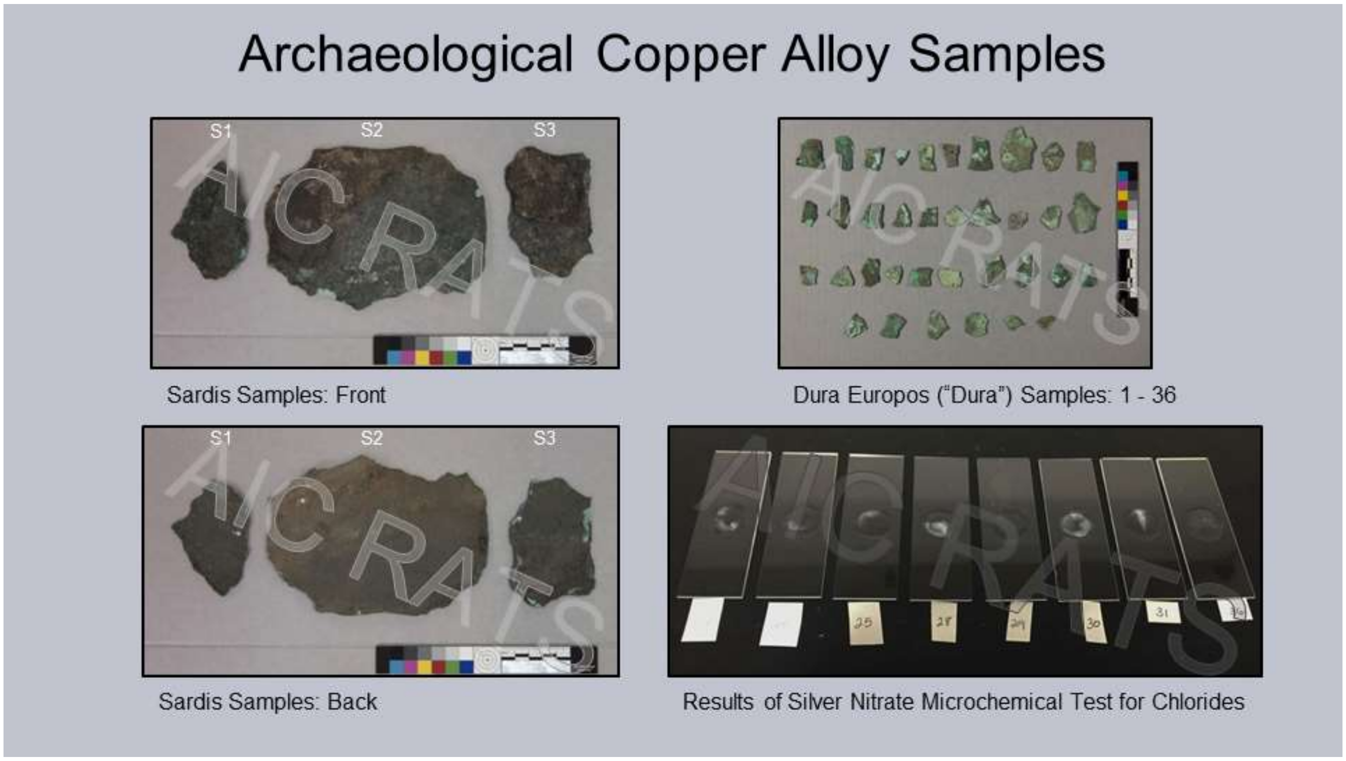
Archaeological Copper Alloy Samples

Sardis Samples: Front

Dura Europos ("Dura") Samples: 1 - 36

Sardis Samples: Back

Results of Silver Nitrate Microchemical Test for Chlorides

Copper Alloy Fragments

To test the efficacy of using a modified energy output laser attachment on small spots of bronze disease, we chose fragments of copper alloy excavated from two archaeological sites: Dura Europos and Sardis.

The site of Dura Europos in modern-day Syria was excavated in the 1920s and 1930s by Yale University and the French Academy of Inscriptions and Letters. The archives and more than twelve thousand artifacts from those excavations are housed within the collections of the Yale University Art Gallery. Samples of copper alloy fragments were selected from a larger group of unidentified fragments from unknown locations on the site. It is not certain if they received treatment between excavation and current storage. However, many of the fragments were almost completely mineralized and some of the corrosion colors and textures suggest possible past chemical intervention, though no treatment records exist for these fragments.

Harvard-Cornell excavations carried out over the last sixty years at Sardis, Turkey, the capital of the Lydian Empire in the sixth century BCE, have produced a collection of more than two thousand copper alloy finds. These finds have been stored on site, and their treatments have been recorded since their excavation. We were given permission to take samples lacking good context from the site for the purpose of testing the viability of laser-based treatment. According to the conservation records, the Sardis fragments tested were all untreated. Additionally, some samples were tested on site with a laser held by the excavation. Those samples were left in storage at Sardis where there is no climate control and relative humidity can reach 100% in the off-season.

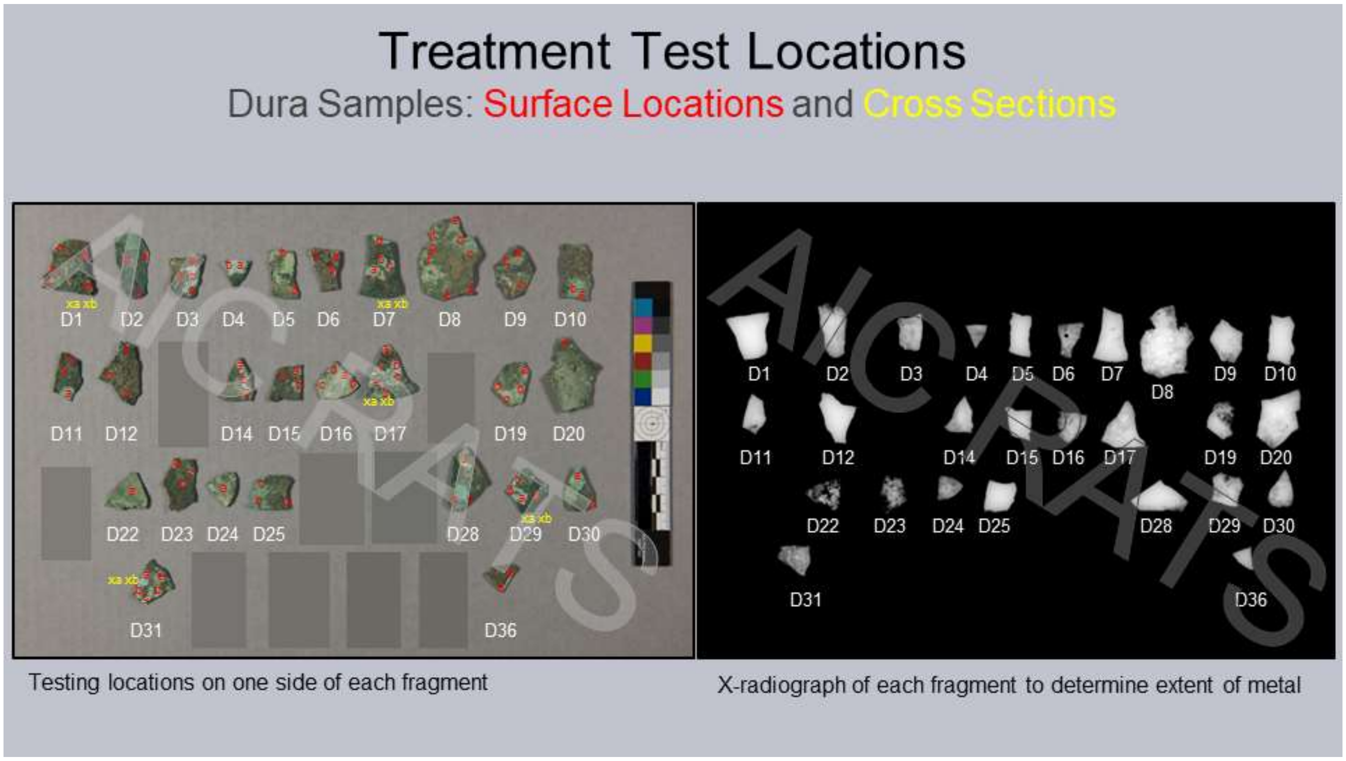

Treatment Test Locations

Dura Samples: Surface Locations and Cross Sections

Testing locations on one side of each fragment

X-radiograph of each fragment to determine extent of metal

Sample Preparation

To narrow down the sample set, multiple fragments from the Dura Europos group and the three Sardis samples brought to the U.S. were x-radiographed to determine the extent of uncorroded metal still present.

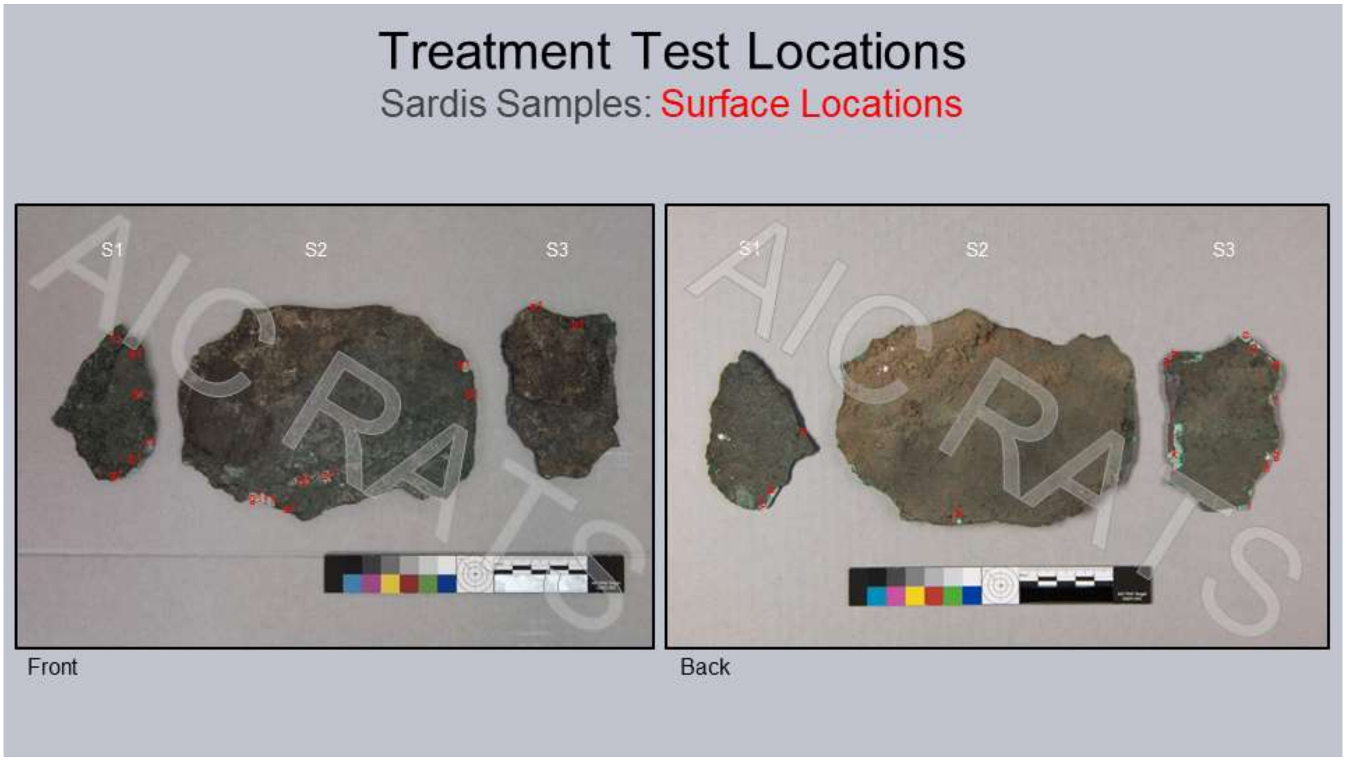

Treatment Test Locations

Sardis Samples: Surface Locations

Front

Back

In all cases, hypothesized bronze disease on the chosen samples was confirmed by the presence of chlorides using silver nitrate microchemical tests (Odegaard 2005, 108-109; see Slide 3). All of the fragments were documented with photography before testing in order to track visible changes. Based on the x-rays and silver nitrate tests, we chose thirty-one areas on the three samples from Sardis and eighty-six locations on twenty-seven fragments from Dura Europos to test laser spot treatments on the surface (see Slide 4).

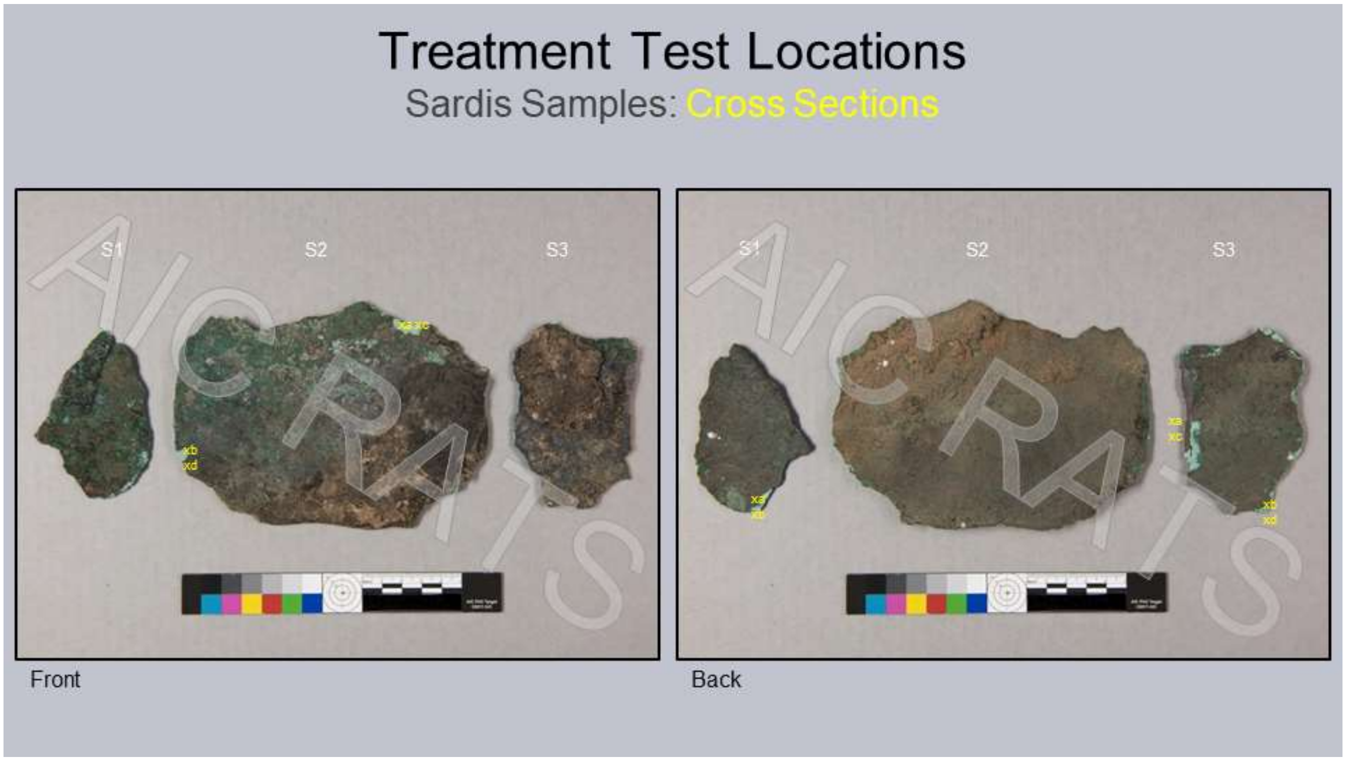

Treatment Test Locations

Sardis Samples: Cross Sections

Front

Back

These treatment tests aimed to examine the effects of the laser on the underlying corrosion and metal and to specifically evaluate the ability of the laser to remove chlorides. Additionally, we chose five large areas at the edges of the Sardis samples and five areas from five Dura fragments (see Slide 4) that tested positive for chlorides to examine in cross section. We cut “before treatment” cross sections, bisecting each area with a jeweler's saw. These untreated halves were set in resin with the relevant edge down and prepared for analysis with a scanning electron microscope. Then, the adjacent surfaces in each area were test treated with the laser, cut in the same manner, and prepared as "after treatment" cross sections for comparison.

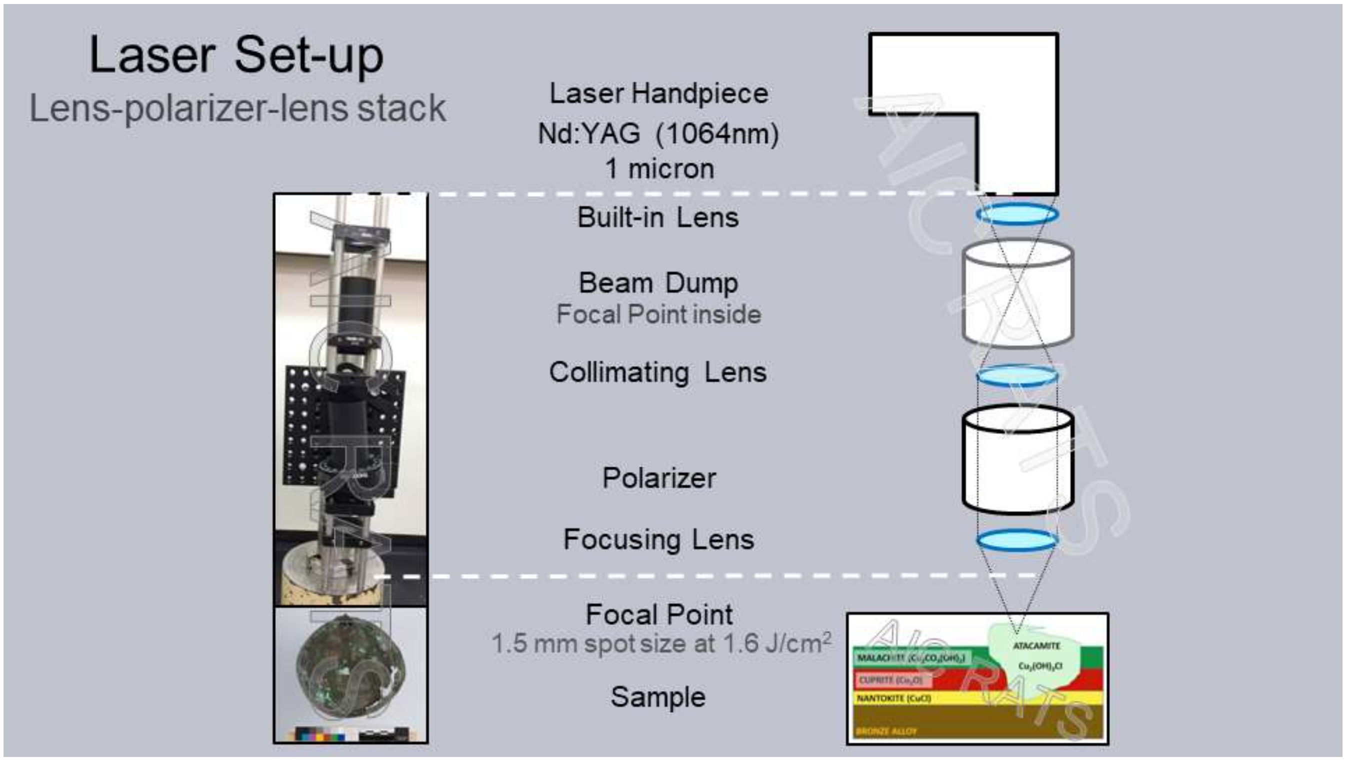

Laser Set-up

Lens-polarizer-lens stack

Laser Handpiece
Nd:YAG (1064nm)
1 micron

Built-in Lens

Beam Dump
Focal Point inside

Collimating Lens

Polarizer

Focusing Lens

Focal Point
1.5 mm spot size at 1.6 J/cm^2

Sample

Laser Equipment and Modifications

Since the Compact Phoenix does not allow for the manipulation of energy output through the unit, we developed and designed a stacked system of lenses and a polarizer through which the beam can pass in order to control the energy while maintaining constant spot size (see Slide 7).

| Laser | Focus | Lens (to collimate beam) | Polarizer | Lens (to refocus beam) | Sample |

Yale University Art Gallery's Lynton Compact Phoenix™ laser unit can operate at three different wavelength options: (1) Nd:YAG | 532 nm and 1064 nm combined in a 1:4 ratio; (2) Nd:YAG | 1064 nm; and (3) Er:YAG | 2940 nm. The 2940 nm wavelength worked poorly in preliminary, uncontrolled testing, yielding an unacceptable color change. Additionally, though the components of our modification are quite broadband, they are not designed to work deeply in the infrared (IR). The reflectance spectra of test fragments measured with an integrating sphere peaked at about 540 nm, suggesting the fragments would largely reflect the 532 nm component of the mixed beam obtained using the KTP (potassium titanyl phosphate crystal) attachment on the Nd:YAG (neodymium: yttrium aluminum garnet) laser handpiece. Thus, this study focused on the 1064 nm wavelength delivered via the Nd:YAG laser handpiece.

Laser fluence is constant over the surface when the beam is perpendicular to the surface to be treated. In order to use this geometry conveniently, several choices were made. The fragments used in this study could lie flat on a table. We created a vertically stacked system with a 3D printed nylon and fiberglass holder for the handpiece and rigged together our stacked modification system of lenses and polarizer with various lab stands and clamps. This setup stabilized and focused the beam in order to prevent human aim error (see Slide 8). Ideally, the modification set-up would be held in a pre-fabricated cage system using rods into which components (i.e. crystal holder, lens with frame, etc.) could be slotted. Unfortunately, this was too limited for two reasons. (1) The polarizer needs to be slightly tilted for the safety of the operator and equipment (because we are working vertically, without this tilt, the beam would scatter directly up into the operator and/or back into the laser). This tilt does not leave the beam in the same line, so the second lens in the stack cannot be centered. (2) The rotating polarizer holder for most standard cages from Glan-Thompson polarizers was too big. The stacked system we fabricated allows a 1.5 mm (0.15 cm) spot size diameter to reach the surface of the fragments. The spot size can be changed, if desirable, by placing an aperture in the beam dump, or by adjusting the focal length of the final lens in the stack.

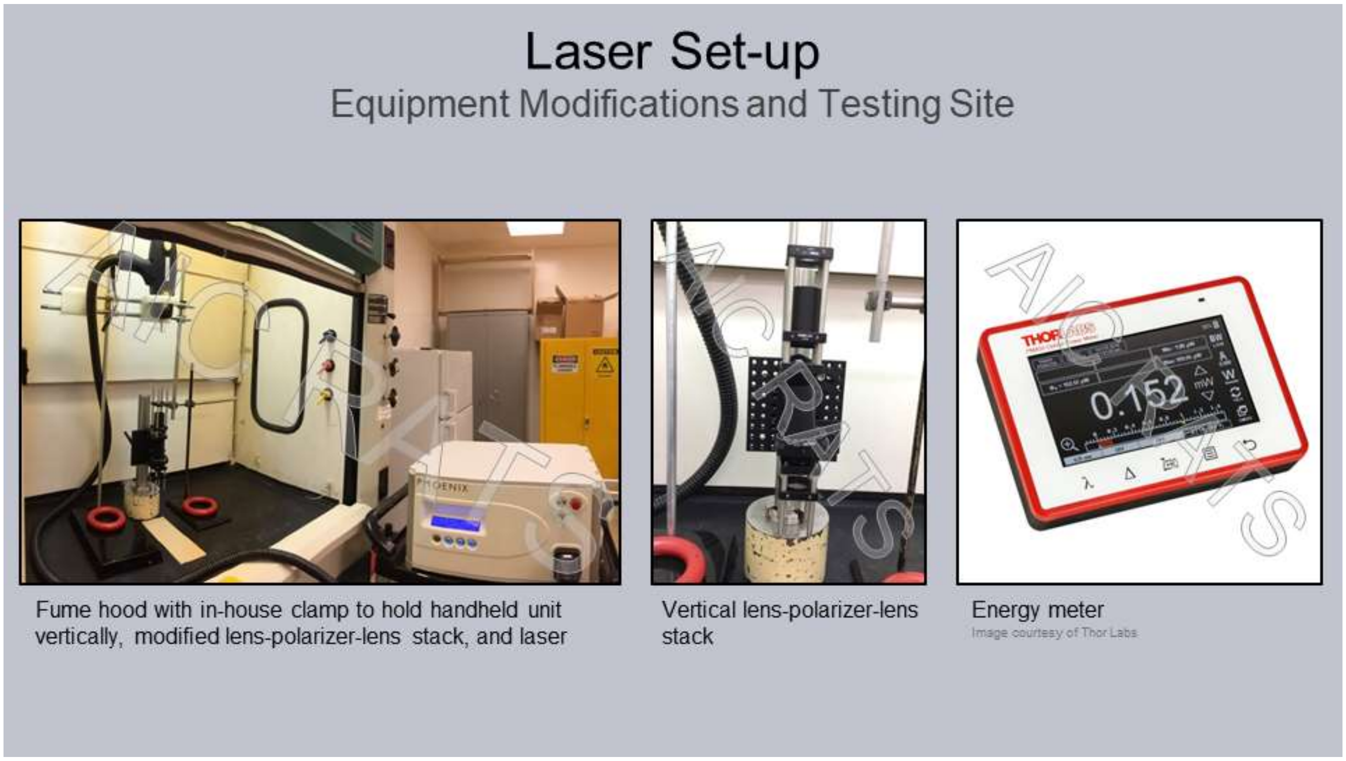

Laser Set-up

Equipment Modifications and Testing Site

Fume hood with in-house clamp to hold handheld unit vertically, modified lens-polarizer-lens stack, and laser

Vertical lens-polarizer-lens stack

Energy meter

Image courtesy of Thor Labs

We determined that the energy must be approximately 0.03 Joules (30 mJ) to approximate the desired fluence of 1.6 J/cm2 (as per Abdel-Karrem et al. 2016, 139) at the spot size of 1.5 mm. The energy of the beam through the system was measured with an energy meter at different rotations of the polarizer.

118° = 0.05 Joules (at 0.018 cm2) → 2.8 J/cm2

180° = 0.035 Joules (at 0.018 cm2) → 2.0 J/cm2

200° = 0.04 Joules (at 0.018 cm2) → 2.3 J/cm2

The above fluence values (J/cm2) are the maximum values at that particular polarizer position. Slight fluctuations due to the ionization of the surrounding air as the beam passes through the polarizer and lens system are inevitable because of the length of our setup, i.e. the distance between the handheld unit and the fragment.

The damage threshold for cast bronze coupons has been tested via a laser cleaning published in Siatou et al. (2006, 5), suggesting that micromelting can occur at a fluence as low as 0.4 J/cm2. Since many of the powdery chloride layers on the selected fragments of this study are thick and there is no pure metal initially visible, we aimed to reach 1.6 J/cm2 to replicate the removal of chlorides documented by Abdel-Kareem et al. (2016) while cleaning archaeological silver alloy coins. Though there is no standard way of measuring fluence, we used the most straightforward method – dividing the output energy by the spot size – to approximate this value. The lowest fluence achievable without modifying the chosen spot size is 2.0 J/cm2, which we considered acceptable as a starting point to best target the small bronze disease spots on the small copper alloy fragments. It is possible, with this system, to lower the fluence, to 1.6 J/cm2 for example, by enlarging the spot size.

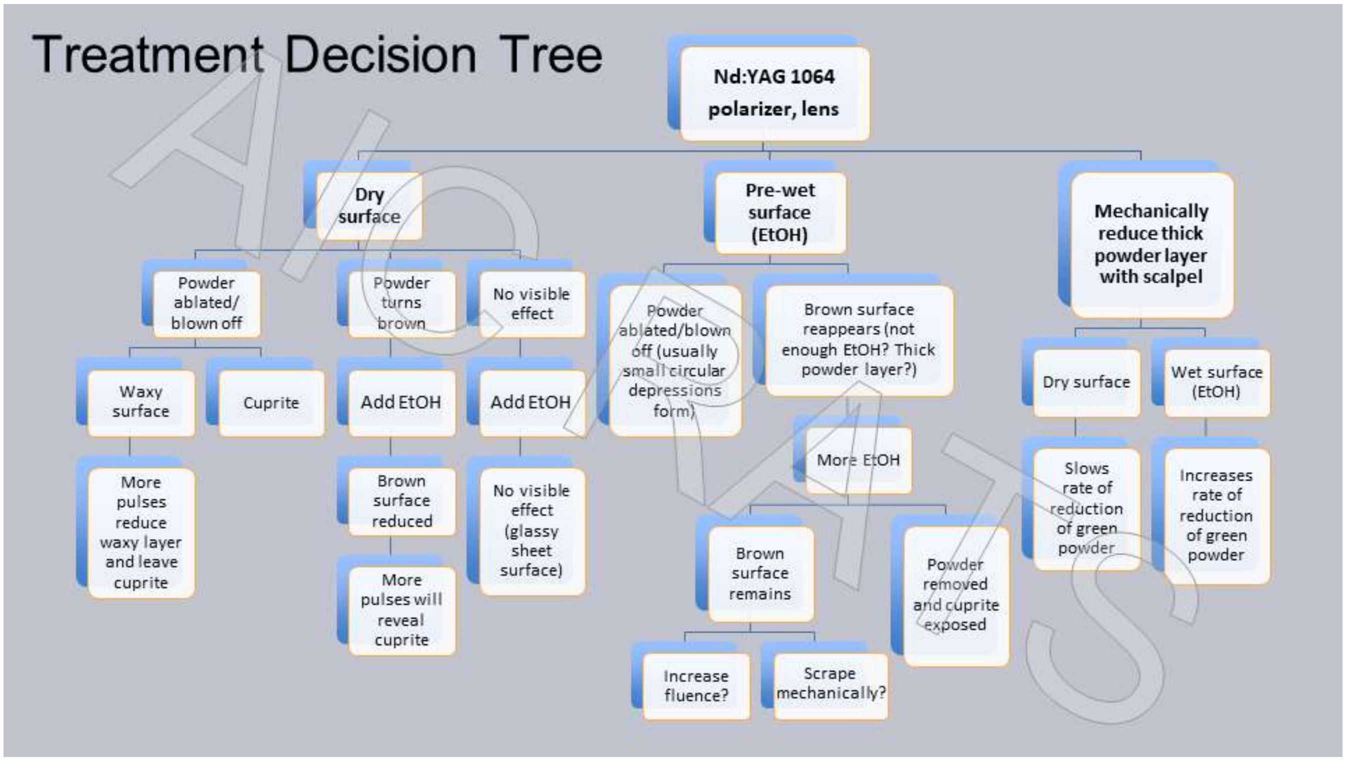

Treatment Decision Tree

- Nd:YAG 1064 polarizer, lens
  - Dry surface
    - Powder ablated/ blown off
      - Waxy surface
        - More pulses reduce waxy layer and leave cuprite
      - Cuprite
    - Powder turns brown
      - Add EtOH
        - Brown surface reduced
          - More pulses will reveal cuprite
    - No visible effect
      - Add EtOH
        - No visible effect (glassy sheet surface)
  - Pre-wet surface (EtOH)
    - Powder ablated/blown off (usually small circular depressions form)
    - Brown surface reappears (not enough EtOH? Thick powder layer?)
      - More EtOH
        - Brown surface remains
          - Increase fluence?
          - Scrape mechanically?
        - Powder removed and cuprite exposed
  - Mechanically reduce thick powder layer with scalpel
    - Dry surface
      - Slows rate of reduction of green powder
    - Wet surface (EtOH)
      - Increases rate of reduction of green powder

Methodology

In addition to noting the removal of chlorides from archaeological silver alloy coins, Abdel-Kareem et al. (2016) also discuss the number of pulses they delivered to the surface of these coins to clean “thin vs thick” corrosion layers. These pulses fluctuated between five for thin and fifteen for thick. This information provided reference points for our tests on copper alloys.

To begin our testing, we visually assessed the samples from Sardis and Dura to determine thickness and, in general, all sample spots were shot with an initial five pulses, one on top of another, to remove a significant visible area of the powdery green corrosion. The number of pulses was increased depending upon visible responses in the corrosion products, tracked visibly with a stereomicroscope. For the purposes of the preliminary tests, we did not consider pulse duration, assuming that the thermal response is so slow on the time scale on which we were working that the difference in pulse duration between the available repetition rates (single, double, triple; at 5 ns per pulse) was inconsequential. All tests were conducted using single pulses delivered mechanically, one on top of another, to reduce the number of variables in the study. We also assumed that the metal had time to stabilize between pulses.

In some cases, five pulses were delivered and then a few drops of ethanol were pipetted onto the surface. This proved effective; therefore ethanol was also delivered first to some of the sample surfaces prior to any laser testing. We mechanically reduced thick pustules with a scalpel before proceeding with the laser. We generated a flowchart (see Slide 9) based on the way we progressed with test treatment of spots on the fragments. When “cuprite” is suggested as a stopping point in fig. 4, it means that a layer of well-bound reddish-brown corrosion was reached and treatment was stopped to avoid revealing bare metal. The presence of cuprite was not confirmed for all samples, but later analysis of some samples with SEM-EDS and Raman spectroscopy indicated the reddish-brown areas exposed are, in fact, copper oxide.

In sum, treatment of the fragments included (1) varying the number of pulses, (2) pre-wetting the surface with ethanol, and/or (3) mechanical removal of some of the thickest pustules in order to assess the efficiency with which the laser removed the powdery chloride corrosion. Fragments were not completely treated; instead small areas of corrosion were removed in order to later analyze treated against untreated areas on the same fragment. After treatment, samples were checked for extant chlorides—to determine removal or reduction—and micromelting, to assess surface changes.

Laser Treatment Test: D17 Surface

Fluence: 1.6
5-10 pulses delivered over green powder

Results

Of the thirty fragments tested, the following three examples are representative of some of the visible effects noted after testing with a laser at the consistent low fluence of 2.0 J/cm2, following the decision flowchart (see Slide 9).

Dura fragment 17, spot a (D17a), was treated with the initial five pulses, and then another five, specifically targeting the bright green corrosion visible on the left. Much of the light green powder was removed, with only a few areas at the very end that developed a light brown surface on the top that would not be reduced further with the laser alone.

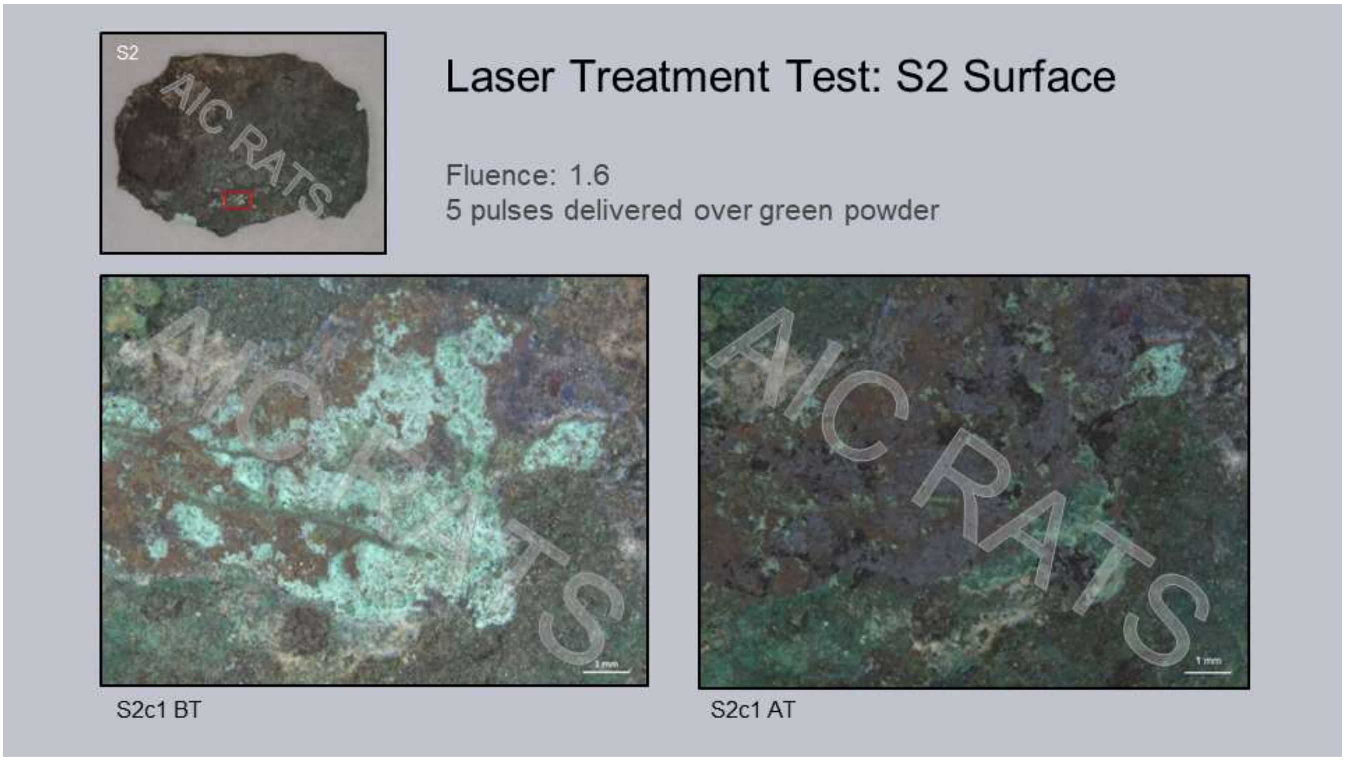

Laser Treatment Test: S2 Surface

Fluence: 1.6
5 pulses delivered over green powder

Sardis fragment 2, spot c1 (S2c1), was also treated with few pulses, but the light green corrosion layer was clearly thinner, so testing was stopped early. The dark, purplish black material visible on the surface in the after treatment photomicrograph was a consistent visible phenomenon created by the laser and will be discussed in Slides 16 and 17 along with other Raman spectroscopy results.

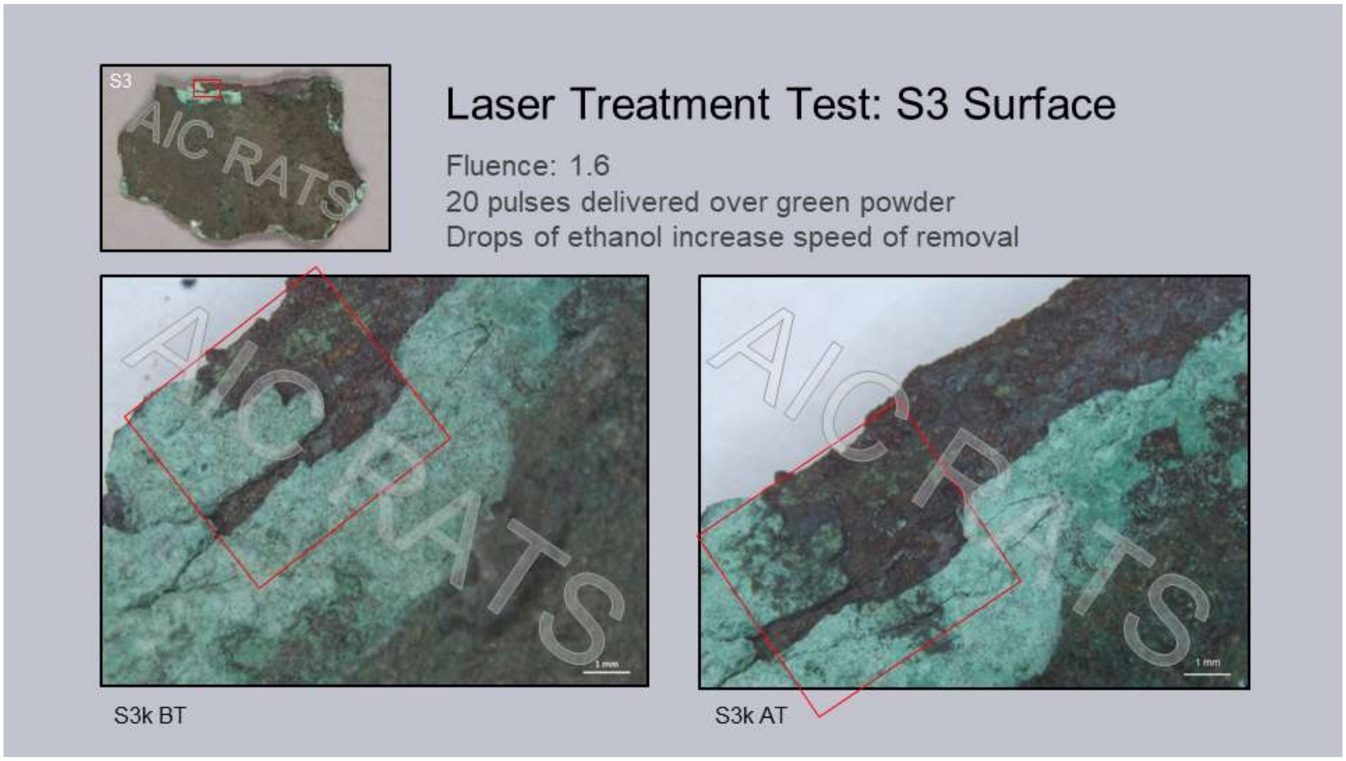

Laser Treatment Test: S3 Surface

Fluence: 1.6
20 pulses delivered over green powder
Drops of ethanol increase speed of removal

S3k BT

S3k AT

The third and final example is one of the more complex surfaces. Sardis fragment 3, spot k (S3k), received the initial five pulses over the bright green corrosion and then an additional five, to little effect. With the addition of a few drops of ethanol over the area of interest, the following ten pulses became much more effective in removing the undesired material. This sample was not fully treated; we stopped when a method appeared to be effective and continued on to the next fragment.

The surfaces of the fragments during and after treatment displayed a variety of phenomena: (1) relatively complete powder removal with well-adhered green or reddish-brown corrosion layers exposed, (2) partial powder removal with a light brown protective layer formed on the surface that can be reduced with ethanol but not the laser alone (up to fifty-sixty pulses tested with no effect until ethanol was used), (3) powder removal with the formation of a patchy purple-black material, and (4) powder removal with the formation of a translucent waxy material that can be removed with further laser treatment.

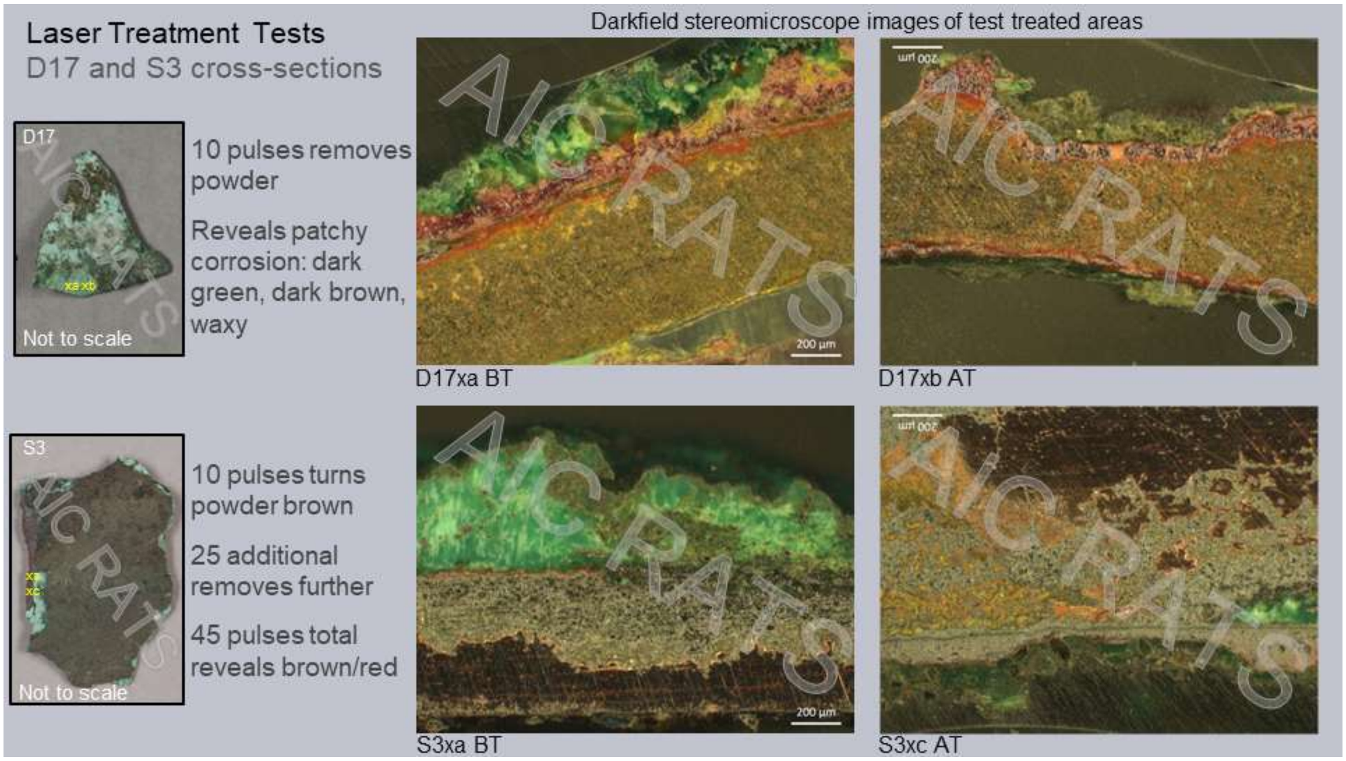

Laser Treatment Tests

D17 and S3 cross-sections

Darkfield stereomicroscope images of test treated areas

10 pulses removes powder

Reveals patchy corrosion: dark green, dark brown, waxy

10 pulses turns powder brown

25 additional removes further

45 pulses total reveals brown/red

Analysis and Discussion

We assessed the results of our tests in a number of ways: visual examination, stereomicroscopy and SEM/EDS of cross sections, and Raman spectroscopy and x-ray diffraction of corrosion products.

We took cross sections from adjacent areas before and after treatment in order to observe the stratigraphy with a stereomicroscope and a scanning electron microscope. The darkfield images here are examples of adjacent areas of metal removed from a fragment, one untreated (on the left), and one treated with the laser (on the right). Some of the analyzed fragments displayed intact stable corrosion stratigraphy on both the untreated and the treated sections. Both halves have a visible metallic core and initial reddish copper oxide layer, with green carbonates mixed in with chlorides on the untreated side, and the comparative reduction of the chlorides and top surface of corrosion on the treated sample. Aesthetically, the result is convincing. The treatment appears to maintain the topography of the underlying corrosion (see Slide 10), and in theory, one could continue mechanically, with less scraping than would have been required initially, or chemically, for passivation of remaining chloride corrosion. The other samples, generally ones that were determined to be “thin” in our initial qualitative decision-making, displayed overcleaning, or the exposure of metallic copper and the reduction of stable cuprite.

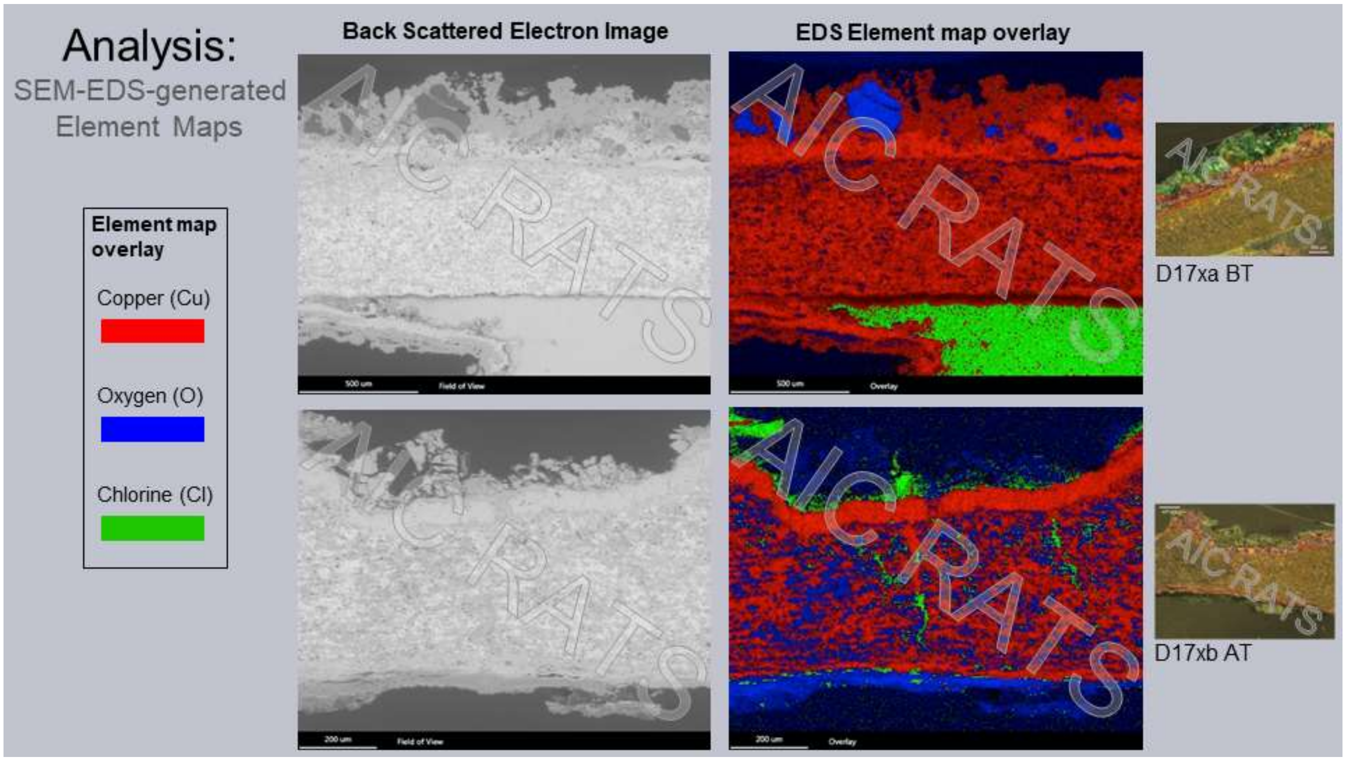

Analysis:

SEM-EDS-generated Element Maps

Back Scattered Electron Image

EDS Element map overlay

Element map overlay

Copper (Cu) 🟥

Oxygen (O) 🟦

Chlorine (Cl) 🟩

D17xa BT

D17xb AT

Analysis with a scanning electron microscope and the production of element maps through SEM-EDS revealed that we successfully removed chlorides from the surface of the samples, though not from the interior geometry where the light is inhibited by thick, stable corrosion. Element maps support the visual observation that much of the oxide layer in some samples was removed during laser treatment (see Slide 15). Raman analysis supports this as well, though more investigation would be needed to confirm that the entirety of the layer is removed or if its disappearance is a product of its initial sparseness on the fragment. Chlorine is visible in protected crevasses, which would require chemical passivation or more invasive mechanical treatment to be fully removed or passivated. Since the fragments all received a different number of pulses, the results show two general categories of possibilities of laser treatment: overcleaning or the continued presence of chloride corrosion in recesses.

In this slide, element maps support the visual observation that superficial chlorides were removed during laser treatment. On the top left, a backscattered electron (BSE) image of D17xaBT and top right, an EDS Element map overlay of D17xaBT. On the lower left, a BSE image of D17xbAT and on the lower right, an EDS Element map overlay of D17xbAT. In the upper right image, a large chlorine-rich mass skewed the normalized image, so an actual averaged image is overlaid for clarity (click in presentation view) – chloride corrosion is visible in the top layer, which is clearly reduced in the after treatment element map. According to Raman results, there is cuprite in both the BT and AT sections, and the primary trihydroxychloride is clinoatacamite (or atacamite). The large chlorine-rich mass is not nantokite, though results for this are not conclusive.

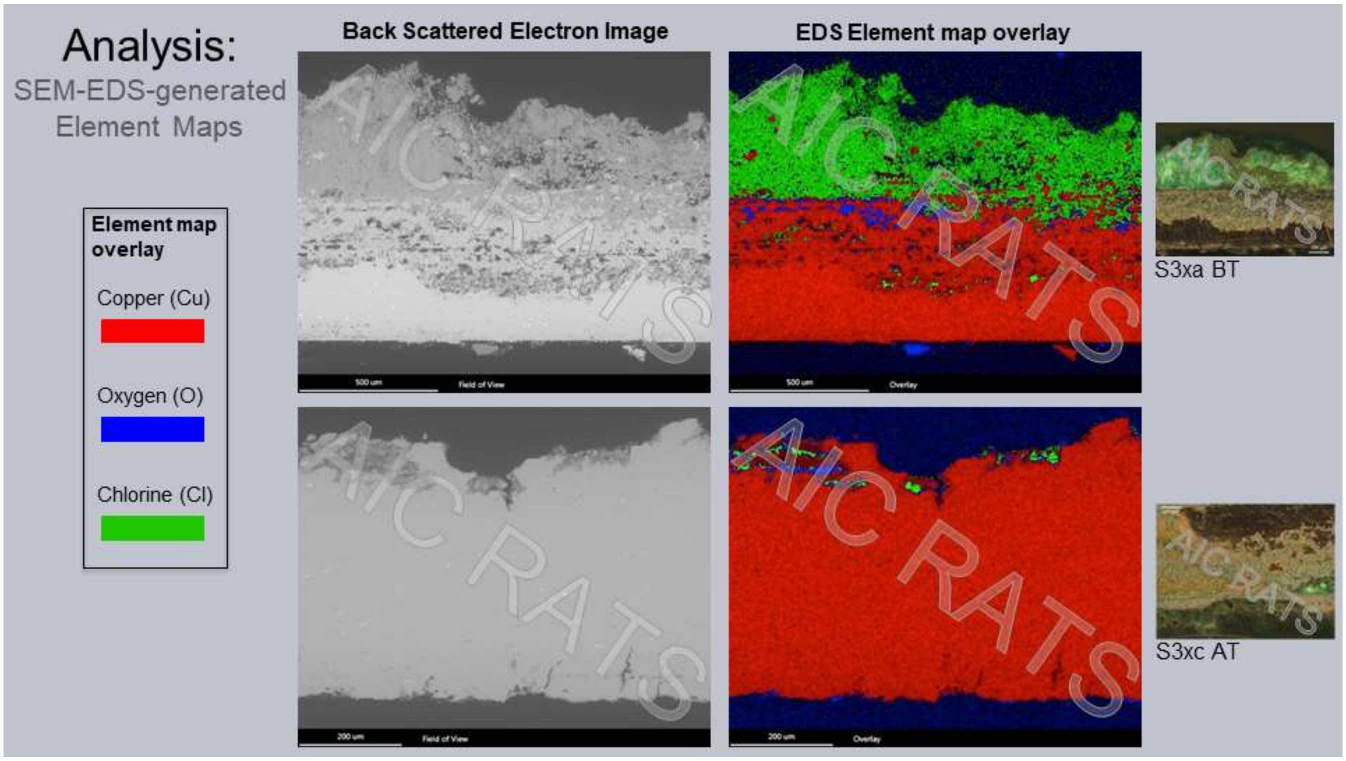

Analysis:

SEM-EDS-generated Element Maps

Element map overlay

Copper (Cu) 🟥

Oxygen (O) 🟦

Chlorine (Cl) 🟩

Back Scattered Electron Image

EDS Element map overlay

S3xa BT

S3xc AT

In this slide, element maps support the visual observation that superficial chlorides were removed, in some cases along with the oxide layer during laser treatment. Upper left, a BSE image of S3xaBT and in the upper right, an EDS Element map overlay of S3xaBT. In the lower left, a BSE image of S3xcAT and in the lower right EDS Element map overlay of S3xcAT

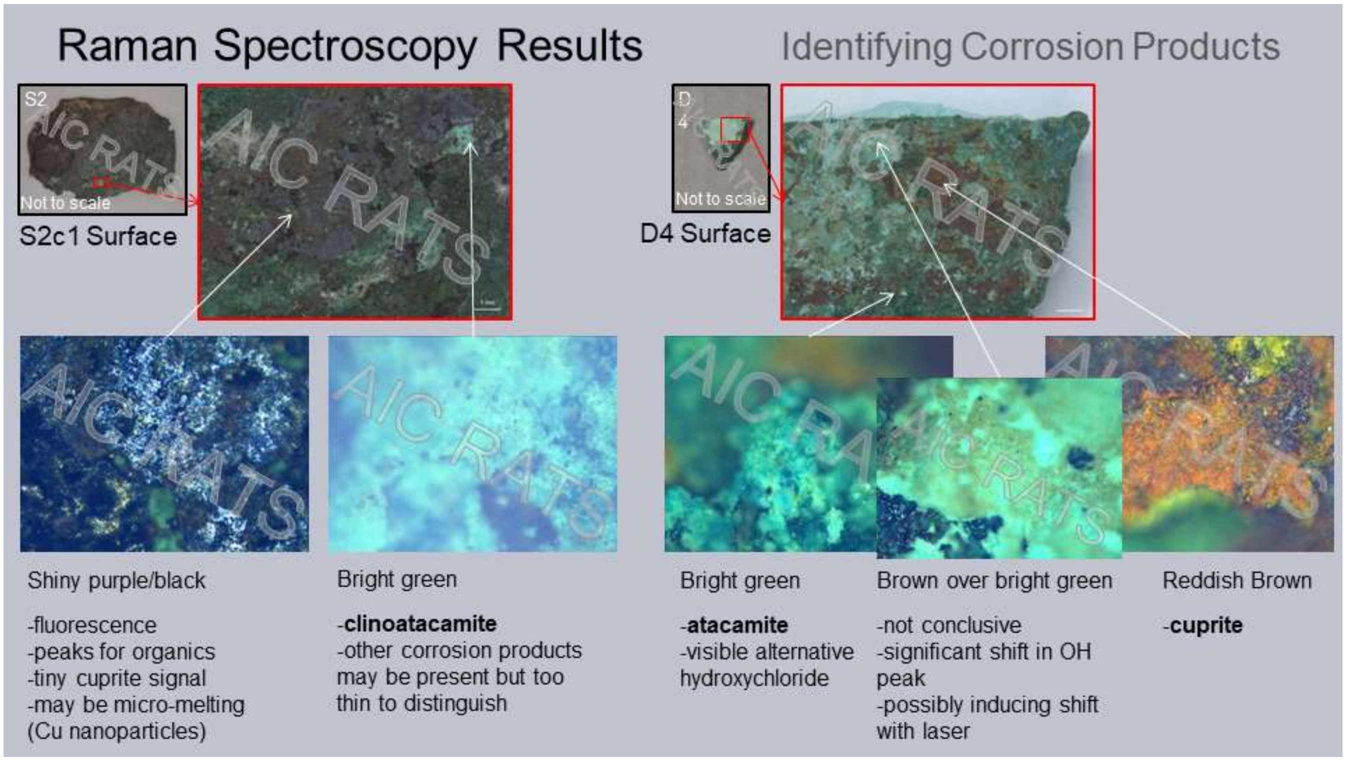

Raman Spectroscopy Results

Identifying Corrosion Products

S2c1 Surface

D4 Surface

Shiny purple/black	Bright green	Bright green	Brown over bright green	Reddish Brown
-fluorescence -peaks for organics -tiny cuprite signal -may be micro-melting (Cu nanoparticles)	-**clinoatacamite** -other corrosion products may be present but too thin to distinguish	-**atacamite** -visible alternative hydroxychloride	-not conclusive -significant shift in OH peak -possibly inducing shift with laser	-**cuprite**

Analysis of corrosion products with Raman spectroscopy supports the SEM-EDS maps. Spectra from test spots on the surfaces of fragments show slightly different corrosion products across the board, which is interesting, though it may be a coincidence within the relatively small number of samples. In general, Raman detected the presence of cuprite, two different copper hydroxychlorides, and the chemical alteration of hydroxychloride compounds in some laser-cleaned areas. The two fragments on this slide display the materials found throughout the treated samples that were analyzed.

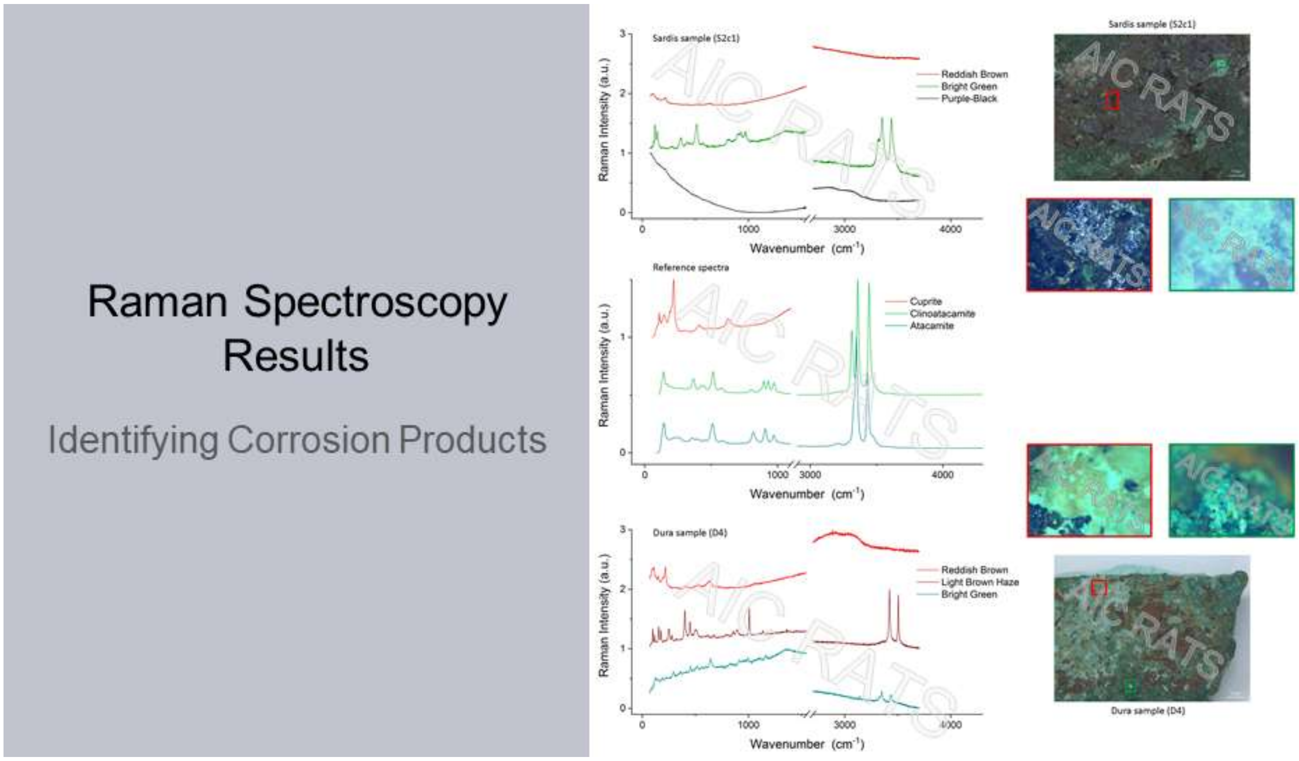

Raman Spectroscopy Results

Identifying Corrosion Products

On the Sardis sample at the top, cuprite and clinoatacamite were identified. The purple/black areas created by the laser are fluorescent in Raman (i.e. as seen on Slide 11), with weak, broad peaks in the 2700-3100 cm-1 region that could correspond to organic material. The black itself remains analytically unidentified, but may be copper nanoparticles from micromelted metallic copper that mixed with organic material present in the corrosion. On the Dura sample at the bottom, cuprite and atacamite were identified. The light brown haze noted as the first phenomenon (discussed on Slides 10 and 12) refers to material that forms on top of some of the light green powder and requires the addition of ethanol to remove with the laser. This haze has a Raman signal that is significantly altered in the OH region, with two sharp peaks appearing at 3402 and 3505 cm-1, rather than the peaks typically observed for a copper hydroxychloride in the 3150-3450 cm-1 region. This shift suggests a chemical alteration of the OH bonds by the cleaning laser, though the precise nature of the chemistry is unclear.

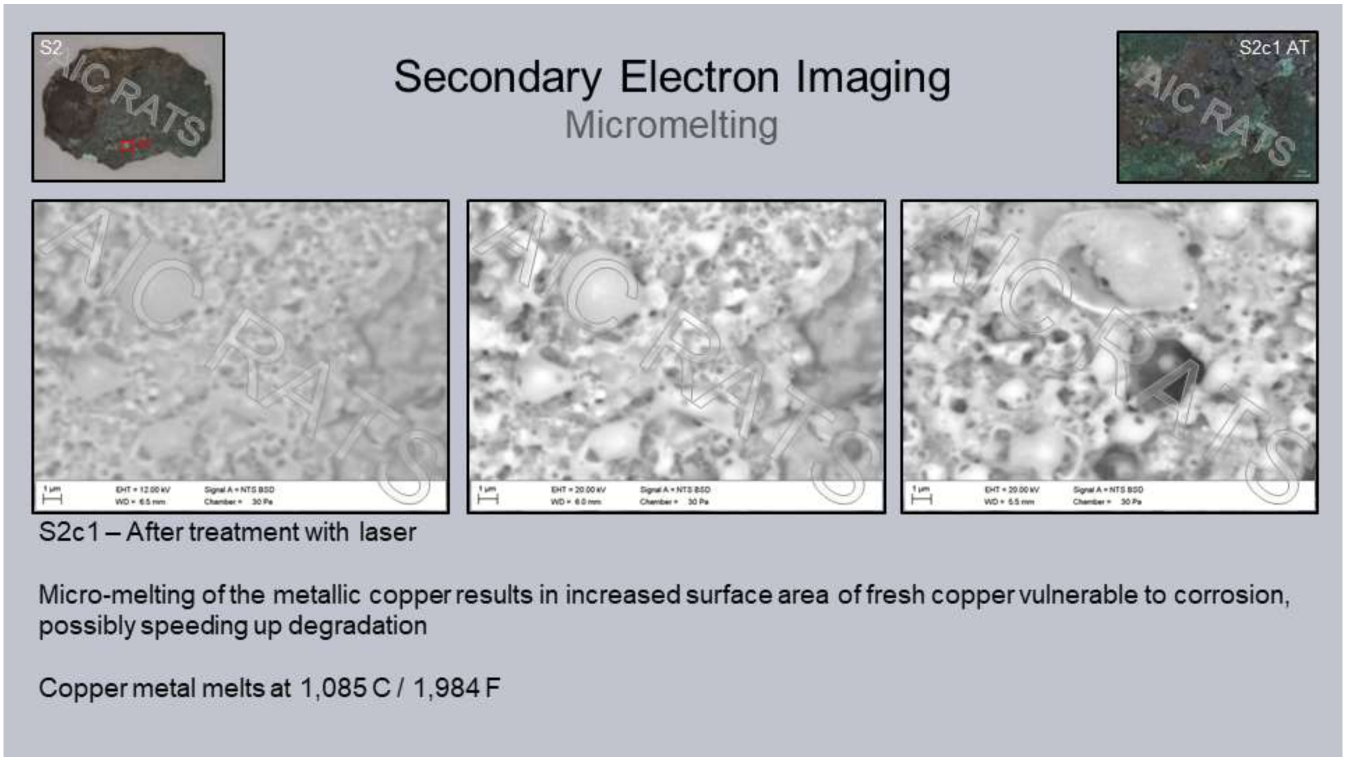

Secondary Electron Imaging

Micromelting

S2c1 – After treatment with laser

Micro-melting of the metallic copper results in increased surface area of fresh copper vulnerable to corrosion, possibly speeding up degradation

Copper metal melts at 1,085 C / 1,984 F

After initial analysis to determine extant chloride corrosion, we looked more closely at the surface morphology of treated copper samples to find evidence of micromelting. Micromelting is generally considered to be undesirable due to its possible role in increasing the rate of continuing corrosion. In theory, the small bubbles of rapidly melted and cooled metallic copper may increase the surface area of fresh copper vulnerable to corrosion more than any shallow grooves created while cleaning by mechanical scraping with a scalpel if bare metal is reached. In secondary electron images, it appears as if we are creating these bubbles, though possibly only on samples that were overcleaned, with the thinnest powdery corrosion to treat initially.

It is not clear if surfaces that experienced less 'cleaning' also reached the specific heat capacity of copper, at which micromelting will occur. The short pulse duration of the Q-switched laser used in this study almost guarantees that temperatures on metal surfaces will be high enough to cause micromelting, probably affecting a thin layer at the surface of a few microns (Martin Cooper, personal correspondence). Some authors used fluence values lower than 1.6 J/cm2 in their studies, which are less likely to negatively affect metallic surfaces (Siatou et al. 2006, Abdel-Kareem et al. 2016, Yandrisevits et al. 2017). The impact of micromelted surfaces on future degradation is not known and merits testing, specifically with the Er:YAG laser due to its longer pulse length and, thus, lower temperature increase (Martin Cooper, personal correspondence).

As mentioned above, we did not consider repetition rate, based on the assumption that the thermal response is slow enough that the metal could stabilize between pulses; confirmation of the practical validity of this assumption requires further testing.

Investigating Color Change

Experiments conducted with pulses delivered by Er:YAG laser attachment (2940 nm), observed blackening of surface.

Experiments conducted with pulses delivered by Nd:YAG laser attachment (1064 nm), observed purpling of surface.

Conclusions and Future Directions

One of the outstanding questions that came out of this analysis is: What is the laser creating on the surface? We know that we are successfully removing chloride-containing layers, sometimes along with more stable copper corrosion products, but we also see the possible formation of various amorphous and crystalline layers post laser treatment. Though the majority of this work was done with a 1064 nm laser, we also had done initial, uncontrolled tests with an Er:YAG 2940 nm laser that consistently showed the creation of a blackened surface (see Slide 19).

Analysis of the blackened material formed, initially posited to be tenorite, was inconclusive, with Raman spectroscopy resulting in spectra with similar peaks in the adjacent black, green, and brown areas, suggesting mixed, non-crystalline materials. Similarly, X-ray diffraction results showed unidentifiable amorphous structures, not clearly identifiable crystalline compounds.

We know the laser both removes and creates material on the surface of archaeological copper alloy fragments. What remains to be seen is if the process can be refined enough to focus on removing or converting the undesirable material while preserving the desired topography. We feel the modifications used in this project are a good, if imperfect, step towards rethinking the possibilities of controlled laser use in conservation in general.

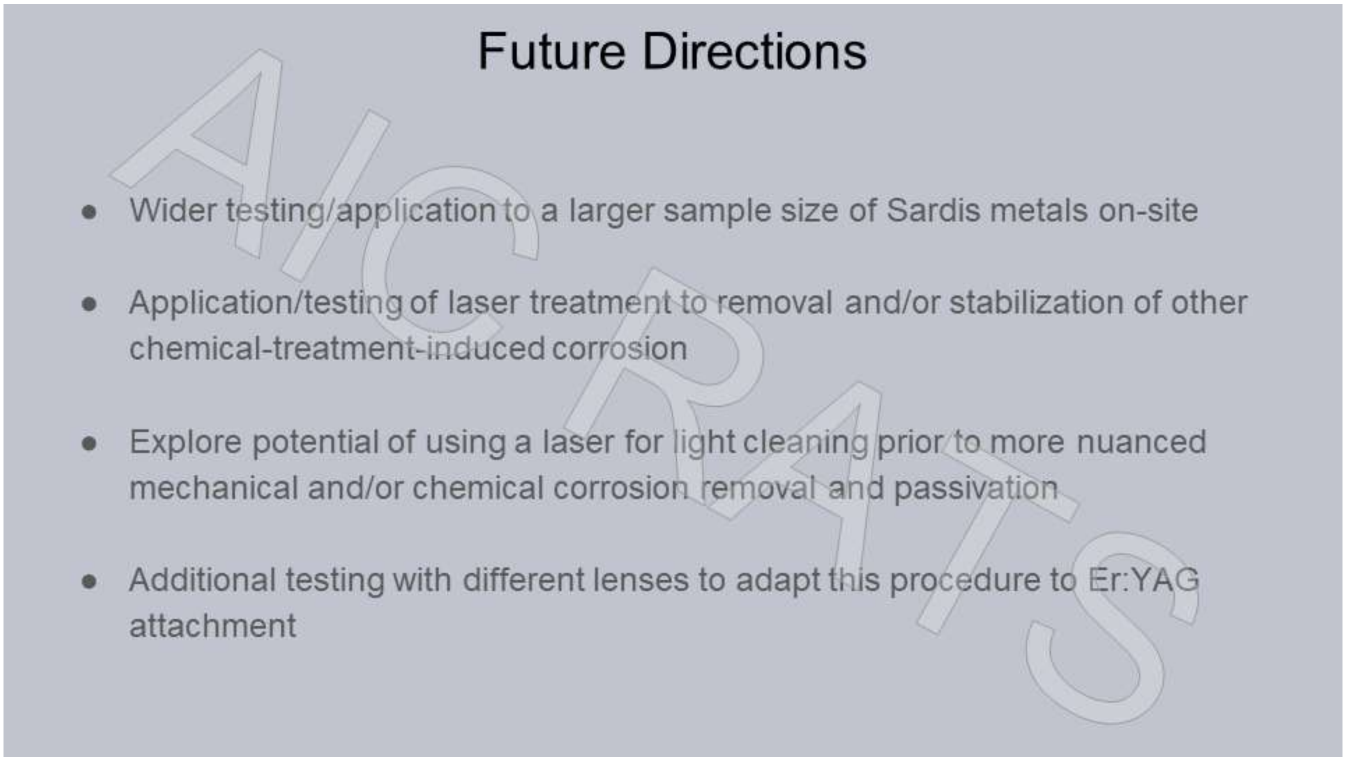

Future Directions

- Wider testing/application to a larger sample size of Sardis metals on-site
- Application/testing of laser treatment to removal and/or stabilization of other chemical-treatment-induced corrosion
- Explore potential of using a laser for light cleaning prior to more nuanced mechanical and/or chemical corrosion removal and passivation
- Additional testing with different lenses to adapt this procedure to Er:YAG attachment

For future study, it would be productive to test a larger sample size of Sardis metals on-site. Additionally, this treatment could be applied to the removal of other chemical-treatment-induced corrosion. Using the modified laser for cleaning that is followed by more nuanced mechanical and/or chemical surface corrosion removal or passivation, such as with BTA and/or aminomercaptothiadiazole (AMT) (De Alarcón 2013, 117) may also prove efficient. It would also be important to determine whether micromelting is significant enough to increase the speed of corrosion or a bronze disease relapse more than other more traditional mechanical cleaning. According to other sources, “nanosecond laser pulses can be useful for ablating incoherent mineral distributions when the metal surface is shielded by relatively thick corrosion, which can avoid surface micromelting effects” (Siano 2012, 430). This theory also suggests that testing with the 532 nm attachment may result in more delicate cleaning. Though initial treatments with the Er:YAG attachment produced a disfiguring black surface, controlled testing - as done in this study with the Nd:YAG attachment - and perhaps using aqueous solutions and organic compounds with hydroxyl groups, should be explored.

It is our further hope that the testing protocols shared in this publication will encourage other conservators and scientists to perform more tests on the application of lasers to stabilize active corrosion on copper alloys and other metal objects.

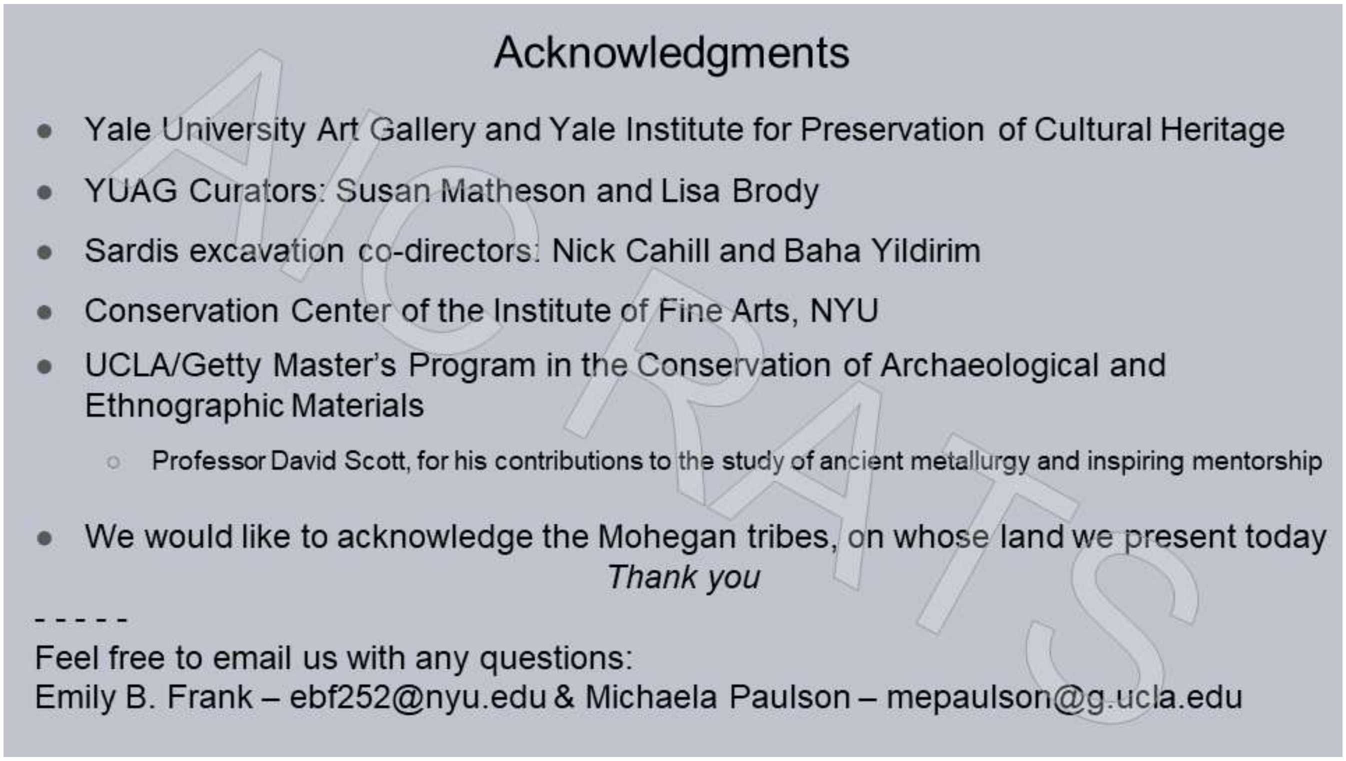

Acknowledgments

- Yale University Art Gallery and Yale Institute for Preservation of Cultural Heritage
- YUAG Curators: Susan Matheson and Lisa Brody
- Sardis excavation co-directors: Nick Cahill and Baha Yildirim
- Conservation Center of the Institute of Fine Arts, NYU
- UCLA/Getty Master's Program in the Conservation of Archaeological and Ethnographic Materials
  - Professor David Scott, for his contributions to the study of ancient metallurgy and inspiring mentorship
- We would like to acknowledge the Mohegan tribes, on whose land we present today

Thank you

\- - - - -

Feel free to email us with any questions:
Emily B. Frank – ebf252@nyu.edu & Michaela Paulson – mepaulson@g.ucla.edu

We would like to thank curators Susan Matheson and Lisa Brody of the Yale University Art Gallery and directors Nicholas Cahill and Baha Yildirim of the Harvard/Cornell Archaeological Exploration of Sardis for their support for this project and allowing us access to archaeological samples. We greatly appreciate the generosity of Edward and Anne Teppo for providing a laser to the Sardis field project, a gift that will enhance treatment protocols in the field and facilitate many other research projects. We are grateful to Yale conservation assistants Eric Stegmaier and Andres Garces for assisting us with x-radiography and 3D-printing. We thank scientist Aniko Bezur for making numerous analytical resources available for this study. Finally, thank you to Stacey Mandelbaum for her generous editing support.

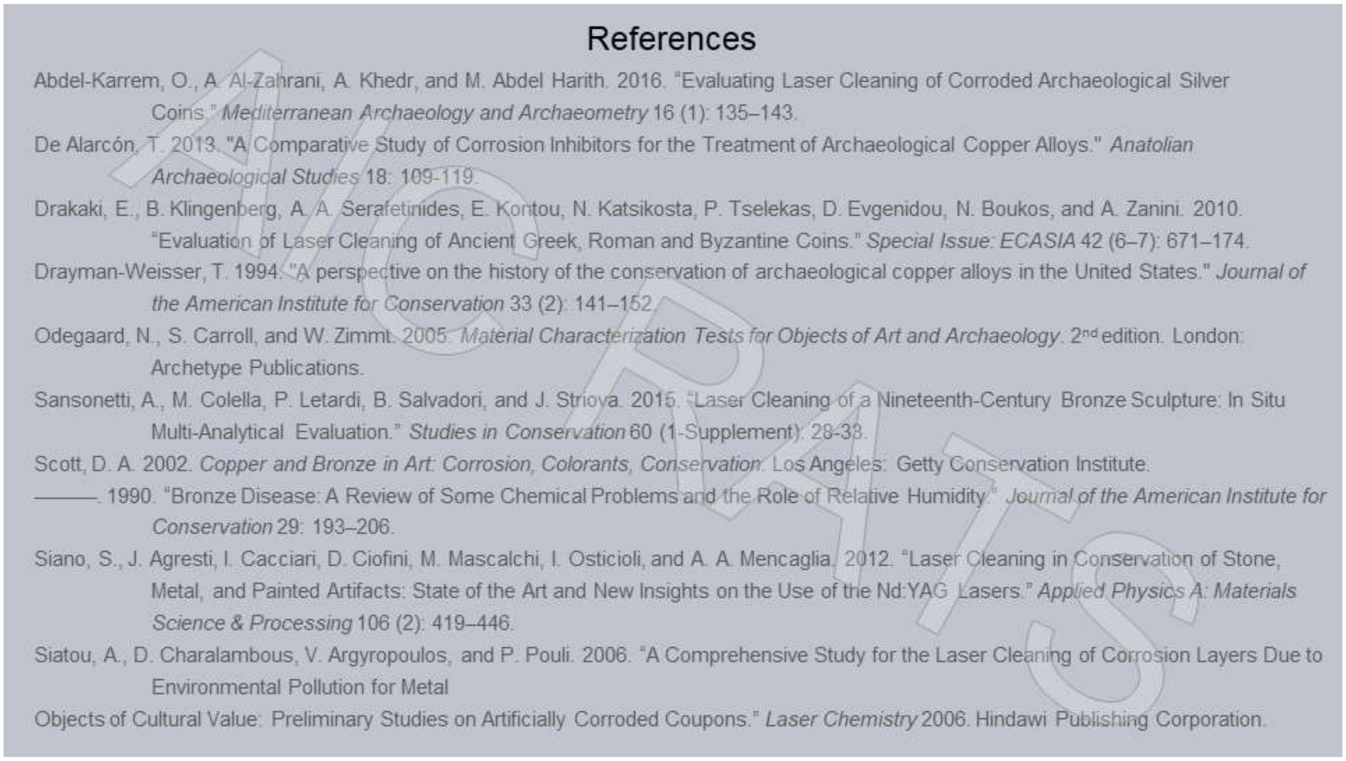

References

Abdel-Karrem, O., A. Al-Zahrani, A. Khedr, and M. Abdel Harith. 2016. "Evaluating Laser Cleaning of Corroded Archaeological Silver Coins." *Mediterranean Archaeology and Archaeometry* 16 (1): 135–143.

De Alarcón, T. 2013. "A Comparative Study of Corrosion Inhibitors for the Treatment of Archaeological Copper Alloys." *Anatolian Archaeological Studies* 18: 109-119.

Drakaki, E., B. Klingenberg, A. A. Serafetinides, E. Kontou, N. Katsikosta, P. Tselekas, D. Evgenidou, N. Boukos, and A. Zanini. 2010. "Evaluation of Laser Cleaning of Ancient Greek, Roman and Byzantine Coins." *Special Issue: ECASIA* 42 (6–7): 671–174.

Drayman-Weisser, T. 1994. "A perspective on the history of the conservation of archaeological copper alloys in the United States." *Journal of the American Institute for Conservation* 33 (2): 141–152.

Odegaard, N., S. Carroll, and W. Zimmt. 2005. *Material Characterization Tests for Objects of Art and Archaeology*. 2nd edition. London: Archetype Publications.

Sansonetti, A., M. Colella, P. Letardi, B. Salvadori, and J. Striova. 2015. "Laser Cleaning of a Nineteenth-Century Bronze Sculpture: In Situ Multi-Analytical Evaluation." *Studies in Conservation* 60 (1-Supplement): 28-33.

Scott, D. A. 2002. *Copper and Bronze in Art: Corrosion, Colorants, Conservation*. Los Angeles: Getty Conservation Institute.

———. 1990. "Bronze Disease: A Review of Some Chemical Problems and the Role of Relative Humidity." *Journal of the American Institute for Conservation* 29: 193–206.

Siano, S., J. Agresti, I. Cacciari, D. Ciofini, M. Mascalchi, I. Osticioli, and A. A. Mencaglia. 2012. "Laser Cleaning in Conservation of Stone, Metal, and Painted Artifacts: State of the Art and New Insights on the Use of the Nd:YAG Lasers." *Applied Physics A: Materials Science & Processing* 106 (2): 419–446.

Siatou, A., D. Charalambous, V. Argyropoulos, and P. Pouli. 2006. "A Comprehensive Study for the Laser Cleaning of Corrosion Layers Due to Environmental Pollution for Metal

Objects of Cultural Value: Preliminary Studies on Artificially Corroded Coupons." *Laser Chemistry* 2006. Hindawi Publishing Corporation.

Further Reading

Batishche, S., A. Kouzmouk, H. Tatur, T. Gorovets, U. Pilipenka, and V. Ukhau. 2005. "1320-Nm Range Nd:YAG-Laser in Restoration of Artworks Made of Bronze and Other Metals." In Lasers in the Conservation of Artworks. Vol. 100. Springer Proceedings in Physics. Berlin, Heidelberg: Springer.

Bertolotti, G., D. Bersani, P. P. Lottici, M. Alesiani, T. Malcherek, and J. Schlüter. 2012. "Micro-Raman Study of Copper Hydroxychlorides and Other Corrosion Products of Bronze Samples Mimicking Archaeological Coins." Analytical and Bioanalytical Chemistry 402: 1451–1457.

Bozzini, B., B. Alemán, M. Amati, M. Boniardi, V. Caramia, G. Giovannelli, L. Gregoratti, and M. Kazemian Abyaneh. 2017. "Novel Insights into Bronze Disease Gained by Synchrotron-Based Photoelectron Spectroscopy, in Support of Electrochemical Treatment Strategies." Studies in Conservation 62 (8): 465-473.

Dajnowski, A. "Laser as a Cleaning Tool for the Treatment of Large Scale Bronze Monuments." In Lasers in the Conservation of Artworks: Proceedings of the International Conference LACONA VII, M. Lasers in the Conservation of Artworks: Proceedings of the International Conference LACONA VII, edited by M. Castillejo, P. Moreno, M. Oujja, R. Radvan, and J. Ruiz, 303-308. Madrid, Spain, 17-21 September 2007. London: Taylor & Francis Ltd.

Dajnowski, A. and B. A. Dajnowski. 2017. "Using the new G.C. Laser Cleaning System for cleaning and surface preparation for re-gilding of a large outdoor bronze monument of Alexander

Hamilton." In Lasers in the Conservation of Artworks: Proceedings of LACONA XI, edited by P. Targowski, M. Walczak, and P. Pouli, 217-228. NCU Press.

Dajnowski, B. A. 2013. "Laser ablation cleaning of an underwater archaeological bronze spectacle plate from the H.M.S. DeBraak shipwreck." Society of Photographic Instrumentation Engineers (SPIE) Proceedings 8790, Optics for Arts, Architecture, and Archaeology IV, edited by L. Pezzati and P. Targowski.

Drayman-Weisser, T. 1987. "The use of sodium carbonate as a pre-treatment for difficult-to-stabilize bronzes". In Recent advances in the conservation and analysis of artifacts. ed. J. Black. London: Summer Schools Press. 105–108.

Fotakis, C., D. Anglos, V. Zafiropulos, S. Georgiou, and V. Tornari. 2007. Lasers in the Preservation of Cultural Heritage: Principles and Applications. Vol. 2. Series in Optics and Optoelectronics. New York, London: Taylor & Francis Ltd.

Froidevaux, M., P. Platt, M. Cooper, and K. Watkins. 2008. "Laser Interactions with Copper, Copper Alloys and Their Corrosion Products Used in Outdoor Sculpture in the United Kingdom." In Lasers in the Conservation of Artworks: Proceedings of the International Conference LACONA VII, edited by M. Castillejo, P. Moreno, M. Oujja, R. Radvan, and J. Ruiz, 277–284. Madrid, Spain, 17-21 September 2007. London: Taylor & Francis Ltd.

Frondel, C. 1950. "On Paratacamite and Some Related Copper Chlorides." Mineralogical Magazine, 34-45.

Garbacz, H., A. Koss, J. Marczak, J. Mróz, T. Onyszczuk, A. Rycyk, A. Sarzyski, W. Skrzeczanowski, M. Strzelec, and A. Zatorska. 2010. "Optimized Laser Cleaning of Metal Artworks - Evaluation of Determinants." Physics Procedia 5: 457–466.

Kurganov, N. 2018. "Possibility of laser application for bronze disease treatment." Poster presentation, Lacona XII, Paris, 10th-14th September 2018. (Proceedings to be published in Studies in Conservation, http://lacona12.org/program accessed June 27, 2019).

Pflugfelder, C., N. Mainusch, W. Viöl, and J. Ihlemann. 2008. "Removal of Unwanted Material from Surfaces of Artistic Value by Means of Nd:YAG Laser in Combination with Cold Atmospheric-Pressure Plasma." In Lasers in the Conservation of Artworks: Proceedings of the International Conference LACONA VII, edited by M. Castillejo, P. Moreno, M. Oujja, R. Radvan, and J. Ruiz, 55-58. Madrid, Spain, 17-21 September 2007. London: Taylor & Francis Ltd.

Pollard, A. M., R. G. Thomas, and P. A. Williams. 1992. "Copper Chloride System and Corrosion, a Complex Interplay of Kinetic and Thermodynamic Factors." In Dialogue|89: The Conservation of Bronze Sculpture in the Outdoor Environment: A Dialogue among Conservators, Curators, Engineering Scientists and Corrosion Engineers, edited by T. Drayman-Weisser, 123–133. Houston, TX: ASTM.

Scott, D. A. 2017. "New Insights on the Corrosion of Ancient Bronzes Using X-Ray Powder Diffraction: The Importance of Paratacamite, Sampleite, and Connellite." Studies in Conservation 62 (8): 410-418.

———. 2000. "A Review of Copper Chlorides and Related Salts in Bronze Corrosion and as Painting Pigments." Studies in Conservation 45 (1): 39-53.

Thompson, H. and M. Cooper. 2010. "The Use of Laser Cleaning in the Conservation of Public Copper-Alloy Monuments in the UK." Journal of Architectural Conservation 16 (1): 7-24.

Wing, N. 2017. "Comparison of Nd:YAG Laser and Mechanical Cleaning Methods on Ancient Roman Copper Coinage." Yale University Art Gallery. Internal Report. Unpublished.

Yandrisevits, M. A., P. Londero, F. Carò, A. Rizzo, and C. Cappuccini. 2017. "Wavelength-Dependent Absorption and Scattering Effects on Laser Cleaning of a Corroded Iron Alloy European Scale Armor." In LACONA XI, 27–45. Toruń: NCU Press.

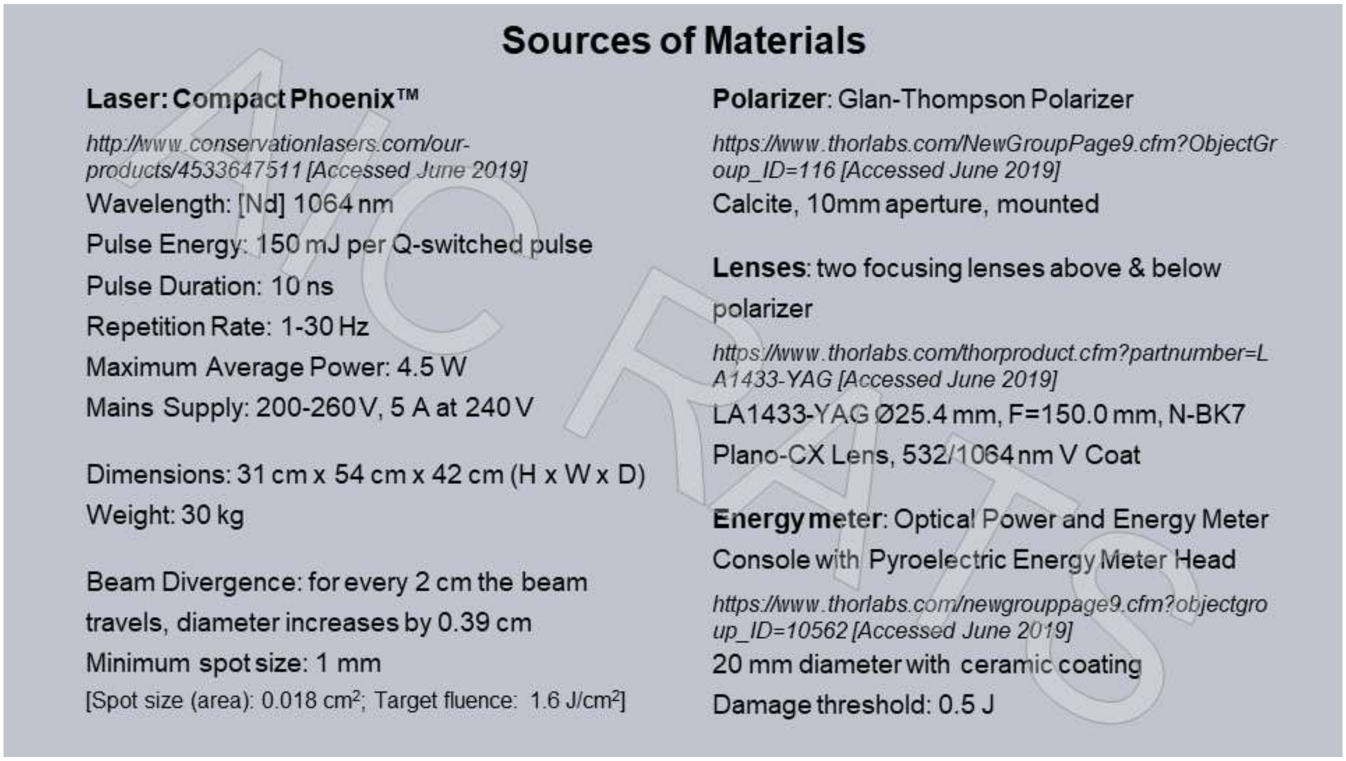

Sources of Materials

Laser: Compact Phoenix™

http://www.conservationlasers.com/our-products/4533647511 [Accessed June 2019]

Wavelength: [Nd] 1064 nm

Pulse Energy: 150 mJ per Q-switched pulse

Pulse Duration: 10 ns

Repetition Rate: 1-30 Hz

Maximum Average Power: 4.5 W

Mains Supply: 200-260 V, 5 A at 240 V

Dimensions: 31 cm x 54 cm x 42 cm (H x W x D)

Weight: 30 kg

Beam Divergence: for every 2 cm the beam travels, diameter increases by 0.39 cm

Minimum spot size: 1 mm

[Spot size (area): 0.018 cm^2; Target fluence: 1.6 J/cm^2]

Polarizer: Glan-Thompson Polarizer

https://www.thorlabs.com/NewGroupPage9.cfm?ObjectGroup_ID=116 [Accessed June 2019]

Calcite, 10mm aperture, mounted

Lenses: two focusing lenses above & below polarizer

https://www.thorlabs.com/thorproduct.cfm?partnumber=LA1433-YAG [Accessed June 2019]

LA1433-YAG Ø25.4 mm, F=150.0 mm, N-BK7 Plano-CX Lens, 532/1064 nm V Coat

Energy meter: Optical Power and Energy Meter Console with Pyroelectric Energy Meter Head

https://www.thorlabs.com/newgrouppage9.cfm?objectgroup_ID=10562 [Accessed June 2019]

20 mm diameter with ceramic coating

Damage threshold: 0.5 J